

**NUMERICAL STUDY IN DELAWARE
INLAND BAYS**

BY

LONG XU, DOMINIC DiTORO AND JAMES T. KIRBY

RESEARCH REPORT NO. CACR-06-04
AUGUST 2006



CENTER FOR APPLIED COASTAL RESEARCH

Ocean Engineering Laboratory
University of Delaware
Newark, Delaware 19716

ACKNOWLEDGEMENT

This study was supported by the Delaware Sea Grant Program, Project Number SG2003-2005 R/OE-32.

TABLE OF CONTENTS

LIST OF FIGURES	vi
LIST OF TABLES	xiii
ABSTRACT	xiv

Chapter

1 INTRODUCTION	1
1.1 Background	1
1.2 Outline of Present Work	6
2 NUMERICAL MODELS	9
2.1 Hydrodynamic Model (ECOMSED)	9
2.1.1 Hydrodynamic Module	10
2.1.2 Surface Heat Flux Module	12
2.1.3 Boundary Conditions	14
2.1.4 Numerical Techniques	15
2.2 Water Quality Model (RCA)	16
2.2.1 Conservation of Mass	16
2.2.2 Model Kinetics	17
2.2.3 Boundary Conditions	19
3 MODEL IMPLEMENTATION FOR DELAWARE INLAND BAY SYSTEM	20
3.1 Model Domain	20
3.2 Model Grid	21

3.3	Model Settings	21
3.4	Indian River Inlet Boundary Condition	21
3.5	Freshwater Discharge	22
3.6	Meteorological Data	22
3.7	Model Systems Coupling	23
4	MODEL CALIBRATION AND EVALUATION	28
4.1	Data	28
4.2	Hydrodynamic Model Calibration	29
4.3	Water Quality Model Calibration	33
4.4	Summary	36
5	MODEL-DATA COMPARISON AND MODEL VALIDATION	69
5.1	Hydrodynamic Model Validation	69
5.2	Water Quality Model Validation	70
5.3	Summary	71
6	CONCLUSION AND DISCUSSION	99
6.1	Conclusion	99
6.2	Limitations and Proposed Future Work	100
	BIBLIOGRAPHY	102

LIST OF FIGURES

1.1	Location of Delaware Inland Bays in Sussex County, Delaware (from Wang, 2005).	8
3.1	Bathymetry in the model domain. (Unit in color bar is m)	24
3.2	Grid cells in the model domain.	25
3.3	Locations of the two USGS tidal stations in Delaware Inland Bays.	26
3.4	Distribution of streams that link to Delaware Inland Bays (JEEAI, 2004).	27
4.1	Station locations of EPA’s STORET data in Delaware Inland Bays (from DNREC Database)	39
4.2	Station locations of State’s Pfiesteria water quality data in Delaware Inland Bays (from DNREC Database)	40
4.3	Station locations of Conectiv’s instantaneous survey in Indian River Bay (from DNREC Database)	41
4.4	Tide calibration result at Rosedale Beach in Indian River Bay in the year 1998 (model results in black solid lines, and field data in blue dash lines)	42
4.5	Tide calibration result at Rosedale Beach in Indian River Bay in the year 1998 (model results in black solid lines, and GEMSS in green dash lines)	43
4.6	Temperature and salinity calibration result at Conectiv’s station 1 in the year 1998 (model results in black dashed lines, GEMSS in green solid lines, and field data in red triangles)	44

4.7	Temperature and salinity calibration result at Conectiv’s station 2 in the year 1998 (model results in black dashed lines, GEMSS in green solid lines, and field data in red triangles)	44
4.8	Temperature and salinity calibration result at Conectiv’s station 3 in the year 1998 (model results in black dashed lines, GEMSS in green solid lines, and field data in red triangles)	45
4.9	Temperature and salinity calibration result at Conectiv’s station 6 in the year 1998 (model results in black dashed lines, GEMSS in green solid lines, and field data in red triangles)	45
4.10	Temperature and salinity calibration result at Conectiv’s station 7 in the year 1998 (model results in black dashed lines, GEMSS in green solid lines, and field data in red triangles)	46
4.11	Temperature and salinity calibration result at Conectiv’s station 8 in the year 1998 (model results in black dashed lines, GEMSS in green solid lines, and field data in red triangles)	46
4.12	Temperature and salinity calibration result at State’s Pfiesteria station I-1 in the year 1998 (model results in black solid lines, and field data in red triangles)	47
4.13	Temperature and salinity calibration result at State’s Pfiesteria station IRB-5 in the year 1998 (model results in black solid lines, and field data in red triangles)	47
4.14	Temperature and salinity calibration result at State’s Pfiesteria station IRB-6 in the year 1998 (model results in black dashed lines, GEMSS in green solid lines, and field data in red triangles)	48
4.15	Temperature and salinity calibration result at State’s Pfiesteria station IP-1 in the year 1998 (model results in black solid lines, and field data in red triangles)	48
4.16	Temperature and salinity calibration result at State’s Pfiesteria station RB-1 in the year 1998 (model results in black solid lines, and field data in red triangles)	49

4.17	Temperature and salinity calibration result at State's Pfiesteria station RB-5 in the year 1998 (model results in black solid lines, and field data in red triangles)	49
4.18	Temperature and salinity calibration result at State's Pfiesteria station RB-7 in the year 1998 (model results in black dashed lines, GEMSS in green solid lines, and field data in red triangles)	50
4.19	Temperature and salinity calibration result at State's Pfiesteria station IWC-2 in the year 1998 (model results in black dashed lines, GEMSS in green solid lines, and field data in red triangles)	50
4.20	Temperature and salinity calibration result at STORET station 306091 in the year 1998 (model results in black dashed lines, GEMSS in green solid lines, and field data in red triangles)	51
4.21	Temperature and salinity calibration result at STORET station 306121 in the year 1998 (model results in black dashed lines, GEMSS in green solid lines, and field data in red triangles)	51
4.22	Scatterplot comparison between model and data for temperature in the year 1998 (part 1)	52
4.23	Scatterplot comparison between model and data for temperature in the year 1998 (part 2)	53
4.24	Scatterplot comparison between model and data for temperature in the year 1998 (part 3)	54
4.25	Scatterplot comparison between model and data for salinity in the year 1998 (part 1)	55
4.26	Scatterplot comparison between model and data for salinity in the year 1998 (part 2)	56
4.27	Scatterplot comparison between model and data for salinity in the year 1998 (part 3)	57
4.28	Transect plot of statistical parameters for temperature in the year 1998	58

4.29	Transect plot of statistical parameters for salinity in the year 1998 .	58
4.30	Partitions of model domain based on chlorophyll's distribution (red lines are segmentation lines. IRI: Indian River Inlet; RB: Rehoboth Bay; IRB: Indian River Bay; White Creek (WC) is to the south of IRI; the rest are all the other rivers and creeks (RAC))	59
4.31	Linear relation between P_{av} and Chlorophyll (left panel), and R and Chlorophyll (right panel) in the year 1998	60
4.32	DO calibration summary 1 in the year 1998 (model results in grey lines, DO saturation in blue lines, and field data in triangles (blue: morning; red: afternoon))	61
4.33	DO calibration summary 2 in the year 1998 (model results in grey lines, DO saturation in blue lines, and field data in triangles (blue: morning; red: afternoon))	62
4.34	DO calibration summary 3 in the year 1998 (model results in grey lines, DO saturation in blue lines, and field data in triangles (blue: morning; red: afternoon))	63
4.35	DO calibration summary 4 in the year 1998 (model results in grey lines, DO saturation in blue lines, and field data in triangles (blue: morning; red: afternoon))	64
4.36	Scatterplot comparison between model and data for DO in the year 1998 (blue: morning; red: afternoon. part 1)	65
4.37	Scatterplot comparison between model and data for DO in the year 1998 (blue: morning; red: afternoon. part 2)	66
4.38	Scatterplot comparison between model and data for DO in the year 1998 (blue: morning; red: afternoon. part 3)	67
4.39	Transect plot of statistical parameters for DO in the year 1998 . . .	68
5.1	Tide validation result at Rosedale Beach in Indian River Bay in the year 1999 (model results in black solid lines, and field data in blue dash lines)	75

5.2	Temperature and salinity validation result at Conectiv’s station 1 in the year 1999 (model results in black solid lines, and field data in red triangles)	76
5.3	Temperature and salinity validation result at Conectiv’s station 2 in the year 1999 (model results in black solid lines, and field data in red triangles)	76
5.4	Temperature and salinity validation result at Conectiv’s station 3 in the year 1999 (model results in black solid lines, and field data in red triangles)	77
5.5	Temperature and salinity validation result at Conectiv’s station 6 in the year 1999 (model results in black solid lines, and field data in red triangles)	77
5.6	Temperature and salinity validation result at Conectiv’s station 7 in the year 1999 (model results in black solid lines, and field data in red triangles)	78
5.7	Temperature and salinity validation result at Conectiv’s station 8 in the year 1999 (model results in black solid lines, and field data in red triangles)	78
5.8	Temperature and salinity validation result at State’s Pfiesteria station IR-2 in the year 1999 (model results in black solid lines, and field data in red triangles)	79
5.9	Temperature and salinity validation result at State’s Pfiesteria station IRB-2 in the year 1999 (model results in black solid lines, and field data in red triangles)	79
5.10	Temperature and salinity validation result at State’s Pfiesteria station IRB-4 in the year 1999 (model results in black solid lines, and field data in red triangles)	80
5.11	Temperature and salinity validation result at State’s Pfiesteria station RB-1 in the year 1999 (model results in black solid lines, and field data in red triangles)	80

5.12	Temperature and salinity validation result at State’s Pfisteria station IWC-2 in the year 1999 (model results in black solid lines, and field data in red triangles)	81
5.13	Temperature and salinity validation result at STORET station 306091 in the year 1999 (model results in black solid lines, and field data in red triangles)	81
5.14	Temperature and salinity validation result at STORET station 306121 in the year 1999 (model results in black solid lines, and field data in red triangles)	82
5.15	Temperature and salinity validation result at STORET station 306321 in the year 1999 (model results in black solid lines, and field data in red triangles)	82
5.16	Scatterplot comparison between model and data for temperature in the year 1999 (part 1)	83
5.17	Scatterplot comparison between model and data for temperature in the year 1999 (part 2)	84
5.18	Scatterplot comparison between model and data for temperature in the year 1999 (part 3)	85
5.19	Scatterplot comparison between model and data for salinity in the year 1999 (part 1)	86
5.20	Scatterplot comparison between model and data for salinity in the year 1999 (part 2)	87
5.21	Scatterplot comparison between model and data for salinity in the year 1999 (part 3)	88
5.22	Transect plot of statistical parameters for temperature in the year 1999	89
5.23	Transect plot of statistical parameters for salinity in the year 1999 .	89
5.24	Linear relation between P_{av} and Chlorophyll (left panel), and R and Chlorophyll (right panel) in the year 1999	90

5.25	DO calibration summary 1 in the year 1999 (model results in grey lines, DO saturation in blue lines, and field data in triangles (blue: morning; red: afternoon))	91
5.26	DO calibration summary 2 in the year 1999 (model results in grey lines, DO saturation in blue lines, and field data in triangles (blue: morning; red: afternoon))	92
5.27	DO calibration summary 3 in the year 1999 (model results in grey lines, DO saturation in blue lines, and field data in triangles (blue: morning; red: afternoon))	93
5.28	DO calibration summary 4 in the year 1999 (model results in grey lines, DO saturation in blue lines, and field data in triangles (blue: morning; red: afternoon))	94
5.29	Scatterplot comparison between model and data for DO in the year 1999 (blue: morning; red: afternoon. part 1)	95
5.30	Scatterplot comparison between model and data for DO in the year 1999 (blue: morning; red: afternoon. part 2)	96
5.31	Scatterplot comparison between model and data for DO in the year 1999 (blue: morning; red: afternoon. part 3)	97
5.32	Transect plot of statistical parameters for DO in the year 1999 . . .	98

LIST OF TABLES

4.1	Statistical parameters for tide (<i>m</i>) calibration (year 1998)	37
4.2	Statistical summary for temperature ($^{\circ}C$) calibration (year 1998) .	37
4.3	Statistical summary for salinity (<i>ppt</i>) calibration (year 1998)	37
4.4	Calibration parameters for RCA model in the year 1998 (Unit of chlorophyll is $\mu g/l$; units of both photosynthesis rate and respiration rate are $gC/m^2 - day$)	38
4.5	Statistical summary for DO (<i>mg/l</i>) calibration (year 1998)	38
5.1	Statistical parameters for tide (<i>m</i>) validation (year 1999)	73
5.2	Statistical summary for temperature ($^{\circ}C$) validation (year 1999) . .	73
5.3	Statistical summary for salinity (<i>ppt</i>) validation (year 1999)	73
5.4	Calibration parameters for RCA model in the year 1999 (Unit of chlorophyll is $\mu g/l$; units of both photosynthesis rate and respiration rate are $gC/m^2 - day$)	74
5.5	Statistical summary for DO (<i>mg/l</i>) validation (year 1999)	74

ABSTRACT

The purpose of this study is to explore the physical transport and water quality in the Delaware Inland Bays through coupling two models: ECOMSED and RCA. ECOMSED is a fully integrated three-dimensional hydrodynamic model, and RCA is a general purpose water quality model.

The Delaware Inland Bays, located in Sussex County, Delaware, consist of two interconnected shallow coastal lagoons, Indian River Bay and Rehoboth Bay. The Inland Bays are connected to the Atlantic Ocean via the Indian River Inlet and they are tidally flushed. The Inland Bays are typical shallow bar-built estuaries that play a significant ecological role due to their high primary and secondary productivity.

The entire Inland Bays are the model domain, and a grid generation program, CoastGrid is used to generate the curvilinear grid. The grid has high resolution in the Bays, satisfying the resolution needed along the tortuous rivers. The coupled model systems have been set up, taking account of tidal elevation, freshwater discharges, wind stress, and water surface heat exchange. Also, reactions affecting dissolved oxygen are included in the water quality model, such as plant photosynthesis, respiration, and reaeration. A database of Delaware Inland Bays has been provided by DNREC to calibrate and verify the coupled models. The formatted database contains the available data in the Inland Bays.

The coupled models are calibrated using a year long data set, then they are compared with another year's data for verification. The calibrated models are capable of simulating the hourly tidal surface elevation at Rosedale Beach in Indian River well for the whole year, and the models are also able to reproduce the yearly

variations well with the field measurements for salinity, temperature, and dissolved oxygen.

The Inland Bays are dominated by the semi-diurnal tide, M_2 . The water temperature shows the expected seasonal variations in the entire Bays, while the salinity varies. The water in the upper and middle portions of the Indian River Bays is fresher than the water near the inlet, and the salinity in the Indian River Bay has larger diurnal oscillations than that in Rehoboth Bay. The DO shows large diurnal swings in summer and fall, and the simulations also reveal the super-saturation and near-anoxic conditions inside the Bays.

The results generated from the coupled models are in reasonable agreement with the available data. It has been shown that numerical models are effective tools for simulating water quality in shallow waters.

Chapter 1

INTRODUCTION

1.1 Background

The Delaware Inland Bays, which are located in Sussex County, Delaware, consist of two interconnected shallow coastal lagoons, Indian River Bay and Rehoboth Bay (Figure 1.1). Indian River Bay is connected to the Atlantic Ocean to the east via the Indian River Inlet and to Little Assawoman Bay to the south via the Little Assawoman Canal. Rehoboth Bay is connected to Delaware Bay to the north via the Lewes-Rehoboth Canal and to Indian River Bay to the south. The western portion of Indian River Bay, known as the Indian River, terminates at Millsboro Dam. The eastern part of the Indian River Inlet is an artificially stabilized channel with a width of about 80 *m* and a mean depth of about 20 *m*. Beyond the western end of the inlet, the bay quickly widens to a mean breadth of about 2.5 *km*. The surface areas of Indian River Bay and Rehoboth Bay are 38 *km*² and 35 *km*², respectively (Karpas, 1978). The mean low water depths of the Bays are generally less than 2 *m*. The Inland Bays are typical shallow bar-built estuaries which are common features along the United States East and Gulf coasts (Wong, 1991).

The physical processes in the Inland Bays are forced by a variety of mechanisms over a wide range of time scales. Keulegan (1967) conducted an analysis within the Bays and showed M_2 tide was the dominant tidal response. Wong and DiLorenzo (1988) showed that the semidiurnal tides experience significant damping in the interior of the Inland Bays while low frequency variability suffers relatively

little attenuation. Wong and Lu (1994) examined the subtidal current through the Indian River Inlet based on current measurements. Using relatively short sea level and current data collected in the vicinity of the Indian River Inlet, Lanan and Dalrymple (1977) and Karpas and Jensen (1977) found very strong tidal current in the inlet and the current in the inlet was clearly correlated with the hydraulic head between the ocean and the interior of the bay. The Inland Bays are tidally flushed, with estimates about 90-100 days flushing time for Indian River Bay and 80 days for Rehoboth Bay (Weston, 1993). Tidal flushing is uneven around the estuary because of the restricted connection with the Atlantic Ocean. For example, the east end of Indian River Bay and southern Rehoboth Bay are well flushed by tidal water twice a day, while most of the other waters are replaced at a much slower rate.

Beside the tide, other forcing mechanisms that induce circulation and exchange processes in coastal lagoons are fresh water inflow and wind stress. Fresh water enters the Bays through ground water discharge, by runoff from land, and from tributaries. There are several small creeks and rivers entering both Rehoboth Bay and Indian River Bay. The freshwater from Millsboro Pond to the west of Indian River Bay is the predominant one among all of them. Indian River, with a mean discharge of $2.83 \text{ m}^3/\text{s}$ (Karpas, 1978), accounts for 95% of the freshwater discharge into the bay. This river discharge affects the salinity of Indian River Bay. Karpas (1978) observed that a significant longitudinal salinity gradient exists in Indian River Bay.

The importance of wind forcing to the subtidal variability in estuarine waters has been recognized for quite some time. In a series of studies of Chesapeake Bay and its tributary estuaries, Wang (1979a,b) documented the effect of wind on the subtidal sea level and current fluctuations in that system. Wong (2002) indicated that the subtidal variability in Delaware Inland Bays is induced by winds through a combination of remote and local effects.

Water temperature and salinity are two most important physical characteristics of water systems. Water temperature of the Inland Bays is affected by many factors, including mixing with ocean water at the Indian River Inlet, precipitation, surface runoff, stream and ground water discharge, direct heating by solar energy, cooling by latent heat of vaporization (evaporation) and sensible heat loss. The climate of the watershed is humid-continental with four distinct seasons, which are moderated by the proximity of the Atlantic Ocean. Two years of water temperature data collected in the Inland Bays (Andres et al., 2002) indicated a mean water temperature of $25^{\circ}C$ and standard deviation $3^{\circ}C$ during the summer; in winter, the Indian River Bay and Rehoboth Bay have a mean water temperature of $7^{\circ}C$ and $8^{\circ}C$, respectively, and both have a standard deviation of $2^{\circ}C$. The mean temperatures of spring and fall season are in between. Salinity of the Inland Bays is mainly affected by the mixing of tidal ocean water and fresh water discharge. There is observational evidence that a significant longitudinal salinity gradient ($0.8 ppt/km$) exists in the Inland Bays (Karpas, 1978). The well-mixed Inland Bays rarely exhibit stratification with respect to temperature and salinity (Entrix, 2001).

Although the Inland Bays are slowly and unevenly flushed, they create a natural estuarine environment for finfish, shellfish, and waterfowl, which can be supported by high biological productivity. This high productivity depends upon the delicate balance between the living resources of the estuary and the quality of their physical environment. In general, the water quality of Rehoboth Bay is healthy, while the water quality of Indian River Bay ranges from healthy to degraded (Center for the Inland Bays (CIB), 1995). The large nutrient load from the watershed, and the natural circulation and flushing characteristics of the Inland Bays, result in over-enrichment of nitrate and phosphorous in the waters. In general, the Inland Bays are highly eutrophic. Using a classification scheme developed for the Chesapeake

Bay, the Inland Bays are among the most highly nutrient enriched of the 32 sub-estuarine systems in the Chesapeake Bay rankings (CIB, 1995). The middle and upper segments of Indian River Bay are more nutrient enriched than any segment of the Chesapeake Bay.

The nutrient inputs to the Delaware Inland Bays affect the abundance and distribution of bay life. The microscopic floating plants (phytoplankton) are most prolific in the upper and middle portions of Indian River Bay, while Rehoboth Bay generally represents an intermediate level of ambient nutrient and chlorophyll concentration, and the area nearest Indian River Inlet has the lowest concentration of both. Eutrophication is a condition in an aquatic ecosystem where high nutrient concentrations stimulate blooms of algae. The algal blooms cause the level of dissolved oxygen (DO) to decrease in the evening, resulting in fish kills (Price, 1998). Hypoxia occurs when DO concentration becomes sufficiently low to harm biota directly or to adversely affect normal ecological interactions. The occurrence of hypoxic events in coastal environments has increased in recent years, due to the continual development of human activities along the coasts (Orel et al., 1986; Baden et al., 1990). Price (1998) showed that increasing eutrophication has a debilitating effect on the benthic invertebrate community and shifts the shore-zone fish community from low-oxygen intolerant species (bay anchovy, menhaden, spot) to low-oxygen tolerant species (*Fundulus* sp. and *Cyprinodon* sp.). In addition, oxygen availability is one of the main factors affecting the swimming activity of fish. Domenici et al. (2000) indicated that schools of herring exposed to progressive hypoxia show a peak in velocity during severe hypoxia, followed by a decrease in swimming speed until school disruption occurred. They observed that fish increased the swimming speed during severe hypoxia to find more favorable conditions. Further, low nighttime oxygen levels in poorly mixed waters can result in fish and shellfish stress or even death if they cannot avoid anoxic areas.

The dissolved oxygen concentration is dependent on the physical and ecological characteristics of the estuarine waters (Chapra, 1997). Steele (1962) gave a theoretical equation for the photosynthesis-light relation. The photosynthesis of phytoplankton mainly depends on the light intensity, temperature, extinction coefficient, and chlorophyll concentration. D'Avanzo and Kremer (1994) showed diel oxygen dynamics is related to light, temperature, and wind. Under normal weather conditions in the summer, the variation of DO is dominated by reaeration from photosynthesis and consumption from respiration and decomposition, and thus exhibits the pattern of large diurnal swings (Wang, 2005). Wang also mentioned that rainfall can inhibit photosynthesis by light limitation and higher flushing rate, while the consumption of DO by respiration and decomposition can still remain at high levels.

The Inland Bays historically have provided nursery areas and habitats for a variety of shellfish, finfish, and other wildlife as well as their food sources. Over the past century, many of these desirable species have declined in numbers due to the loss of suitable habitat and the availability of appropriate food. Numerous fish kills in recent years have been related either to low-oxygen or anoxic waters or to "red tides". There are 26 miles of dead-end lagoons in the Inland Bays, where the water cannot adequately circulate (CIB, 1995). Hundreds of miles of rivers, streams, and Atlantic coastline, and thousands of acres of bays, estuaries and wetland failed to meet the fishable and swimmable water quality standard as required by the Federal Water Pollution Control Act (Wang, 2005). People are paying more attention to the environment in the Delaware Inland Bays. The U.S. Environmental Protection Agency (EPA) has presented the criteria of DO concentration based on the available data to protect aquatic life and its uses. The Total Maximum Daily Loads (TMDLs) have been limited below established water quality standards for the Inland Bays.

Numerical models are widely used to diagnose water quality problems and

predict future water quality status (e.g., Rajar and Cetina, 1997; Cox, 2003; J. E. Edinger Associates, Inc. (JEEAI), 2004). Deterministic water quality models which consist of both physical transport and biogeochemical processes are based on mass balance equations for water quality constituents in the water column. It is important to understand the hydrology of the Inland Bays because the mass of chemical constituents delivered to the water body over a specific time period are strongly dependent on the hydrodynamic transport and mixing. Blumberg and Mellor (1987) developed a three-dimensional coastal ocean circulation model, and this model has been expanded and applied to a variety of coastal ocean numerical studies (e.g., Blumberg and Fitzpatrick, 1999; Ahsan and Blumberg, 1999; Connolly et al., 1999). The hydrodynamic and water quality models have been coupled to understand the complex interrelations and interactions between hydrologic processes and ecological processes (Rajar and Cetina, 1997; Connolly et al., 1999; Karim et al., 2002; JEEAI, 2004). Hydrologic and water quality models of the Delaware Inland Bays will help diagnose and predict water quality status, and can be used as a water resources planning and management tool.

1.2 Outline of Present Work

In this thesis, a state-of-the-art hydrodynamic and water quality models are coupled to study the physical and ecological characteristics of Delaware Inland Bays. The dissolved oxygen will be simulated based on the hydrodynamic transport and the rates of photosynthesis, respiration and reaeration. The model systems will be calibrated and validated with the measured data. The following chapters describe the numerical models, the models calibration, the comparison between the simulated results and measured data, and the conclusion.

Chapter 2 details ECOMSED and RCA models, including the governing equations, model kinetics, numerical scheme, and module components.

Chapter 3 describes the model implementation for Delaware Inland Bays. The model domain and bathymetry are presented. Grids are generated by software, CoastGrid. The tidal boundary condition is specified by the USGS station data. The fresh water boundary and atmospheric boundary conditions are established using the observed data. The two models' coupling are described briefly in the end.

Chapter 4 presents the model system. First, the data are described, which will be used for calibration and validation. Then, the hydrodynamic model and water quality model are calibrated sequentially. Model parameters are adjusted systematically so that the discrepancies between the simulated values and the corresponding observations are minimized. The error analysis will be applied to evaluate the calibration.

Chapter 5 compares the model results with the measured data. In this chapter, the calibrated models will be applied to a different time series of data. The comparison results will show us how well the models perform.

Chapter 6 discusses and summarizes the models' performance. Conclusion will be made, and also with some suggestions for future's work.

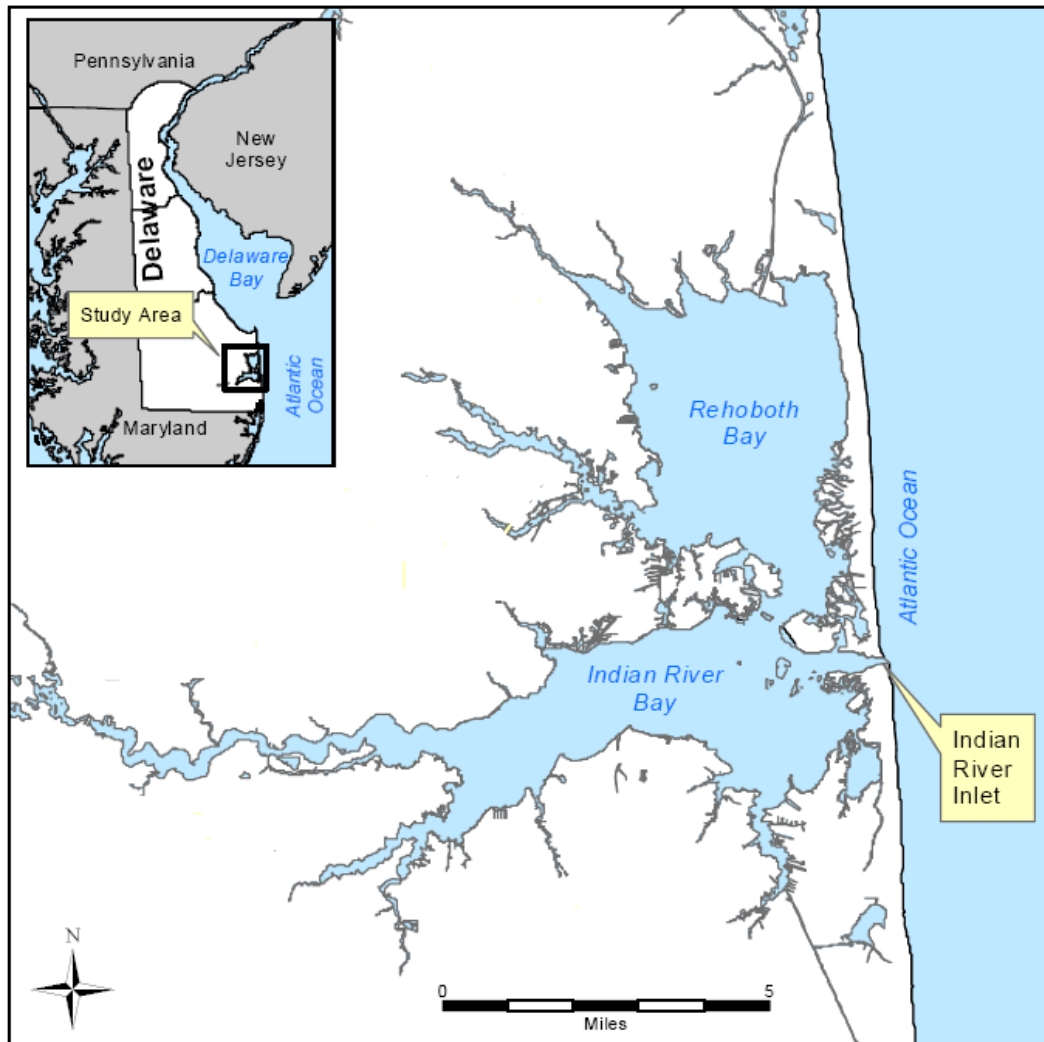


Figure 1.1: Location of Delaware Inland Bays in Sussex County, Delaware (from Wang, 2005).

Chapter 2

NUMERICAL MODELS

The numerical models applied in this thesis are HydroQual's state-of-the-art hydrodynamic model, ECOMSED and water quality model, RCA. The models are in the public domain and are freely available from the HydroQual website (www.hydroqual.com). These two models are coupled to study hydrodynamics and DO in the Delaware Inland Bays. The details of these two models are discussed here.

2.1 Hydrodynamic Model (ECOMSED)

ECOMSED is a fully integrated three-dimensional hydrodynamic model developed by HydroQual for application to marine and freshwater systems. The development of ECOMSED has its origins in the mid-1980s with the creation of the Princeton Ocean Model followed by an upgraded version called ECOM for shallow water environments such as rivers, lakes, estuaries and coastal oceans. ECOMSED includes surface wave models, bottom boundary layer physics, noncohesive sediment transport, and dissolved and sediment-bound tracer capabilities (HydroQual, Inc., 2002).

The complete ECOMSED model consists of several modules, including hydrodynamic module, sediment transport module, wind induced wave module, heat flux module and particle tracking module. The ECOMSED is also coupled with HydroQual's state-of-the-art water quality model, RCA by a sophisticated and efficient interface. The modules within the ECOMSED modeling framework are linked

internally. The framework also allows the hydrodynamic module to link with other modules externally. For the modeling framework in this thesis, the hydrodynamic module is run alone and transport information is saved in a separate file. Then the water quality module, RCA is run using the previously saved transport information. The following section describes some of the features of ECOMSED related to this thesis in detail.

2.1.1 Hydrodynamic Module

The hydrodynamic module, ECOM is a three-dimensional, time-dependent model developed by Blumberg and Mellor (1980, 1987). This module of ECOMSED has widely successful applications to oceanic, coastal, and estuarine waters.

The governing equations describe the velocity, surface elevation, temperature, and salinity fields. Two simplifying approximations in this module are the hydrostatic approximation and Boussinesq approximation. ECOMSED uses a horizontal, orthogonal, curvilinear coordinate system, ξ_1 , ξ_2 , and a vertical σ -coordinate system instead of the ordinary x , y , z coordinate system. The advantage of using orthogonal, curvilinear coordinate is to obtain high resolution where it is required without paying the penalty of unnecessarily high resolution in other parts of the modeled region. The metric coefficients, h_1 and h_2 , are defined so that the differential arc lengths along ξ_1 and ξ_2 are $ds_1 = h_1 d\xi_1$ and $ds_2 = h_2 d\xi_2$. The new vertical independent variable transforms both the free surface, η and the bottom, H into coordinate surfaces. This is used to overcome the computational problems which arise in the vicinity of large bathymetric irregularities. The new vertical coordinate is

$$\sigma = \frac{z - \eta}{H + \eta} \quad (2.1)$$

Let $D = H + \eta$, then under the new coordinate system, the continuity equation is

$$h_1 h_2 \frac{\partial \eta}{\partial t} + \frac{\partial}{\partial \xi_1} (h_2 U_1 D) + \frac{\partial}{\partial \xi_2} (h_1 U_2 D) + h_1 h_2 \frac{\partial \omega}{\partial \sigma} = 0 \quad (2.2)$$

where:

$$\omega = W - \frac{1}{h_1 h_2} \left[h_2 U_1 \left(\sigma \frac{\partial D}{\partial \xi_1} + \frac{\partial \eta}{\partial \xi_1} \right) + h_1 U_2 \left(\sigma \frac{\partial D}{\partial \xi_2} + \frac{\partial \eta}{\partial \xi_2} \right) \right] - \left(\sigma \frac{\partial D}{\partial t} + \frac{\partial \eta}{\partial t} \right) \quad (2.3)$$

The Reynolds momentum equations are

$$\begin{aligned} & \frac{\partial (h_1 h_2 D U_1)}{\partial t} + \frac{\partial}{\partial \xi_1} (h_2 D U_1^2) + \frac{\partial}{\partial \xi_2} (h_1 D U_1 U_2) + h_1 h_2 \frac{\partial (\omega U_1)}{\partial \sigma} \\ & \quad + D U_2 \left(-U_2 \frac{h_2}{\xi_1} + U_1 \frac{h_1}{\xi_2} - h_1 h_2 f \right) \\ & = -g D h_2 \left(\frac{\partial \eta}{\partial \xi_1} + \frac{\partial H_0}{\partial \xi_1} \right) - \frac{g D^2 h_2}{\rho_0} \int_{\sigma}^0 \left[\frac{\partial \rho}{\partial \xi_1} - \frac{\sigma}{D} \frac{\partial D}{\partial \xi_1} \frac{\partial \rho}{\partial \sigma} \right] d\sigma \\ & \quad - D \frac{h_2}{\rho_0} \frac{\partial P_a}{\partial \xi_1} + \frac{\partial}{\partial \xi_1} \left(2 A_M \frac{h_2}{h_1} D \frac{\partial U_1}{\partial \xi_1} \right) + \frac{\partial}{\partial \xi_2} \left(A_M \frac{h_1}{h_2} D \frac{\partial U_1}{\partial \xi_2} \right) \\ & \quad + \frac{\partial}{\partial \xi_2} \left(A_M D \frac{\partial U_2}{\partial \xi_1} \right) + \frac{h_1 h_2}{D} \frac{\partial}{\partial \sigma} \left(K_M \frac{\partial U_1}{\partial \sigma} \right) \end{aligned} \quad (2.4)$$

$$\begin{aligned} & \frac{\partial (h_1 h_2 D U_2)}{\partial t} + \frac{\partial}{\partial \xi_1} (h_2 D U_1 U_2) + \frac{\partial}{\partial \xi_2} (h_1 D U_2^2) + h_1 h_2 \frac{\partial (\omega U_2)}{\partial \sigma} \\ & \quad + D U_1 \left(-U_1 \frac{h_1}{\xi_2} + U_2 \frac{h_2}{\xi_1} + h_1 h_2 f \right) \\ & = -g D h_1 \left(\frac{\partial \eta}{\partial \xi_2} + \frac{\partial H_0}{\partial \xi_2} \right) - \frac{g D^2 h_1}{\rho_0} \int_{\sigma}^0 \left[\frac{\partial \rho}{\partial \xi_2} - \frac{\sigma}{D} \frac{\partial D}{\partial \xi_2} \frac{\partial \rho}{\partial \sigma} \right] d\sigma \\ & \quad - D \frac{h_1}{\rho_0} \frac{\partial P_a}{\partial \xi_2} + \frac{\partial}{\partial \xi_2} \left(2 A_M \frac{h_1}{h_2} D \frac{\partial U_2}{\partial \xi_2} \right) + \frac{\partial}{\partial \xi_1} \left(A_M \frac{h_2}{h_1} D \frac{\partial U_2}{\partial \xi_1} \right) \\ & \quad + \frac{\partial}{\partial \xi_1} \left(A_M D \frac{\partial U_1}{\partial \xi_2} \right) + \frac{h_1 h_2}{D} \frac{\partial}{\partial \sigma} \left(K_M \frac{\partial U_2}{\partial \sigma} \right) \end{aligned} \quad (2.5)$$

with ρ_0 the reference density, ρ the in situ density, f the Coriolis parameter. A_M , K_M are the horizontal and vertical kinematic viscosity, respectively.

The conservation equations for temperature and salinity are

$$\begin{aligned} & h_1 h_2 \frac{\partial (\theta D)}{\partial t} + \frac{\partial}{\partial \xi_1} (h_2 U_1 \theta D) + \frac{\partial}{\partial \xi_2} (h_1 U_2 \theta D) + h_1 h_2 \frac{\partial (\omega \theta)}{\partial \sigma} \\ & = \frac{\partial}{\partial \xi_1} \left(\frac{h_2}{h_1} A_H D \frac{\partial \theta}{\partial \xi_1} \right) + \frac{\partial}{\partial \xi_2} \left(\frac{h_1}{h_2} A_H D \frac{\partial \theta}{\partial \xi_2} \right) + \frac{h_1 h_2}{D} \frac{\partial}{\partial \sigma} \left(K_H \frac{\partial \theta}{\partial \sigma} \right) \end{aligned} \quad (2.6)$$

$$\begin{aligned}
& h_1 h_2 \frac{\partial (SD)}{\partial t} + \frac{\partial}{\partial \xi_1} (h_2 U_1 SD) + \frac{\partial}{\partial \xi_2} (h_1 U_2 SD) + h_1 h_2 \frac{\partial (\omega S)}{\partial \sigma} \\
&= \frac{\partial}{\partial \xi_1} \left(\frac{h_2}{h_1} A_H D \frac{\partial S}{\partial \xi_1} \right) + \frac{\partial}{\partial \xi_2} \left(\frac{h_1}{h_2} A_H D \frac{\partial S}{\partial \xi_2} \right) + \frac{h_1 h_2}{D} \frac{\partial}{\partial \sigma} \left(K_H \frac{\partial S}{\partial \sigma} \right)
\end{aligned} \tag{2.7}$$

where θ is the potential temperature and S is the salinity. A_H , K_H are the horizontal and vertical diffusivity for turbulent mixing of heat and salt, respectively.

A second order turbulence closure scheme (Mellor and Yamada, 1982) characterizes the turbulence by equations for the turbulence kinetic energy, $q^2/2$, and a turbulence macroscale, ℓ , which are

$$\begin{aligned}
& h_1 h_2 \frac{\partial (q^2 D)}{\partial t} + \frac{\partial}{\partial \xi_1} (h_2 U_1 D q^2) + \frac{\partial}{\partial \xi_2} (h_1 U_2 D q^2) + h_1 h_2 \frac{\partial (\omega q^2)}{\partial \sigma} \\
&= h_1 h_2 \left\{ \frac{2K_M}{D} \left[\left(\frac{\partial U_1}{\partial \sigma} \right)^2 + \left(\frac{\partial U_2}{\partial \sigma} \right)^2 \right] + \frac{2g}{\rho_0} K_H \frac{\partial \rho}{\partial \sigma} - \frac{2q^3 D}{A_1} \right\} \\
&+ \frac{\partial}{\partial \xi_1} \left(\frac{h_2}{h_1} A_H D \frac{\partial q^2}{\partial \xi_1} \right) + \frac{\partial}{\partial \xi_2} \left(\frac{h_1}{h_2} A_H D \frac{\partial q^2}{\partial \xi_2} \right) + \frac{h_1 h_2}{D} \frac{\partial}{\partial \sigma} \left(K_q \frac{\partial q^2}{\partial \sigma} \right)
\end{aligned} \tag{2.8}$$

$$\begin{aligned}
& h_1 h_2 \frac{\partial (q^2 \ell D)}{\partial t} + \frac{\partial}{\partial \xi_1} (h_2 U_1 D q^2 \ell) + \frac{\partial}{\partial \xi_2} (h_1 U_2 D q^2 \ell) + h_1 h_2 \frac{\partial (\omega q^2 \ell)}{\partial \sigma} \\
&= h_1 h_2 \left\{ \frac{\ell E_1 K_M}{D} \left[\left(\frac{\partial U_1}{\partial \sigma} \right)^2 + \left(\frac{\partial U_2}{\partial \sigma} \right)^2 \right] + \frac{\ell E_1 g}{\rho_0} K_H \frac{\partial \rho}{\partial \sigma} - \frac{q^3 D}{B_1} \tilde{w} \right\} \\
&+ \frac{\partial}{\partial \xi_1} \left(\frac{h_2}{h_1} A_H D \frac{\partial q^2 \ell}{\partial \xi_1} \right) + \frac{\partial}{\partial \xi_2} \left(\frac{h_1}{h_2} A_H D \frac{\partial q^2 \ell}{\partial \xi_2} \right) + \frac{h_1 h_2}{D} \frac{\partial}{\partial \sigma} \left(K_q \frac{\partial q^2 \ell}{\partial \sigma} \right)
\end{aligned} \tag{2.9}$$

2.1.2 Surface Heat Flux Module

The energy content of water bodies is primarily governed by the surface heat energy exchanges. Heat fluxes are often parameterized by using the most commonly available meteorological data. The processes that control the heat exchange between the water and atmosphere are well documented (Large and Pond, 1982; Rosati and Miyakoda, 1988; Ahsan and Blumberg, 1999). All of these relied mostly on the bulk formulae to evaluate the components of the heat budget.

To estimate net heat flux, the bulk formulae depend on meteorological parameters, such as cloud cover, relative humidity, air temperature, winds, water surface temperature, etc. Computations of four major heat flux components: short wave solar radiation, longwave atmospheric radiation, sensible heat and latent heat fluxes are based on the works of Ahsan and Blumberg (1999). The solar radiation data are provided by the National Climatic Data Center (NCDC) and are directly used by the model; therefore, no estimation for solar radiation is necessary in the current application.

The net atmospheric radiation at the surface is the result of two processes: the downward radiation from the atmosphere and the upward radiation emitted by the water surface. Atmospheric radiation depends primarily on the air temperature, T_a , humidity, and cloud cover, C . The net atmospheric flux is given as

$$H_a = \varepsilon\sigma \left((9.37 \times 10^{-6} T_a^6) (1 + 0.17C^2) - T_s^4 \right) \quad (2.10)$$

where, H_a = net longwave atmospheric radiations (Wm^{-2}); ε = emissivity of the water body (0.97); σ = Stefan-boltzmann constant ($5.67 \times 10^{-8} Wm^{-2}K^{-4}$); and T_s is water temperature ($^{\circ}C$).

Heat exchange can occur between the atmosphere and a water body through conduction. The heat flux may be in either direction, depending on the sense of the temperature difference between the air and the water body. The conductive heat flux is commonly parameterized by the bulk transfer formula with dependency on wind speed as suggested by Edinger et al. (1974):

$$H_c = C_c f(W)(T_s - T_a) \quad (2.11)$$

where H_c = sensible (conduction) heat fluxes (Wm^{-2}); C_c = Bowen's coefficient (0.62 mb/K); and $f(W)$ = wind speed function ($Wm^{-2}mb^{-1}$).

The evaporative heat flux is related to the conductive heat flux by the Bowen ratio, and can be given as a function of wind speed and the difference between the

saturated water vapor pressure at the water surface temperature and the water vapor pressure in the overlying air (Edinger et al. 1974):

$$H_e = f(W)(e_s - e_a) \quad (2.12)$$

where H_e = evaporative heat flux (Wm^{-2}); e_s = saturated vapor pressure (mb); and e_a = air-vapor pressure (mb).

2.1.3 Boundary Conditions

Boundary conditions are applied at the water body surface and bottom as well as open lateral boundaries. Momentum flux at the free surface is imparted by wind stress. The bottom stress is determined by matching velocities with the logarithmic law of the wall. Specifically,

$$\vec{\tau}_b = \rho_0 C_D |\vec{V}_b| \vec{V}_b \quad (2.13)$$

with C_D , the drag coefficient given by

$$C_D = \left[\frac{1}{\kappa} \ln(H + z_b) / z_0 \right]^{-2} \quad (2.14)$$

If the bottom boundary layer is not well resolved, it is more appropriate to specify $C_D = 0.0025$. The actual algorithm is to set C_D to the larger of the two values given by (2.14) and 0.0025.

Open lateral boundary conditions are applied by parameterizing the environment exterior to the relevant domain. Two types of open boundaries exist, inflow and outflow. Temperature and salinity are prescribed from data at boundaries,

$$\frac{\partial}{\partial t}(\theta, S) + U_n \frac{\partial}{\partial n}(\theta, S) = 0 \quad (2.15)$$

where the subscript n is the coordinate normal to the boundary.

For the ocean circulation module, the seaward open boundary conditions are provided to allow long-wave energy (e.g., tides) to enter the model domain as well

as a means of radiating out. There are a number of radiation boundary conditions that can be utilized to achieve these goals. In this study, the clamped boundary condition is used by specifying water level along the boundary grids.

2.1.4 Numerical Techniques

The equations which form the circulation model together with their boundary conditions are solved by finite difference techniques. A staggered “C” grid (Arakawa and Lamb, 1977) is used for horizontal differencing. The arrangement of points has U_1 at points $\pm\Delta\xi_1/2$ away from the points where H and η are defined, and U_2 at points $\pm\Delta\xi_2/2$ away from the H and η points. The finite difference equations have been demonstrated to conserve energy, temperature, salinity, mass, and momentum.

A mode splitting technique is used for computational efficiency. An external mode is derived by vertically integrating Equations (2.2), (2.4), and (2.5). The computational strategy is to solve equations for the external mode with a short time step to resolve high frequency motions. The terms from the internal mode are held constant in time over the external mode integration period. The external mode calculation results in updates for surface elevation, and vertically averaged velocities. The internal mode equations are then solved with a much longer time step, and update velocity, temperature, salinity, and turbulence quantities.

The leap-frog differencing scheme used for the time stepping introduces a tendency for the solution at even and odd time steps to split. This time splitting is removed by a weak filter where the solution is smoothed at each time step according to

$$F_s^n = F^n + \frac{\alpha}{2} (F^{n+1} - 2F^n + F_s^{n-1}) \quad (2.16)$$

where $\alpha = 0.05$ and F_s is a smoothed solution. This technique introduces less damping than either Euler backward or forward stepping technique.

From a viewpoint of computational stability, the Courant-Friedrichs-Levy (CFL) condition on the vertically integrated, external mode, transport equations limits the time step. A rule of thumb for the critical time step is found to be

$$\Delta t_c < \frac{1}{C_e} \left(h_1^{-2} + h_2^{-2} \right)^{-1/2} \quad (2.17)$$

where

$$C_e = 2(gH)^{1/2} + \bar{U}_{max} \quad (2.18)$$

Here, \bar{U}_{max} is the fastest vertically averaged velocity. The internal mode is restricted by a similar condition except that C_e , is replaced by C_i , a value twice the fastest internal wave speed plus the largest current velocity. For most coastal and open ocean situations, C_e/C_i is from 80 to 100, while in estuaries the ratio is somewhat smaller, perhaps 10.

2.2 Water Quality Model (RCA)

RCA is a Row-Column version of AESOP, HydroQual's general purpose water quality modeling computer code. It employs the same variable horizontal grid and vertical σ coordinate system as ECOMSED does.

2.2.1 Conservation of Mass

The modeling framework is based upon the principle of conservation of mass. The conservation of mass accounts for all of a material entering or leaving a body of water, transport of the material within the water body, and physical, chemical and biological transformations of the material (HydroQual, Inc., 2004). For a three-dimensional coordinate system, the conservation of mass can be written as:

$$\begin{aligned} \frac{\partial c}{\partial t} = & \frac{\partial}{\partial x} \left(E_x \frac{\partial c}{\partial x} \right) + \frac{\partial}{\partial y} \left(E_y \frac{\partial c}{\partial y} \right) + \frac{\partial}{\partial z} \left(E_z \frac{\partial c}{\partial z} \right) \\ & - U_x \frac{\partial c}{\partial x} - U_y \frac{\partial c}{\partial y} - U_z \frac{\partial c}{\partial z} \pm S + W \end{aligned} \quad (2.19)$$

where, c is the concentration of water quality variable, E is the dispersion coefficient due to tides, density, and velocity gradients, U is the advective velocity, S is the source and sink of the water quality variable, representing kinetic interactions, and W is the external input of the variable. The modeling framework is made up of two components: (1) the transport due to freshwater flow in riverine systems and tidal, meteorological and density-driven currents in estuarine and coastal systems, and (2) the kinetic interactions between variables and the external inputs. Freshwater flow, density-driven currents, and tidally and wind induced mixing are responsible for the movement of the water quality constituents within the water body.

2.2.2 Model Kinetics

Salinity is included in this model to enable the verification that transport of the hydrodynamic model is transferred to the water quality model properly. The salinity is conservative with no reaction kinetics involved, and there are no direct sources or sinks of salinity.

Dissolved oxygen is one state variable included in this application of the model. The sources of oxygen are algal photosynthesis and reaeration. The sink of oxygen is algal respiration.

In the natural environment, the light intensity to which the phytoplankton are exposed is not at the optimum value uniformly. At the air-water interface, photo inhibition may occur due to high light intensity, while at depths below the euphotic zone, light is not available for photosynthesis due to natural turbidity, such as algal related turbidity. The light formulation in RCA extends from a light curve analysis by Steele (1962), which accounts for both the effects of saturating light intensities and light attenuation through the water column. The incident light intensity I_0 at the water surface, I_{surf} may be evaluated at any time, t within the day by using the

formula:

$$I_{surf}(t) = \frac{\pi I_{tot}}{2f} \sin \left[\frac{\pi (t_d - t_{sunrise})}{f} \right] \quad (2.20)$$

where, I_{tot} is the total daily incident solar radiation (langley/day), f is the fraction of daylight, t_d is the time of day, and $t_{sunrise}$ is the time of sunrise. At night, I_{surf} is set to 0 because of no light. To account for the effect of variations of available light as a function of depth, the light intensity $I_0(H)$ at any depth H is related to the incident surface intensity, I_{surf} , via the extinction coefficient, k_e , through the formula:

$$I_0(H) = I_{surf} \exp(-k_e H) \quad (2.21)$$

In this thesis, the extinction coefficient is considered as constant ($k_e = 1.1 \text{ m}^{-1}$) in the entire Bays. The depth-averaged light attenuated growth rate factor, $G_I(I)$ is

$$G_I(I) = \frac{e}{k_e H} \left[\exp \left(\frac{-I_0(t)}{I_s} e^{-k_e H} \right) - \exp \left(\frac{-I_0(t)}{I_s} \right) \right] \quad (2.22)$$

where I_s is the saturation light intensity (lanleys/day) and $e = 2.718$.

In this model, the photosynthesis rate is directly proportional to the light attenuated growth rate G_I , which is a function of the light intensity I_0 . The empirical formula of photosynthesis rate can be expressed as:

$$P = P_m \theta_{P,T}^{T-20} G_I \quad (2.23)$$

where P_m is the maximum photosynthesis rate ($gC/m^2 - day$), $\theta_{P,T}$ is the temperature correction parameter of photosynthesis. Similarly, the respiration rate R can be expressed based on the temperature correction $\theta_{R,T}$,

$$R = R_T \theta_{R,T}^{T-20} \quad (2.24)$$

where, R_T is the respiration rate ($gC/m^2 - day$) at temperature $20^\circ C$. Another source term, reaeration is a function of reaeration rate at $20^\circ C$, k_a (d^{-1}), temperature

T , and the difference between dissolved oxygen, O (mg/l) and saturated dissolved oxygen, O_s (mg/l):

$$Re = k_a \theta_{Re,T}^{T-20} (O_s - O) \quad (2.25)$$

All the temperature corrections for photosynthesis, respiration, and reaeration are in terms of $20^\circ C$. The empirical values for $\theta_{P,T}$, $\theta_{R,T}$, and $\theta_{Re,T}$ are 1.066, 1.080, and 1.024, respectively.

2.2.3 Boundary Conditions

In the water quality model, since the hydrodynamic transport information has been transferred into this model, only the open lateral boundary conditions need to be specified. DO is discharged into the model domain with the freshwater from rivers and creeks. The formula at boundaries is the same as Eq. (2.15), with the replacement of temperature and salinity by the concentration of DO.

Chapter 3

MODEL IMPLEMENTATION FOR DELAWARE INLAND BAY SYSTEM

In this chapter, both hydrodynamic model, ECOMSED and water quality model, RCA are set up to simulate the tidal current driven by astronomical tide from the Atlantic Ocean via the Inlet, and the resulting transport system of water qualities. First, the model domain will be specified. Then the model grid will be generated accordingly. The seaward boundary condition is specified by the observed sea level data. Other boundary conditions including fresh water boundaries and atmospheric boundary are specified as well. Last, all the other input parameters and time-changed variables in the models are discussed.

3.1 Model Domain

The simulation domain includes the Indian River Bay and Rehoboth Bay. The bathymetric data originally came from combined measurements of Delaware Department of Natural Resources and Environmental Control (DNREC), U.S. Geological Survey (USGS), the Army Corps of Engineers (ACOE), and 1999 field estimates made by ENTRIX, Inc. (ENTRIX). All bathymetric measurements were converted into meters from mean lower-low water (MLLW). Conversion of bathymetry data from NGVD29 datum to MLLW was performed using:

$$MLLW = NGVD29 + 0.408(m) \quad (3.1)$$

After the conversion, the bathymetry of the model domain is shown in Figure 3.1 .

3.2 Model Grid

Figure 3.2 shows the grids in the model domain. This curvilinear grid is generated by CoastGrid (Shi, 2006) developed by Dr. Fenyan Shi at University of Delaware. The grid generation program is based on Brackbill’s adaptive grid generation method (Brackbill and Saltzman, 1982). The advantage of the CoastGrid is its adaptive character which can make the grids fit the boundary well. In this model domain, there are many rivers, among which the Indian River is the biggest one. The grids fit the rivers pretty well with finer cells. The grids contain 68×58 cells including land cells and water cells. Figure 3.2 shows totally 658 water cells in the model domain. The cells’ size changes gradually in the bay systems. The highest horizontal resolution is around 60 *m*, while the lowest resolution is more than 800 *m*. Vertical resolution is provided by 10 sigma levels, which gives enough vertical resolution to resolve the quantities of interest for the present research.

3.3 Model Settings

Model runs use a split time: 3 *sec* for the depth-averaged mode and 30 *sec* for the depth-resolving mode. The external time step is set below the upper bound imposed by the barotropic CFL criterion. Bottom friction follows the quadratic drag law; the bottom friction coefficient C_D has been set to 0.0039. The upwind difference algorithm is chosen not only because of its positive definite salinities, temperatures, and DO, and the most computationally efficient of any of the advective schemes, but also because it best simulates the observed data.

The simulations have been initialized with homogeneous water with a temperature of 4°C, salinity of 30 *ppt*, and DO of 8 *mg/l*.

3.4 Indian River Inlet Boundary Condition

The USGS tidal data at the Indian River Inlet were available near Bethany Beach, DE (Station# 1484683, 38° 27’N, 75° 4’W). Figure 3.3 shows the positions

of Indian River Inlet and Indian River at Rosedale Beach. The latter will be used for the model calibration and comparison. The tidal height was measured in feet every 15 minutes and referenced to the NGVD29. The data were converted to the time series input required by ECOMSED. For a specific year's run, the tides at the Indian River Inlet force the water to flow through the Inlet, and change the surface elevation inside the bays periodically.

The temperature and salinity open boundary conditions at the inlet are specified from the available field database, where the data are sparse. The database will be detailed later, which will be used to calibrate the models.

3.5 Freshwater Discharge

The Inland Bays are connected with a number of streams which continuously feed the Bays with freshwater inflow, shown in Figure 3.4. This freshwater boundary conditions were originally developed by J. E. Edinger Associates, Inc. (JEEAI) for use in Generalized Environmental Modeling System for Surfacewaters (GEMSS). The GEMSS's boundary conditions provide the time series data including volume flow rate (m^3/s), temperature, salinity, and DO for all these streams. The time frequencies are different for these streams. Therefore a linear interpolation has been applied to make all these boundaries have the same time series.

3.6 Meteorological Data

The atmospheric boundary conditions are used for air-sea interaction. The NCDC provided the most complete database of historical meteorological data within the vicinity of the Inland Bays. The closest station that contained a complete database is located in Salisbury, Maryland. The data is converted into the format required by ECOMSED from GEMSS's format. The meteorological data are used in the water surface heat exchange and the wind stress acting on the water surface.

For the RCA model, the solar radiation data are used. A unit conversion ($1\text{watt}/m^2 = 2.3885 \times 10^{-5}\text{langley}/s$) needs to be implemented to get the total daily solar radiation ($\text{langley}/\text{day}$) required by RCA. The fraction of daylight is calculated from the sun rise-set table from Astronomical Applications Department of U.S. Naval Observatory.

3.7 Model Systems Coupling

In this study, the two models are coupled externally. First, the ECOMSED runs with the specific input conditions, and the hydrodynamic information is stored at specific intervals in a file for the desired periods. Here, 1 *hr* is chosen for a whole year's run. The surface elevation, temperature, salinity, volume transport and dispersion as a time history are stored in the unformatted file, `gcm_tran`. The grid segmentation and bathymetry information are stored in the unformatted file, `gcm_geom`. If the wet grid only option is chosen, an unformatted file, `wet_grid` will be output, and only the wet grid information will be stored in `gcm_geom` and `gcm_tran`. The RCA will recognize these unformatted input files, and input the required information for the desired periods as was set from `gcm_tran`. This procedure completes the model systems coupling.

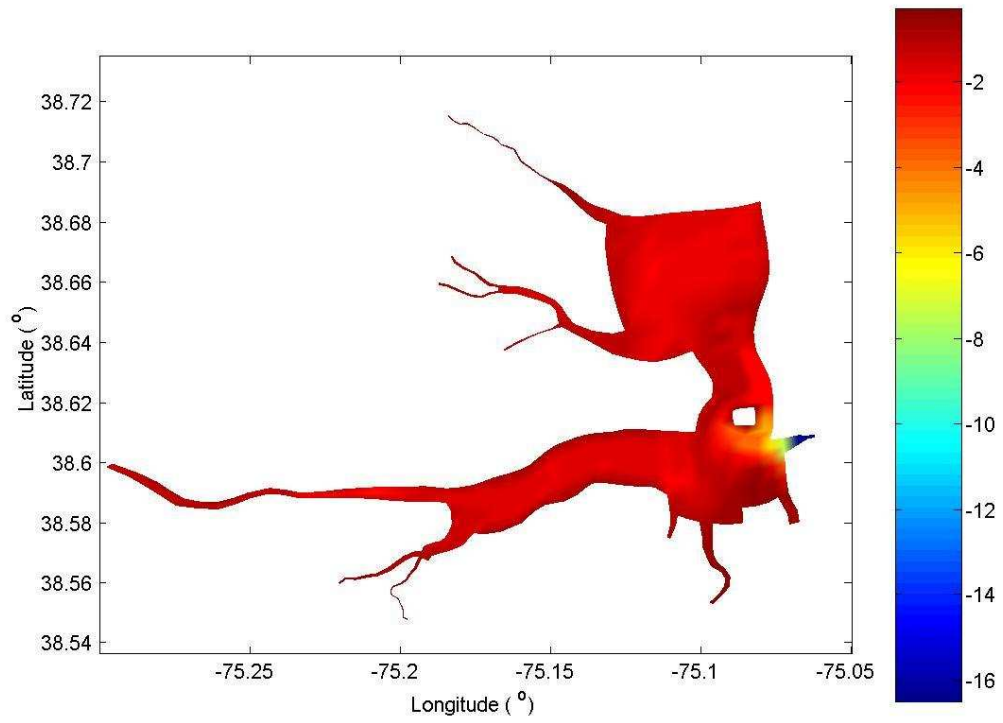


Figure 3.1: Bathymetry in the model domain. (Unit in color bar is *m*)

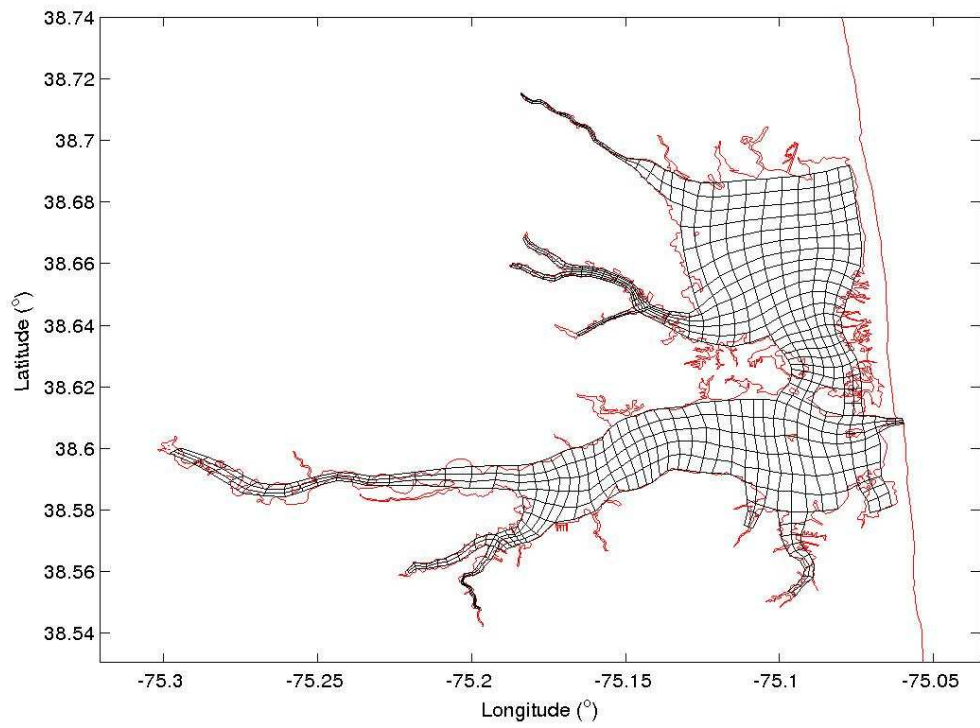


Figure 3.2: Grid cells in the model domain.

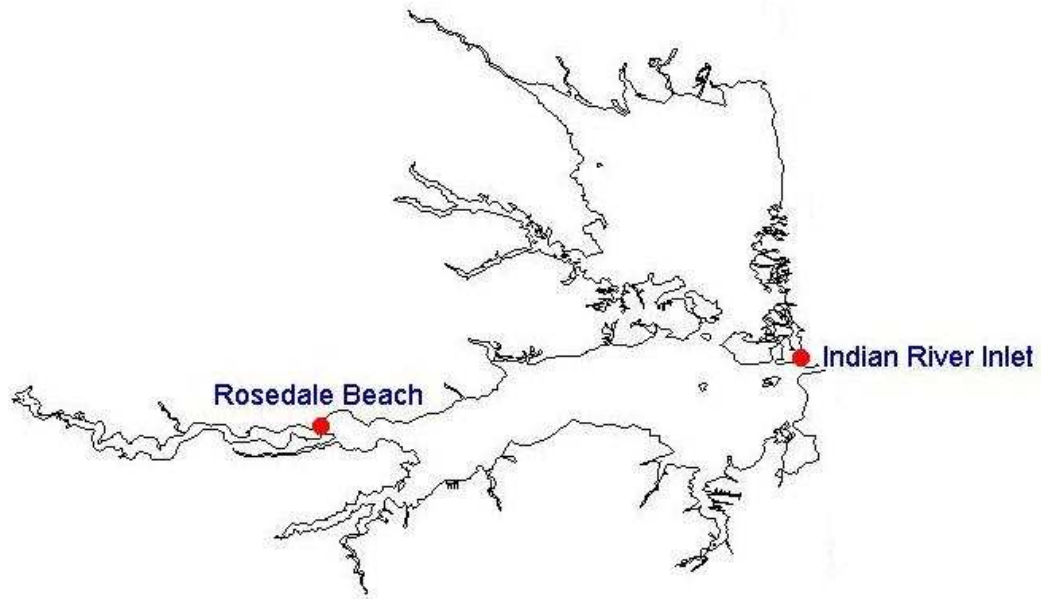


Figure 3.3: Locations of the two USGS tidal stations in Delaware Inland Bays.

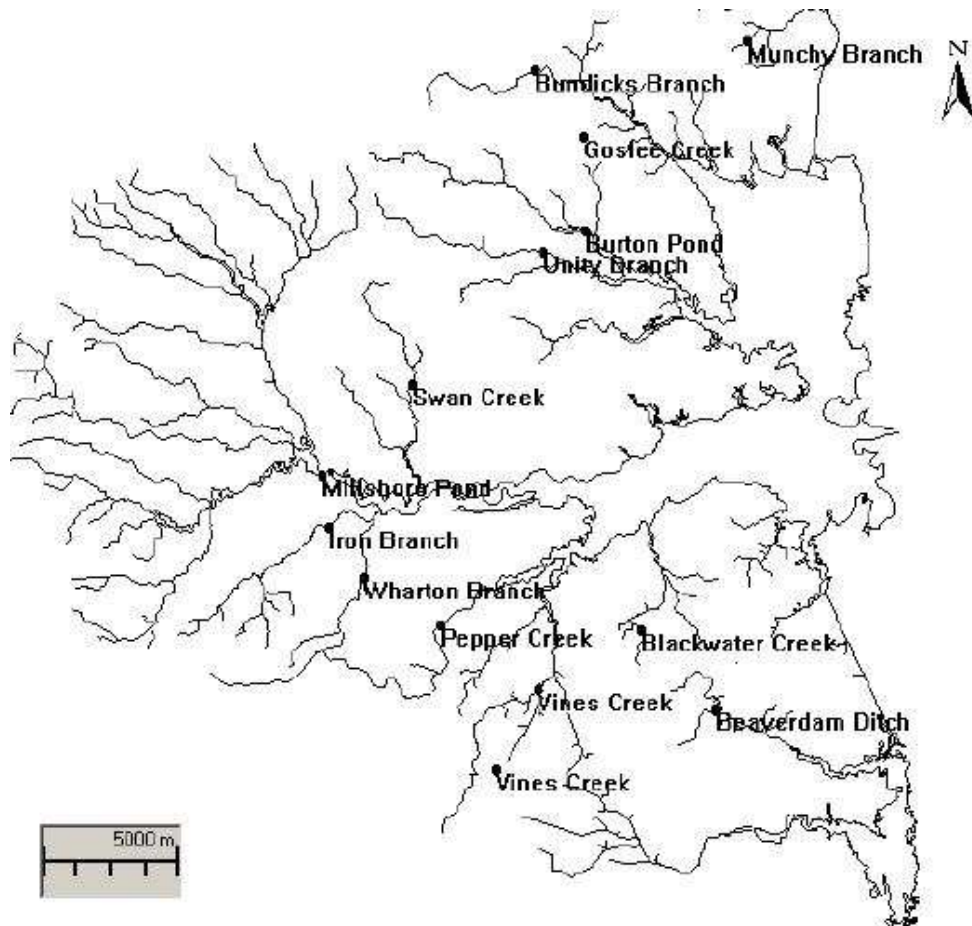


Figure 3.4: Distribution of streams that link to Delaware Inland Bays (JEEAI, 2004).

Chapter 4

MODEL CALIBRATION AND EVALUATION

In this chapter, the hydrodynamic model and water quality model are calibrated sequentially with the in situ data. One whole year's simulation is implemented, and the model results are calibrated with tidal station data and water quality data. The calibration processes involve adjustments of the model parameters to represent the hydrologic process and water quality reaction process, until an acceptable agreement between simulated results and field measurements is achieved.

4.1 Data

The data used in this study for calibration are provided by Division of Water Resources, DNREC. The formatted database contains different data sources. In order to ensure the calibration's accuracy, more than one data source are retrieved. Two integrated years' data sources are chosen for the study in this thesis, which are years 1998 and 1999. One is for the calibration in this chapter, the other is for the validation in the next chapter.

The tide height measurements are from the USGS tide stations. Only one station is located within the model domain, which is Rosedale Beach at Indian River (station# 1484540, $38^{\circ} 35'N$, $75^{\circ} 13'W$, Figure 3.3). Tide heights are measured relative to NGVD29, so the conversion to MLLW is implemented by using Eq. (3.1).

EPA's STORET data source contains an extensive collection of environmental data in Delaware Inland Bays. DNREC provided a set of STORET output from April, 1997 through October, 1999 for 30 stations. Figure 4.1 shows station locations

in the Bays. The disadvantage of this database is that very few data are available during a calendar year for each station.

Water quality data for the State's Pfiesteria monitoring program was obtained by Dr. Edythe Humphries of DNREC for 1998 through 2000. Figure 4.2 shows the distribution of the stations. This data source provides more data than STORET for each station on average.

Sampling surveys were conducted in the Indian River for Conective's Indian River Power Plant 316(a) Demonstration. The surveys were conducted from April through December, 1998 and March through October, 1999 to provide water quality samples. The stations are only located along and near the Indian River, as shown in Figure 4.3. There are only 8 stations, but each of them provides much more data than the previous two data sources.

Most of the stations, spreading over the entire Inland Bays, are chosen from these three data sources to compare with the model results.

4.2 Hydrodynamic Model Calibration

The hydrodynamic calibration is performed prior to the water quality calibration. The calibration process involves adjustments of the model parameters in order to achieve the acceptable agreement between simulated results and field measurements. In this chapter, the data of year 1998 have been chosen to calibrate the models.

The calibration process for the hydrodynamic model includes comparing with surface elevation, temperature, and salinity data. Chapter 3 has described the model settings and provided some model parameters. In this study, since we only care about the dynamic characteristics of water body, the sediment transport is not considered. The bottom friction coefficient is an important one to calibrate the shallow water simulation. The coefficient has been set to 0.0039, which is bigger than the

standard value. This value best matches the model with observed tidal characteristics at the USGS station. The tidal amplitude is not sensitive to the bottom friction within the given range, and only decreases a little with the high bottom friction. All the other coefficients are set to the standard value mainly because they are not sensitive to this study. Three advection algorithms are available for use in ECOMSED: central difference, upwind difference, and the Multidimensional Positive Definite Advection Transport Algorithm (MPDATA). These different advective schemes have been tested and compared with the observed data. The upwind difference algorithm has shown better agreement with the salinity data in the Bays than the other algorithms. Upwind difference is only first-order accurate, but it is stable and does not get negative salinity, temperature, or other concentrations. An advantage of upwind transport is the most computationally efficient of any of the advective schemes. Since there are no field data to be compared with for the first 90 days of the year, these 90 days works as the spin-up period for the model initiation, which is long enough to reach quasi-steady state in the Bays. Therefore, the effect of initial condition is removed no matter what it is.

The tidal elevation inside the Inland Bays is controlled by the astronomical tide through the Indian River Inlet from the Atlantic Ocean. Figure 4.4 shows the time series comparison between the model prediction and the USGS gage data at Rosedale Beach. It can be seen that the model simulates the astronomical tide well except some time in the summer, when the model and data are not in phase. This discrepancy is puzzling since the M_2 tide is dominant in this area, which has the fixed period 12.42 *hrs*. So, GEMSS's (JEEAI, 2004) simulated results have been obtained and compared with the model results as shown in Figure 4.5. It can be seen that the two model results are very similar, not only for the amplitude, but also for the phase. Therefore, the phase shift of the data during that time seems not correct. The success of tide simulation indicates the exchange between ocean

water and bay water is in effect, which is the basis for the other calibration.

Water temperature represents one of the most important physical characteristics of surface water systems. It affects both hydrodynamic and biogeochemical processes. Salinity is also important, which is controlled by the mixing of fresh water and salt water. To calibrate the temperature and salinity, 16 stations have been chosen for two reasons: (1) they are spread over the Inland Bays; and (2) they have the most data. GEMSS's results for these stations are also included as references if available. The temperature and salinity calibration results are shown station by station to evaluate the model results (Figures 4.6 to 4.21). For the temperature calibration, the model simulates the temperature well by successfully reproducing the seasonal variations for all the stations. Figures 4.22 to 4.24 also indicate that the model predicts the temperature well during the whole year. However, sometimes the model still underestimates the observed data at some stations in Indian River Bay, such as stations 3 and IRB-6. For the salinity, the model captures the general trend of salinity variations of the whole year. But at some stations, especially the ones of Conectiv's data, the model underestimates the salinity. This can be seen from the Figures 4.25 to 4.27 clearly. Also there exist some data points which are far from the model results. The discrepancies between model simulation and measured data are caused by a few reasons. First, the model is not as sensitive as the real data suggested. This is because, in the current model, freshwater input rates are in daily intervals, while the temperature and salinity inputs are very coarse based on the limited data. At some boundaries, there may be no data in a specific month. In order to obtain continuous boundary conditions in daily intervals, the data are interpolated according to the contiguous data. Second, some other effects are not included in the current model, which may affect the model results much spatially and temporally. For example, the precipitation can affect the salinity to some extent. Last, it is possible that the data are not correct under special circumstances,

such as instrument error. Since the model only underestimates the salinity near Indian River, it is likely that the freshwater influx there is poorly estimated. Therefore, the discrepancies between model and data are acceptable if they are within the range of error. Moreover, the model results are very close to the GEMSS's results. Generally speaking, the model successfully simulates the variations of temperature and salinity over the whole area.

Some statistical parameters are calculated for data analysis in this study, such as ME, MAE, RE, and RMSE (Wang, 2005). The definitions of these parameters are given below:

1) Mean Error (ME)

$$ME = \frac{1}{N} \sum_{i=1}^N (M_i - O_i) \quad (4.1)$$

where N: number of field observations; M: model results; O: field observations.

2) Mean Absolute Error (MAE)

$$MAE = \frac{1}{N} \sum_{i=1}^N |M_i - O_i| \quad (4.2)$$

3) Relative Error (RE)

$$RE = \frac{\sum_{i=1}^N |M_i - O_i|}{\sum_{i=1}^N |O_i|} \quad (4.3)$$

4) Root Mean Square Error (RMSE)

$$RMSE = \sqrt{\frac{1}{N} \sum_{i=1}^N (M_i - O_i)^2} \quad (4.4)$$

These different errors can evaluate the model performance from different point of view, and be the criteria for the model calibration. In this study, the mean error is subtracted from the model result before calculating the other errors.

Tables 4.1 to 4.3 present the statistical parameters for surface elevation, temperature, and salinity. It can be seen from the tables that the temperature results

have a better agreement than salinity. For the tidal elevation, the hourly results have been compared with measured data. Since some time series data are not in phase, the statistical parameters are a little bigger based on the small surface elevation. Since the data may have problems, the error is still acceptable. The statistical parameters (ME and RMSE) for temperature and salinity along the Bays are shown in Figures 4.28 and 4.29 respectively. Figure 4.28 shows the model underestimates the temperature slightly in Indian River; while in Indian River Bay and Rehoboth Bay, there is not any obvious trend. However, the RMSE is relatively uniform in the Bays after subtracting the ME. Figure 4.29 shows the model underestimates the salinity in Indian River and Indian River Bay, and overestimates at station IWC-2; the model reproduces the salinity well in Rehoboth Bay. The RMSE of salinity is not uniform in the Bays. In general, the hydrodynamic model has simulated the physical characteristics well, and it will provide a solid basis for later water quality calibration.

4.3 Water Quality Model Calibration

The calibrated hydrodynamic model results have been stored hourly for the year 1998, and used as the dynamic environment to drive the water quality model. Salinity is included in this model to verify that transport of the hydrodynamic model is transferred to the water quality model properly. Since DO is the primary concern of this study, the calibration of DO simulation is the upmost issue for the water quality model.

As described in chapter 2, photosynthesis, respiration, and reaeration are the main source/sink terms in the equation of mass conservation for DO. The parameters that control these three processes are calibrated for the water quality model. The maximum photosynthesis rate ($gC/m^2 - d$), P_m , respiration rate ($gC/m^2 - d$), R_T , and reaeration rate (d^{-1}), k_a refer to the rates at $20^\circ C$ respectively. The real reaction rates will be calculated based on the temperature at the simulation time. One of the

reaeration formulae used in streams and rivers, O'Connor-Dobbins formula (Chapra, 1997) has been chosen in this study,

$$k_a = 3.93 \frac{U^{0.5}}{H^{1.5}} \quad (4.5)$$

where H = mean depth (m), and U = mean velocity (m/s). These two variables can be estimated from the hydrodynamic model results directly. In the current water quality model, the rate of photosynthesis is a function of the light energy, $I(t)$. In some other studies, the photosynthesis can be estimated from plant biomass measurements (Chapra, 1997). The plant photosynthesis is directly proportional to concentration of plant biomass ($mgChla/m^3$). Therefore, it is expected that the maximum photosynthesis rate is proportional to the concentration of chlorophyll. The plant respiration rate is also proportional to the concentration of chlorophyll (Chapra, 1997). The average daily photosynthesis rate ($gC/m^2 - d$), P_{av} is

$$P_{av} = P_m \frac{2f}{\pi} \quad (4.6)$$

where f is the fraction of daylight. At $20^\circ C$, the oxygen production ($gO/m^3 - d$), at optimal light levels is

$$P_s = r_{oa} G_{max} a \quad (4.7)$$

where r_{oa} = oxygen generated per unit mass of plant biomass produced ($gO/mgChla$), G_{max} = maximum plant growth rate (d^{-1}), and a = concentration of plant biomass ($mgChla/m^3$). Base on Eqs. (4.6) and (4.7), the average daily photosynthesis rate in this study can be expressed as,

$$P_{av} = \frac{2fH}{\pi r_{oc}} r_{oa} G_{max} a \quad (4.8)$$

where $r_{oc} = 2.67 gO/gC$. This equation shows the average daily photosynthesis rate is proportional to the concentration of chlorophyll. Based on the distribution of chlorophyll from DNREC database, the model domain is divided into several regions

as shown in Figure 4.30. The regions include high primary production parts in rivers and creeks, low primary production part near Indian River Inlet, and Rehoboth Bay and Indian River Bay in between. P_{av} and R are calibrated using mean water depth and yearly averaged chlorophyll data in each region. The respiration rate is calibrated according to the average daily photosynthesis rate. Table 4.4 provides the calibration parameters, P_{av} and R , based on the concentration of chlorophyll in each region. Figure 4.31 shows the linear relation between P_{av}/R and chlorophyll. The black lines in the figure are decided if 2 m is used as the mean water depth of the entire Bays.

The time series calibration results for DO concentration are shown station by station (Figures 4.32 to 4.35). The stations are same as those used for the hydrodynamic model calibration. It can be seen that the model captures the trend of DO variation during the whole year. Nearly all the field data are within the range of model simulations at different stations. The data show that DO concentrations are always lower in the morning than that in the afternoon. The model successfully simulates this diurnal DO variation at all stations during the year, which has the minimum value at sunrise and maximum value at sunset. As shown in Table 4.5, at most of the stations, the differences between the model and data are small. But at stations 1, 2, and IP-1, the errors are comparatively large. These discrepancies can also be seen in Figures 4.36 to 4.38; at these stations, the model-data points scatter far from the lines. These three stations are all in the shallow river regions close to the boundary sites. Figure 4.39 shows the model slightly overestimates the DO in Indian River and underestimates in Rehoboth Bay. The RMSE at station 1 is larger than the other stations evidently. Since the data for the current model boundary conditions are very limited, sometimes even in a monthly frequency, the current model is not sensitive enough to reproduce the DO variations all the time in this area. Using the reactions of photosynthesis and respiration, the model simulates the

DO diurnal swings all over the Bays. In the river area, due to the high concentration of chlorophyll, which means the high activity of biota, the model simulates the large diurnal DO swings in summer and fall, causing the phenomena of super-saturation in the daytime and hypoxia at night and in early morning.

4.4 Summary

Both the hydrodynamic model and water quality model are calibrated and predict reasonable results all over the Inland Bays. The hydrodynamic model reproduces the seasonal variation of temperature very well. In the year 1998, mean water temperature in the Bays is $26.1^{\circ}C$ and standard deviation is $2.0^{\circ}C$ during the summer (June, July, and August); in winter (December, January, and February), mean water temperature is $8.2^{\circ}C$ with a standard deviation of $3.0^{\circ}C$; mean water temperatures in spring and fall are in between, which are $16.0^{\circ}C$ and $17.1^{\circ}C$ respectively, and the standard deviations are $4.2^{\circ}C$ and $6.4^{\circ}C$, respectively.

The salinity in the Bays is not as uniform as temperature. Salinity is sensitive to the freshwater discharge. The water near the river is fresher, such as stations 1 and IP-1, while the water near the inlet is saltier, such as station I-1. There is a significant longitudinal salinity gradient in the Indian River Bay. The salinity in the Indian River Bay has a wide range of diurnal variation than in Rehoboth Bay due to the sharp mixing between the sea water and fresh water.

The water quality model successfully simulates the large diurnal DO variations in summer and fall. In other seasons, the diurnal DO range is small, which is very close to the saturation level. During the summer and fall, there exists much time that the DO concentration is below 4 mg/l , especially in the Indian River and Pepper Creek. This hypoxia phenomenon really affects the activity of the fish as well as decreases some kind of species.

Table 4.1: Statistical parameters for tide (m) calibration (year 1998)

	Rosedale
ME	-0.050
MAE	0.099
RE	0.125
RMSE	0.152

Table 4.2: Statistical summary for temperature ($^{\circ}C$) calibration (year 1998)

	1	2	3	6	7	8	I-1	IRB-5
N	22	23	21	23	23	22	20	21
ME	-1.054	-1.195	-1.132	-0.261	0.113	0.428	0.732	-0.296
MAE	0.944	1.041	1.617	1.236	1.261	1.283	0.705	0.665
RE	0.042	0.048	0.070	0.056	0.058	0.061	0.032	0.026
RMSE	1.235	1.383	1.943	1.508	1.560	1.638	0.997	0.818
	IRB-6	IP-1	RB-1	RB-5	RB-7	IWC-2	306091	306121
N	23	21	19	19	11	20	4	4
ME	-1.500	-0.720	0.109	0.130	-0.898	-0.734	1.500	2.129
MAE	0.879	0.723	0.827	0.751	1.481	0.754	0.980	0.972
RE	0.035	0.028	0.033	0.030	0.059	0.030	0.055	0.058
RMSE	1.207	0.892	1.055	1.010	1.875	0.898	1.215	1.136

Table 4.3: Statistical summary for salinity (ppt) calibration (year 1998)

	1	2	3	6	7	8	I-1	IRB-5
N	22	23	21	23	23	22	20	21
ME	-1.390	-2.322	-2.388	-1.692	-2.828	-2.559	-0.310	-1.343
MAE	1.418	1.081	0.920	0.986	1.214	1.068	0.349	1.467
RE	0.082	0.051	0.039	0.040	0.045	0.037	0.012	0.063
RMSE	2.615	1.421	1.204	1.330	1.517	1.279	0.457	1.884
	IRB-6	IP-1	RB-1	RB-5	RB-7	IWC-2	306091	306121
N	23	21	19	19	11	20	4	4
ME	-1.516	-0.764	0.076	-0.179	-0.311	1.563	0.437	-1.306
MAE	1.336	2.001	1.145	1.063	1.060	1.727	1.218	1.835
RE	0.059	0.096	0.041	0.038	0.037	0.068	0.044	0.065
RMSE	1.700	2.926	1.490	1.354	1.390	2.786	1.520	2.226

Table 4.4: Calibration parameters for RCA model in the year 1998 (Unit of chlorophyll is $\mu g/l$; units of both photosynthesis rate and respiration rate are $gC/m^2 - day$)

	IRI	RB	WC	IRB	RAC
Chlorophyll	7.50	15.50	21.60	27.50	52.20
Pav	0.24	0.51	0.55	0.78	1.40
R	0.23	0.49	0.53	0.76	1.37

Table 4.5: Statistical summary for DO (mg/l) calibration (year 1998)

	1	2	3	6	7	8	I-1	IRB-5
N	22	23	21	23	23	22	20	21
ME	1.083	1.179	0.303	0.595	-0.064	-0.162	0.161	0.195
MAE	2.253	1.539	1.450	1.421	1.040	1.102	0.545	1.380
RE	0.268	0.238	0.216	0.192	0.140	0.146	0.082	0.183
RMSE	3.165	1.931	1.732	1.947	1.268	1.528	0.676	1.669
	IRB-6	IP-1	RB-1	RB-5	RB-7	IWC-2	306091	306121
N	23	21	19	19	11	20	4	4
ME	0.326	-0.397	-0.744	-0.481	-1.290	0.884	0.301	0.318
MAE	1.294	3.050	1.489	1.257	1.580	1.171	1.033	0.723
RE	0.189	0.330	0.226	0.191	0.183	0.177	0.145	0.105
RMSE	1.557	3.853	1.855	1.610	1.984	1.433	1.425	0.868

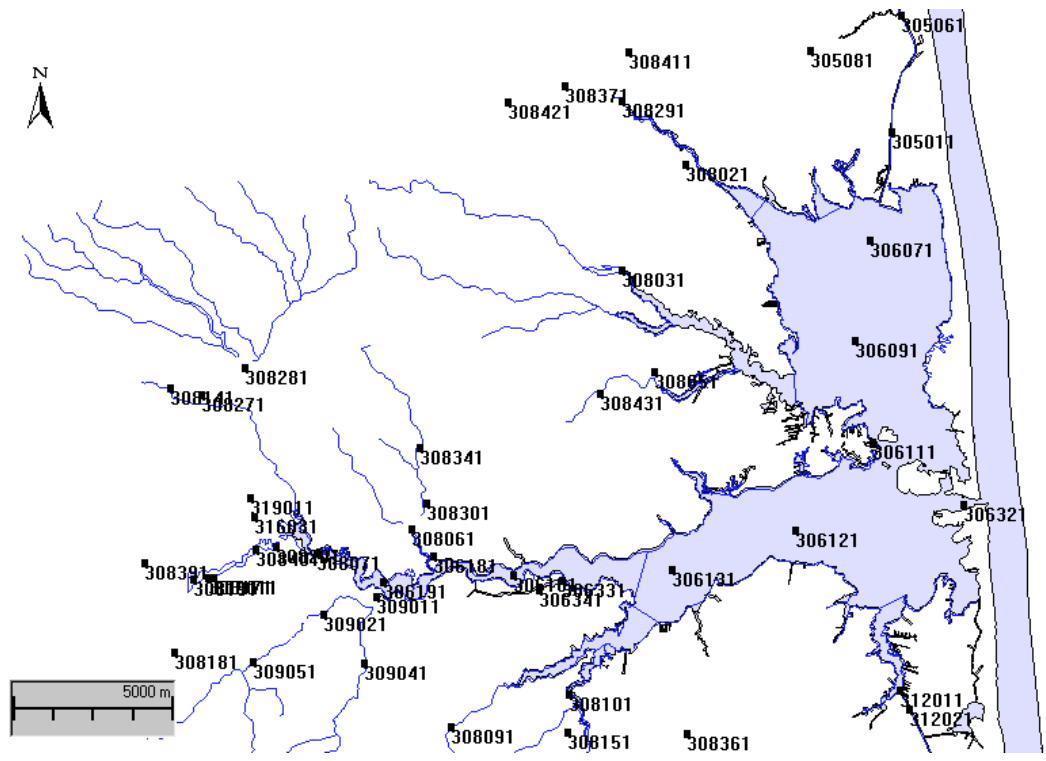


Figure 4.1: Station locations of EPA's STORET data in Delaware Inland Bays (from DNREC Database)

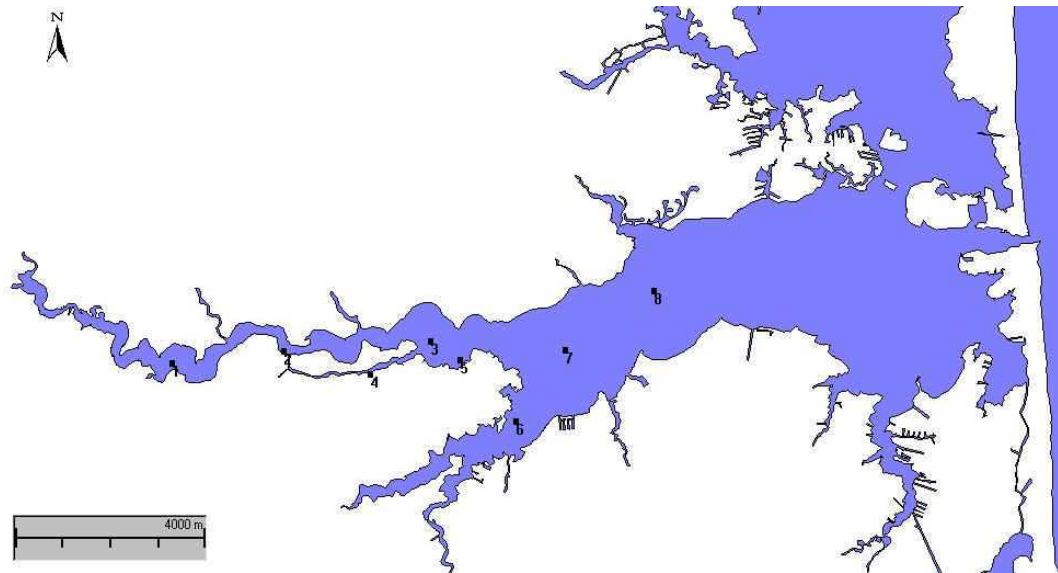


Figure 4.3: Station locations of Conectiv's instantaneous survey in Indian River Bay (from DNREC Database)

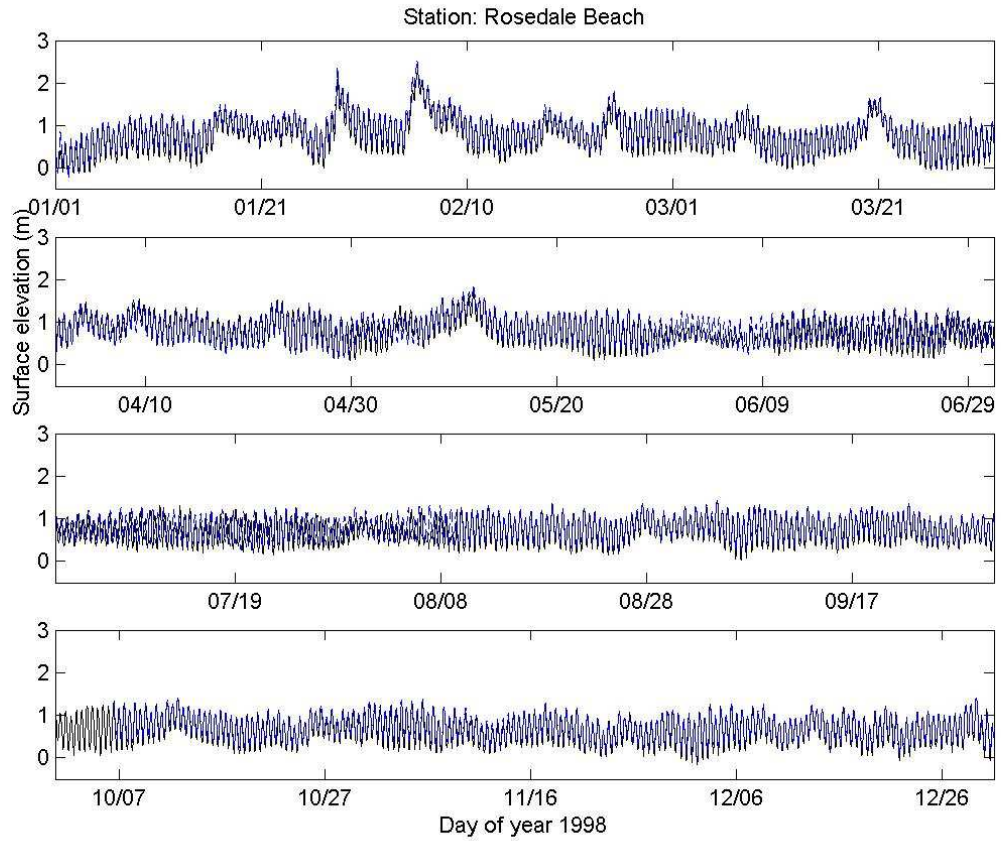


Figure 4.4: Tide calibration result at Rosedale Beach in Indian River Bay in the year 1998 (model results in black solid lines, and field data in blue dash lines)

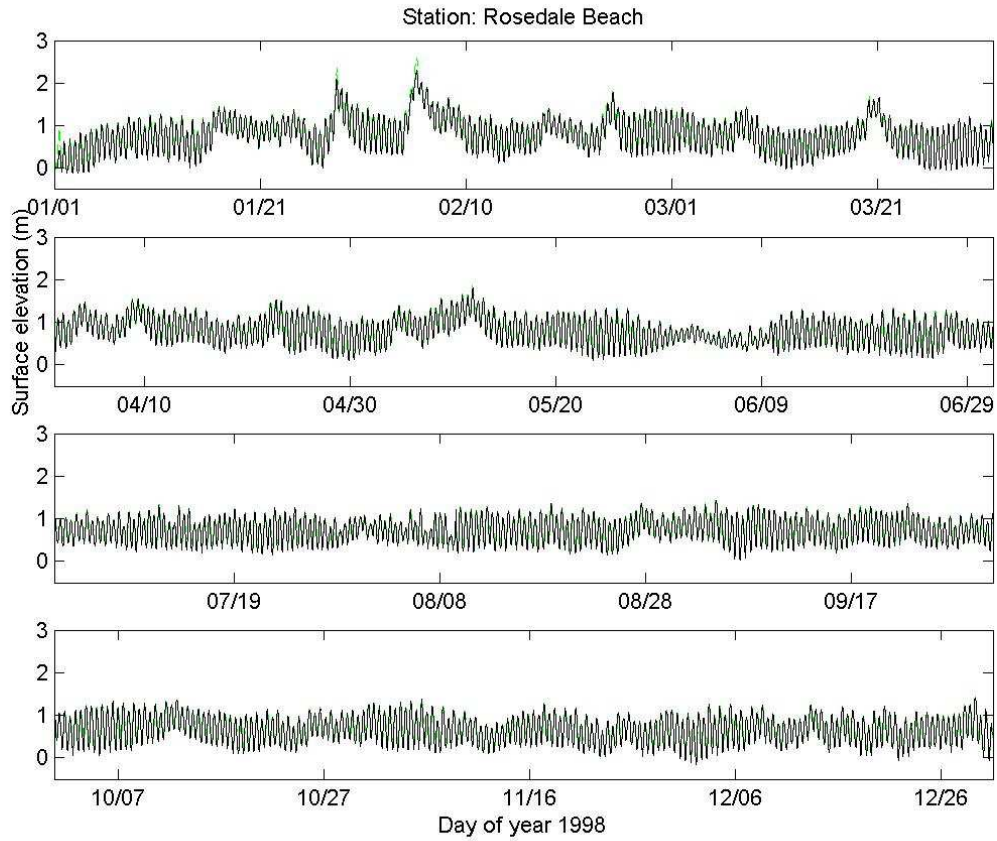


Figure 4.5: Tide calibration result at Rosedale Beach in Indian River Bay in the year 1998 (model results in black solid lines, and GEMSS in green dash lines)

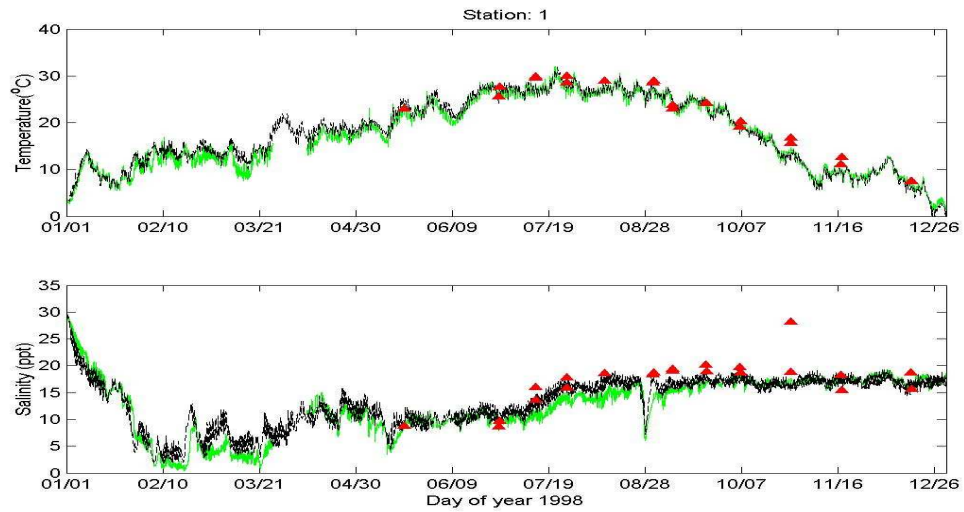


Figure 4.6: Temperature and salinity calibration result at Conectiv's station 1 in the year 1998 (model results in black dashed lines, GEMSS in green solid lines, and field data in red triangles)

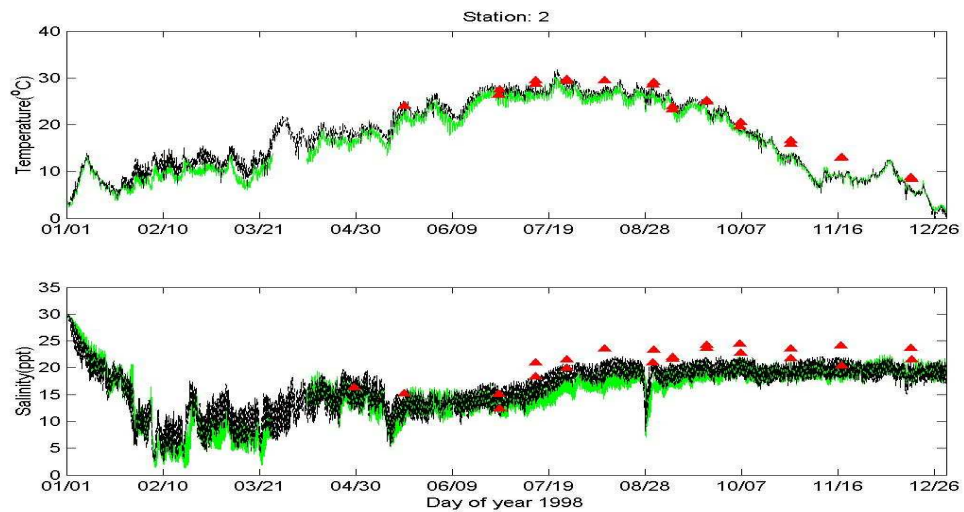


Figure 4.7: Temperature and salinity calibration result at Conectiv's station 2 in the year 1998 (model results in black dashed lines, GEMSS in green solid lines, and field data in red triangles)

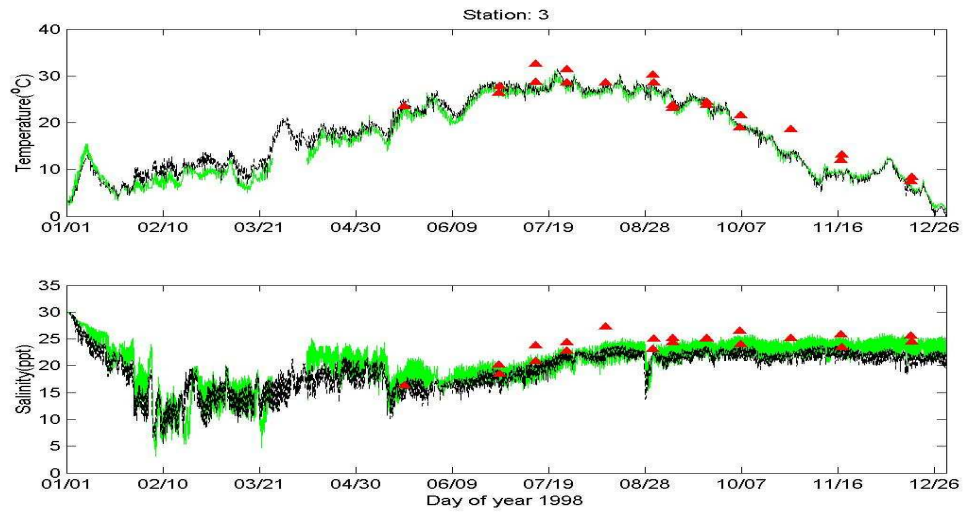


Figure 4.8: Temperature and salinity calibration result at Conectiv's station 3 in the year 1998 (model results in black dashed lines, GEMSS in green solid lines, and field data in red triangles)

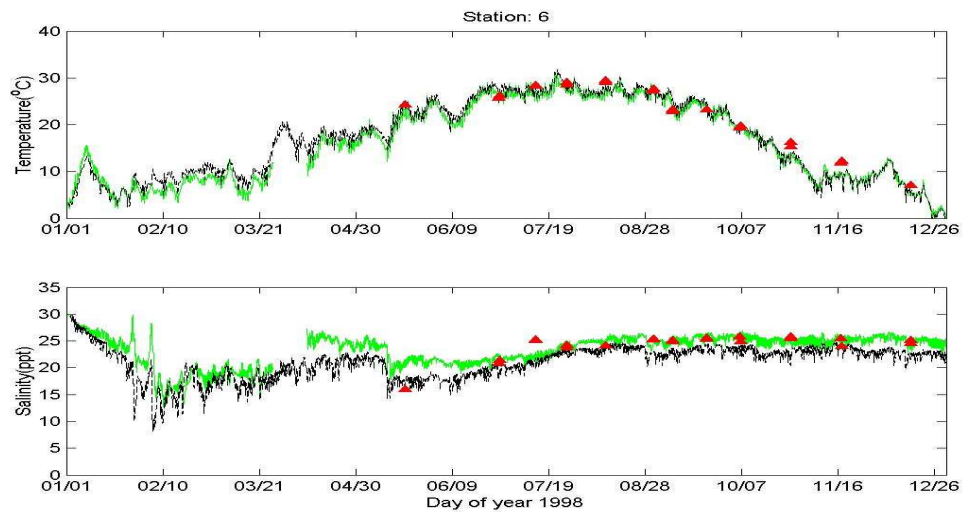


Figure 4.9: Temperature and salinity calibration result at Conectiv's station 6 in the year 1998 (model results in black dashed lines, GEMSS in green solid lines, and field data in red triangles)

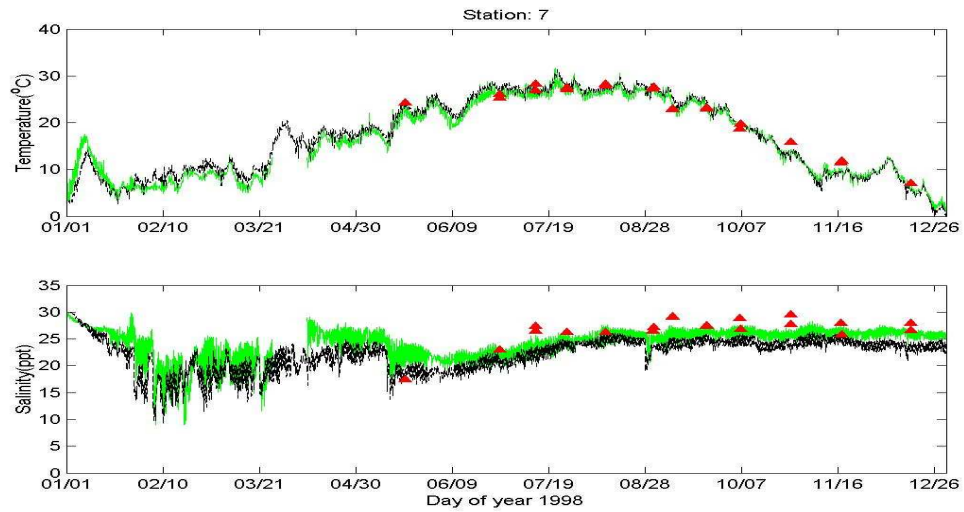


Figure 4.10: Temperature and salinity calibration result at Conectiv’s station 7 in the year 1998 (model results in black dashed lines, GEMSS in green solid lines, and field data in red triangles)

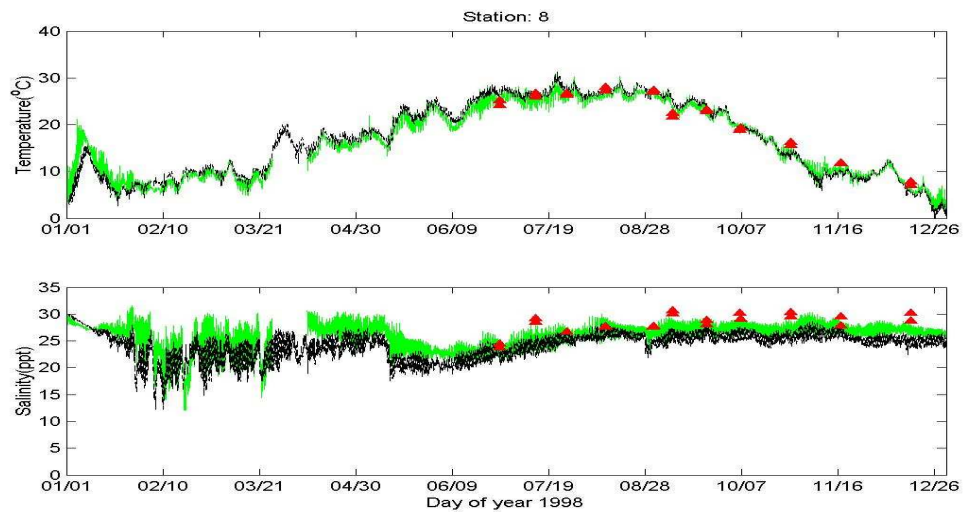


Figure 4.11: Temperature and salinity calibration result at Conectiv’s station 8 in the year 1998 (model results in black dashed lines, GEMSS in green solid lines, and field data in red triangles)

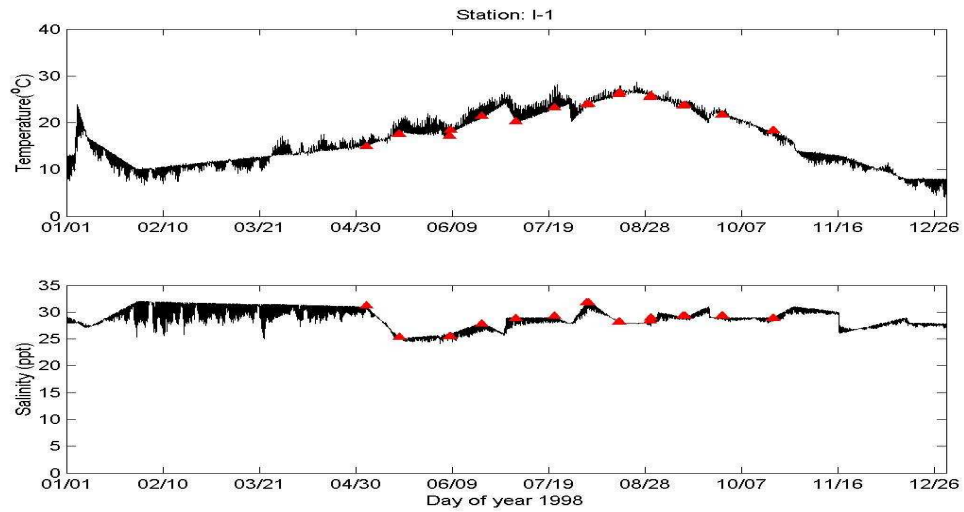


Figure 4.12: Temperature and salinity calibration result at State’s Pfiesteria station I-1 in the year 1998 (model results in black solid lines, and field data in red triangles)

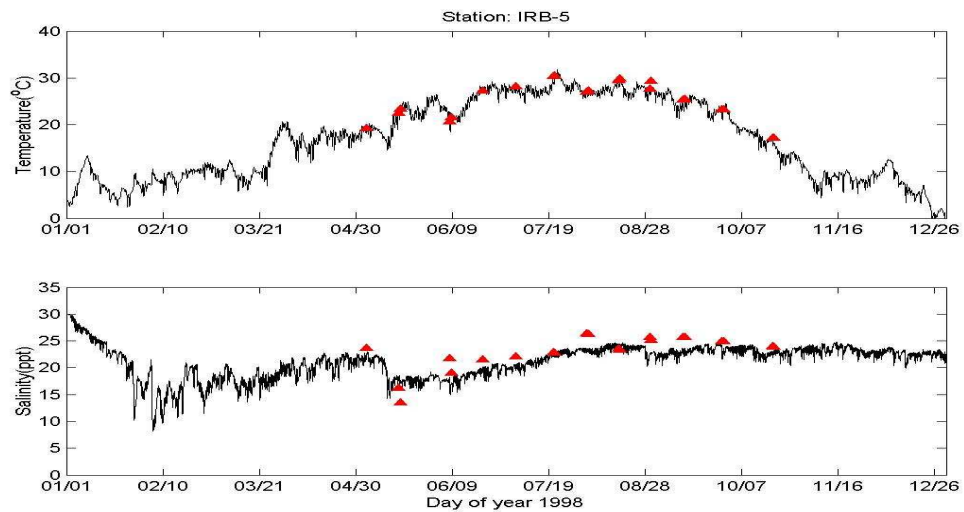


Figure 4.13: Temperature and salinity calibration result at State’s Pfiesteria station IRB-5 in the year 1998 (model results in black solid lines, and field data in red triangles)

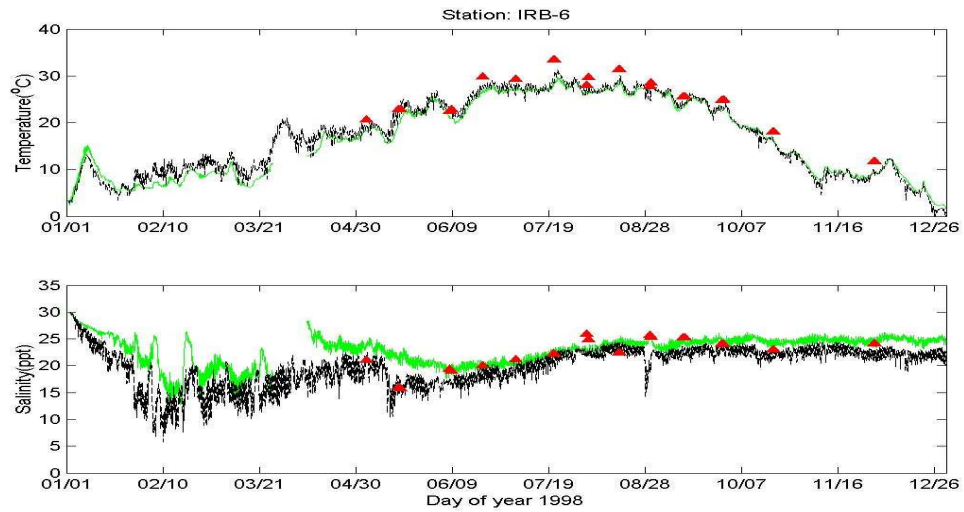


Figure 4.14: Temperature and salinity calibration result at State's Pfiesteria station IRB-6 in the year 1998 (model results in black dashed lines, GEMSS in green solid lines, and field data in red triangles)

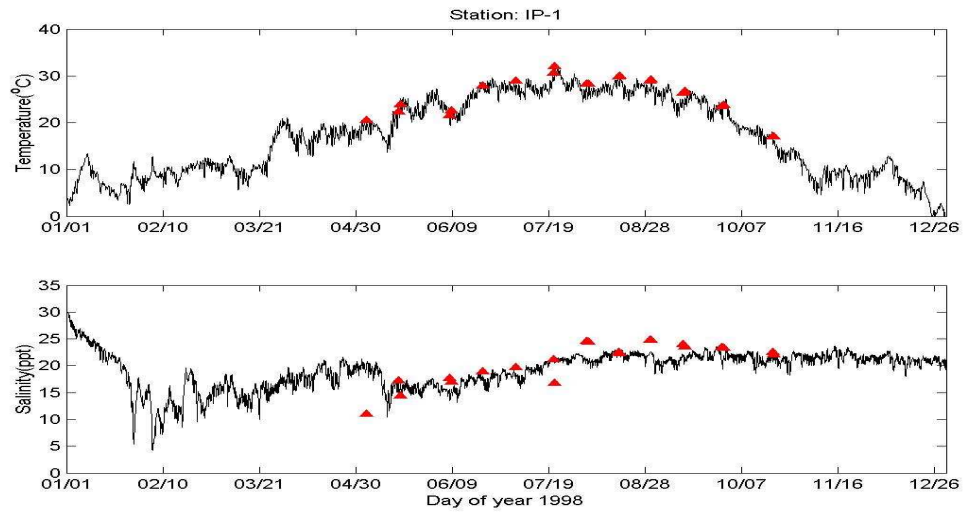


Figure 4.15: Temperature and salinity calibration result at State's Pfiesteria station IP-1 in the year 1998 (model results in black solid lines, and field data in red triangles)

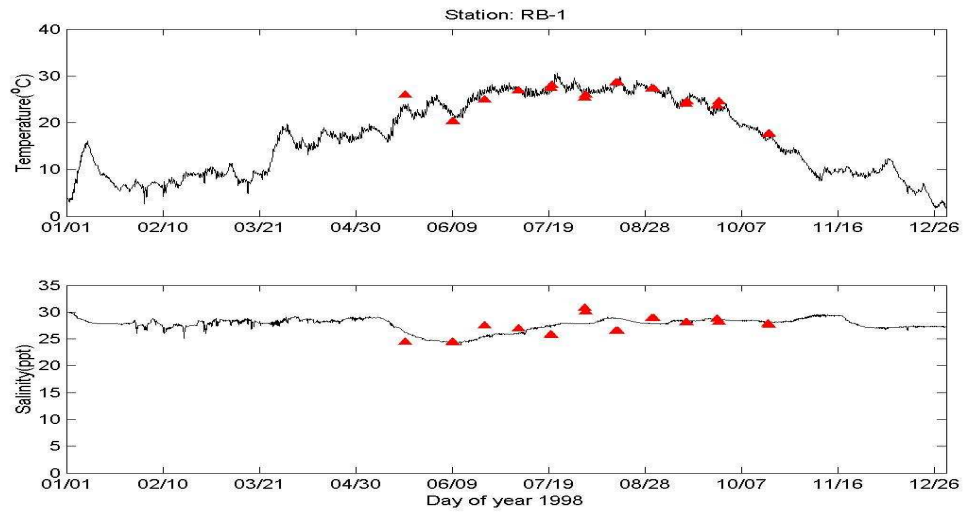


Figure 4.16: Temperature and salinity calibration result at State’s Pfiesteria station RB-1 in the year 1998 (model results in black solid lines, and field data in red triangles)

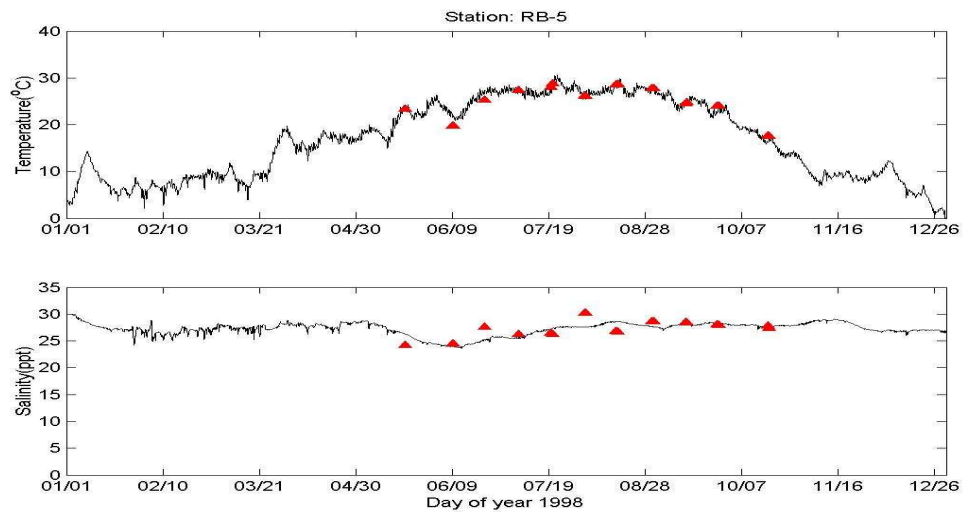


Figure 4.17: Temperature and salinity calibration result at State’s Pfiesteria station RB-5 in the year 1998 (model results in black solid lines, and field data in red triangles)

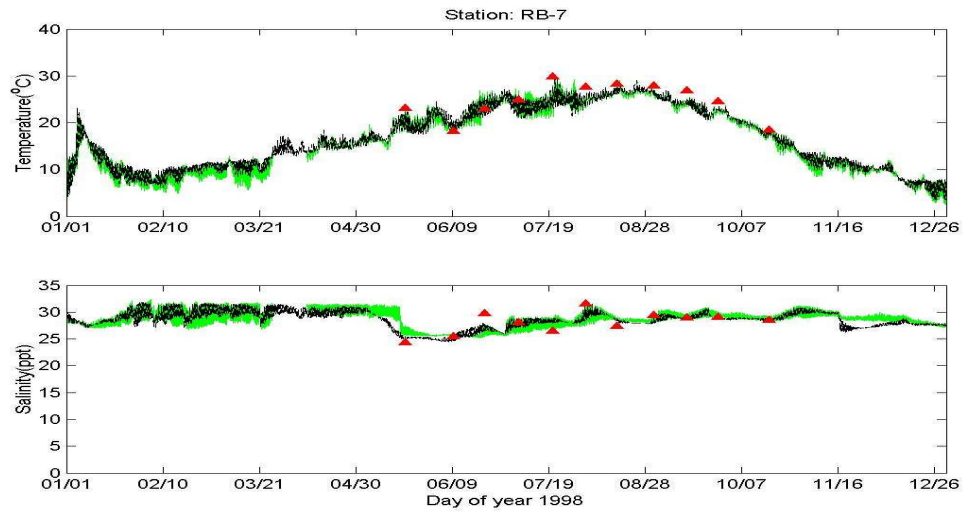


Figure 4.18: Temperature and salinity calibration result at State’s Pfiesteria station RB-7 in the year 1998 (model results in black dashed lines, GEMSS in green solid lines, and field data in red triangles)

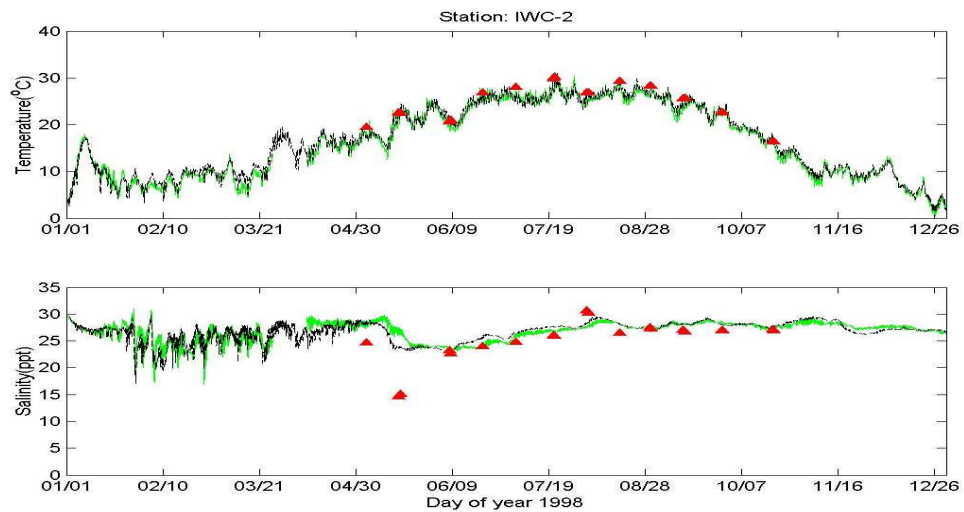


Figure 4.19: Temperature and salinity calibration result at State’s Pfiesteria station IWC-2 in the year 1998 (model results in black dashed lines, GEMSS in green solid lines, and field data in red triangles)

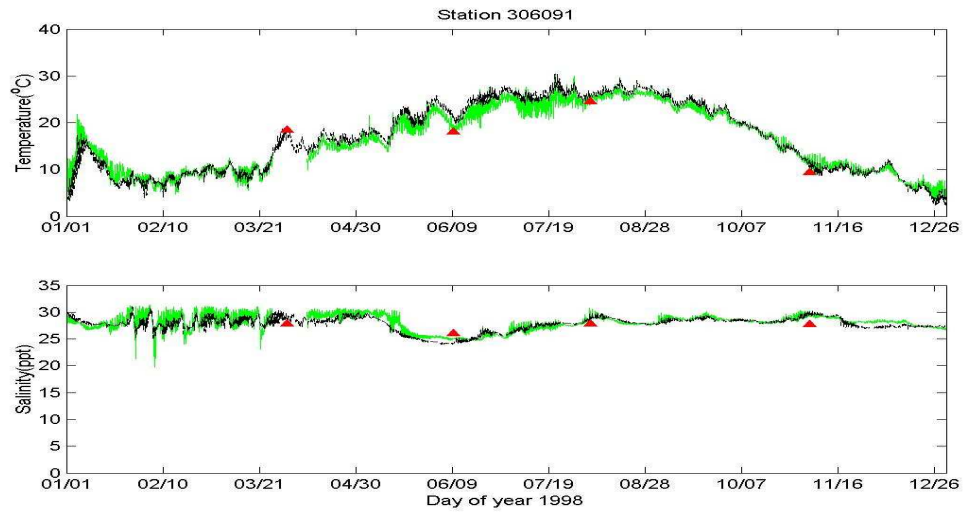


Figure 4.20: Temperature and salinity calibration result at STORET station 306091 in the year 1998 (model results in black dashed lines, GEMSS in green solid lines, and field data in red triangles)

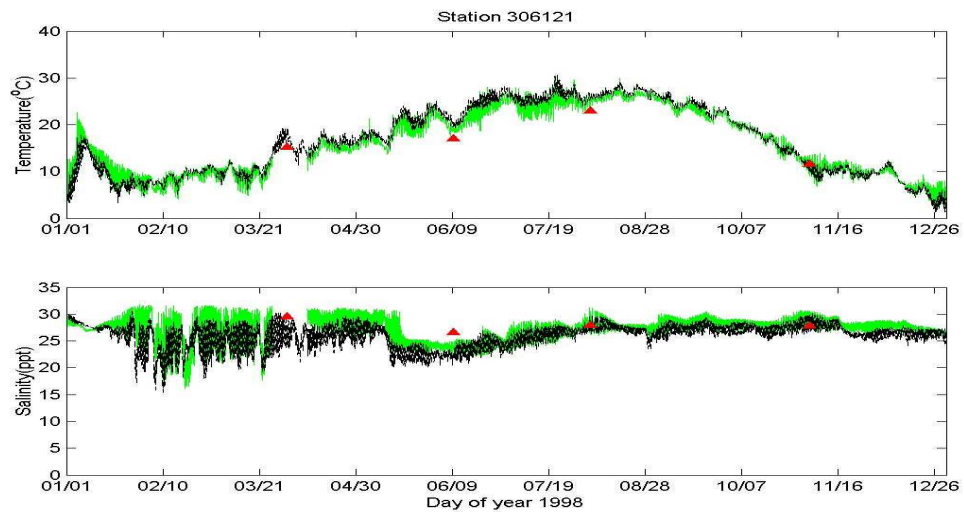


Figure 4.21: Temperature and salinity calibration result at STORET station 306121 in the year 1998 (model results in black dashed lines, GEMSS in green solid lines, and field data in red triangles)

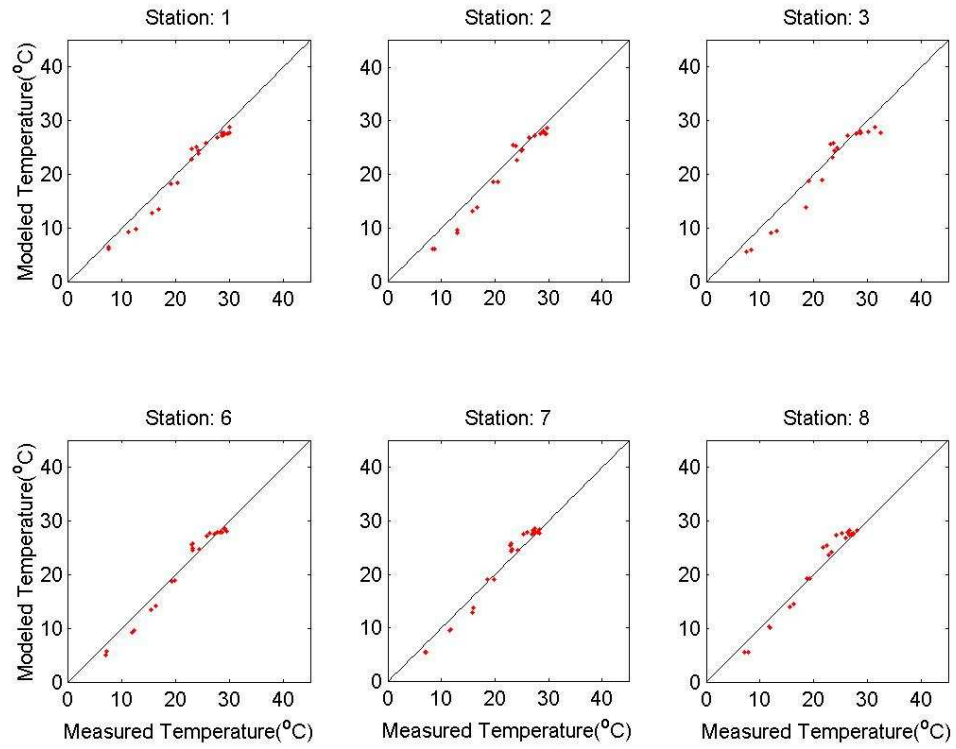


Figure 4.22: Scatterplot comparison between model and data for temperature in the year 1998 (part 1)

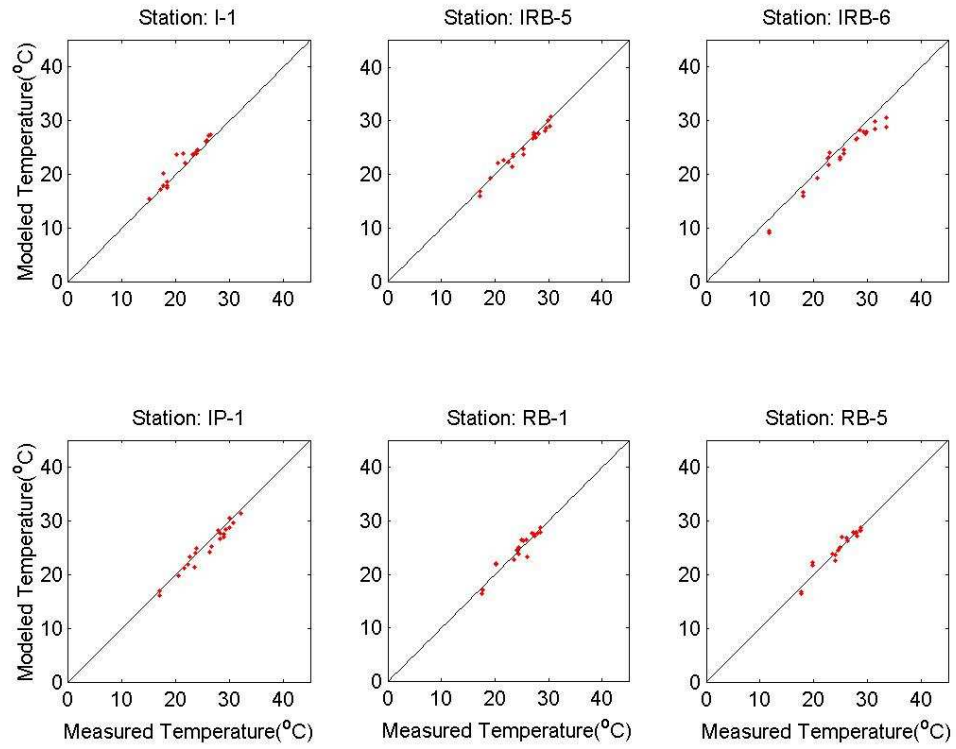


Figure 4.23: Scatterplot comparison between model and data for temperature in the year 1998 (part 2)

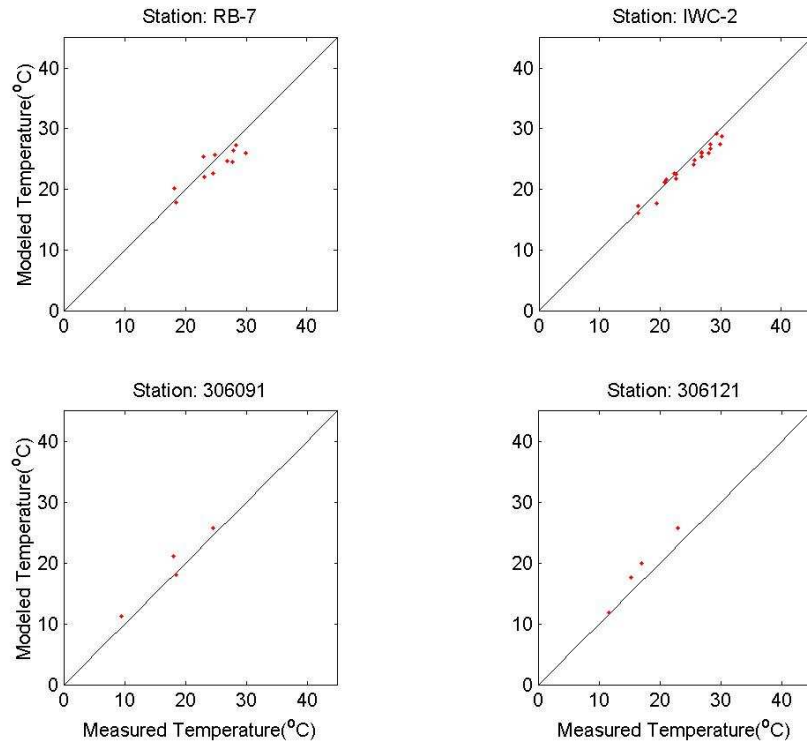


Figure 4.24: Scatterplot comparison between model and data for temperature in the year 1998 (part 3)

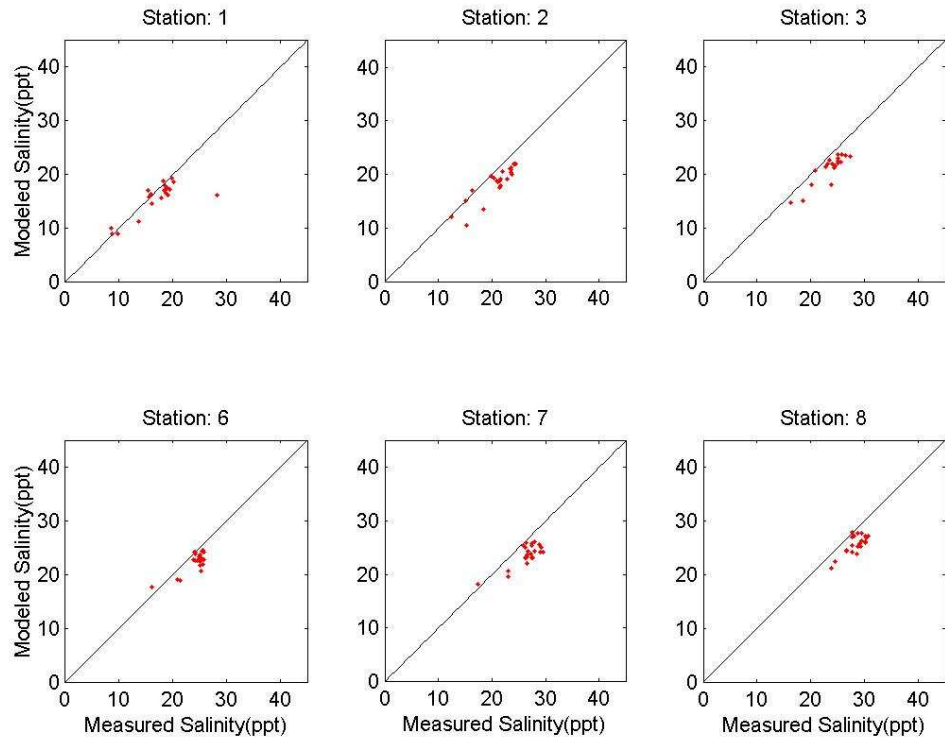


Figure 4.25: Scatterplot comparison between model and data for salinity in the year 1998 (part 1)

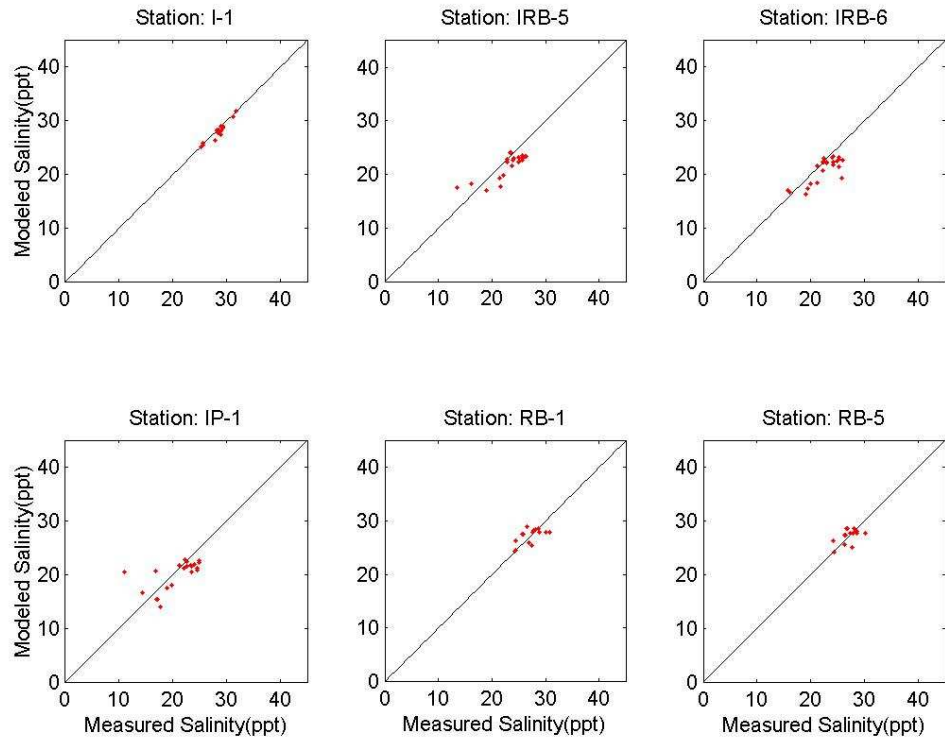


Figure 4.26: Scatterplot comparison between model and data for salinity in the year 1998 (part 2)

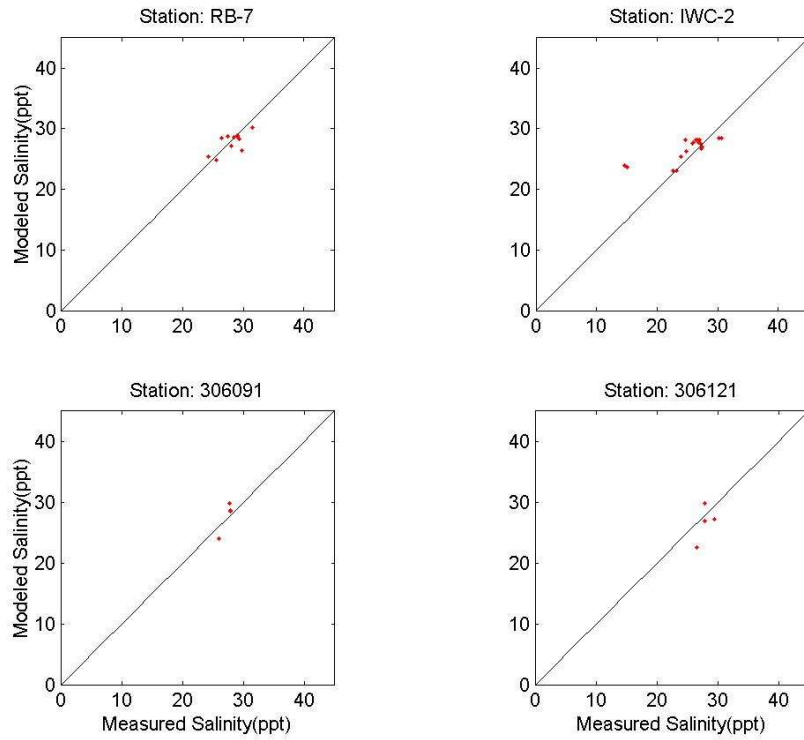


Figure 4.27: Scatterplot comparison between model and data for salinity in the year 1998 (part 3)

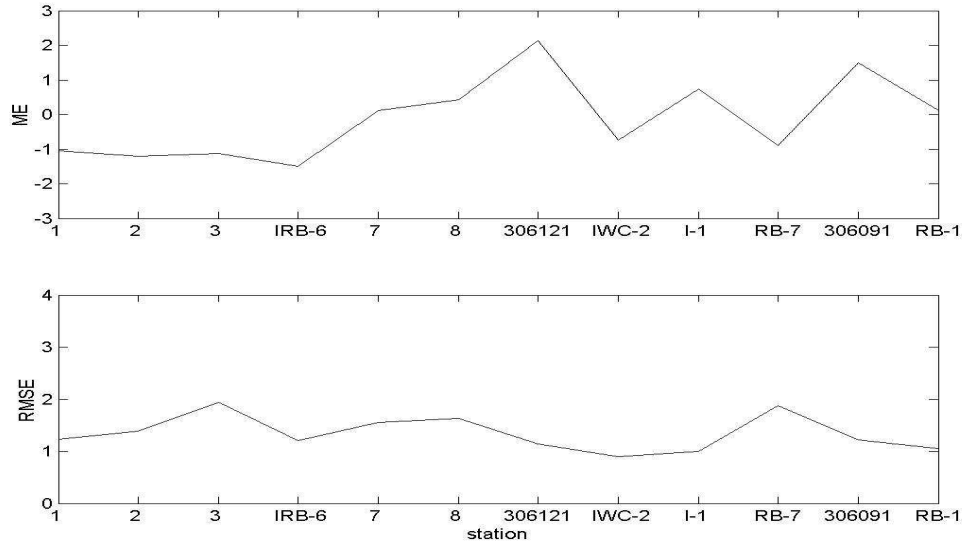


Figure 4.28: Transect plot of statistical parameters for temperature in the year 1998

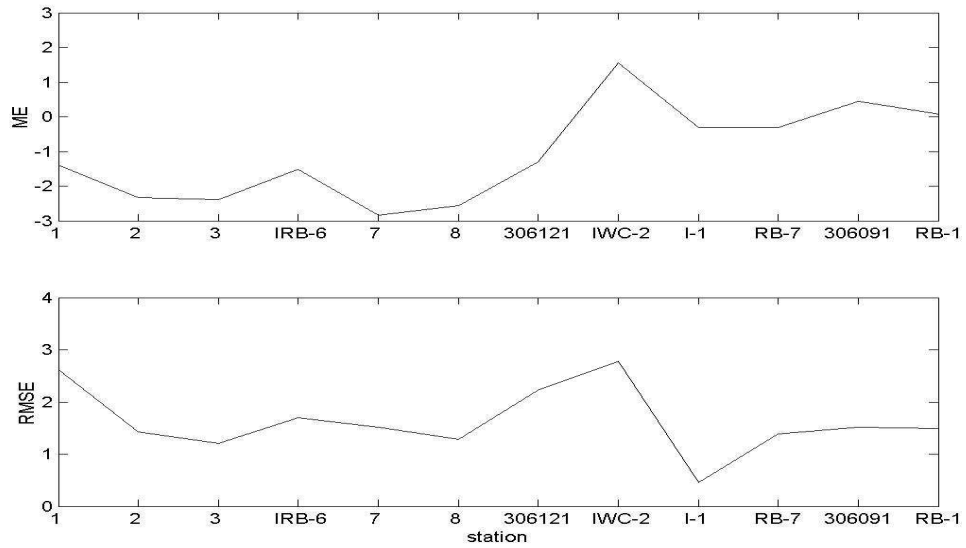


Figure 4.29: Transect plot of statistical parameters for salinity in the year 1998

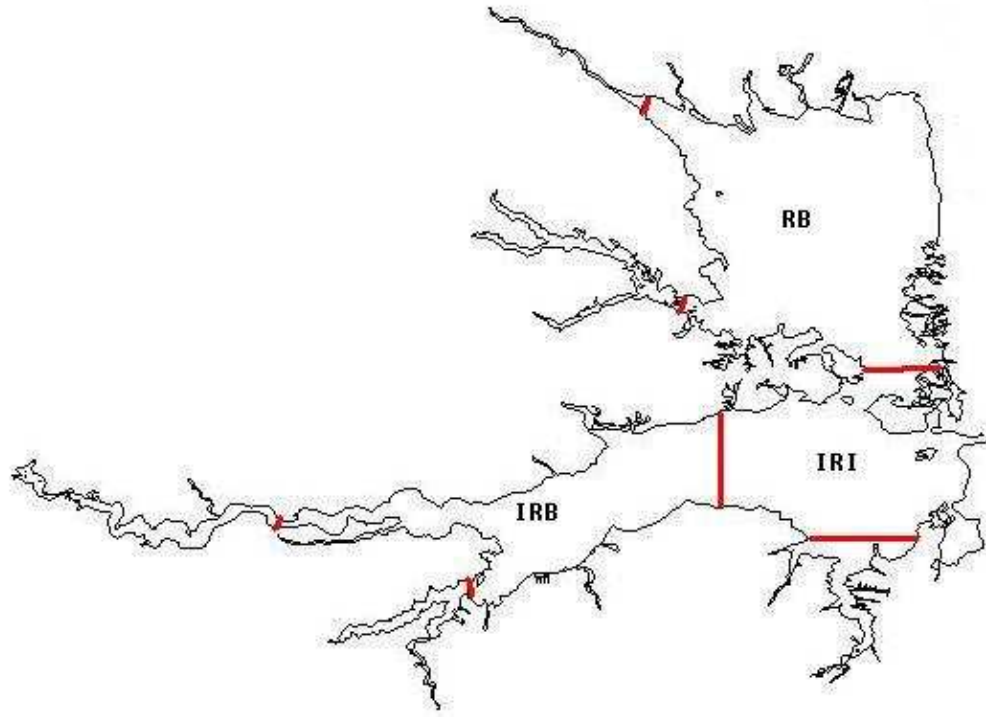


Figure 4.30: Partitions of model domain based on chlorophyll's distribution (red lines are segmentation lines. IRI: Indian River Inlet; RB: Rehoboth Bay; IRB: Indian River Bay; White Creek (WC) is to the south of IRI; the rest are all the other rivers and creeks (RAC))

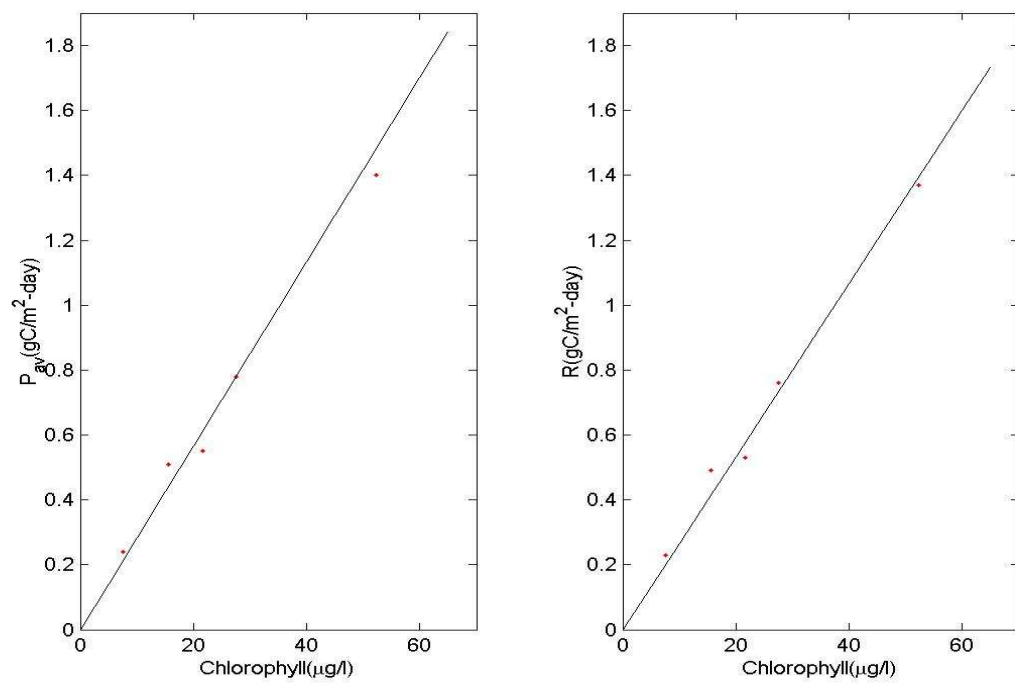


Figure 4.31: Linear relation between P_{av} and Chlorophyll (left panel), and R and Chlorophyll (right panel) in the year 1998

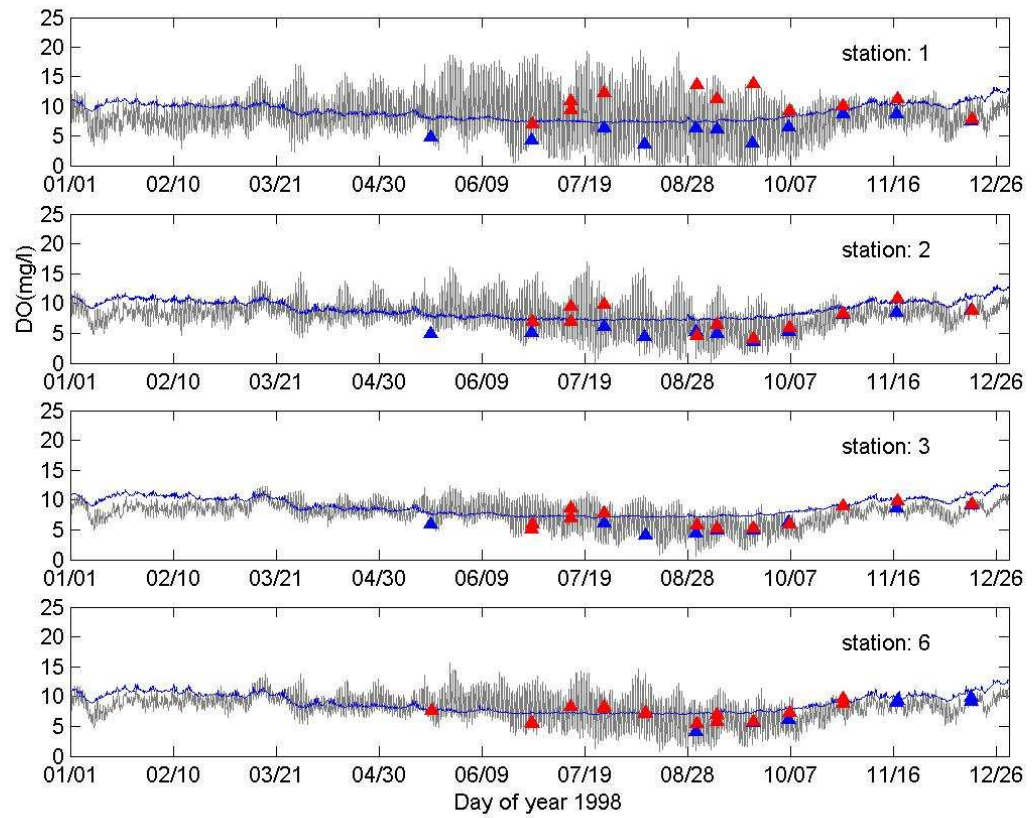


Figure 4.32: DO calibration summary 1 in the year 1998 (model results in grey lines, DO saturation in blue lines, and field data in triangles (blue: morning; red: afternoon))

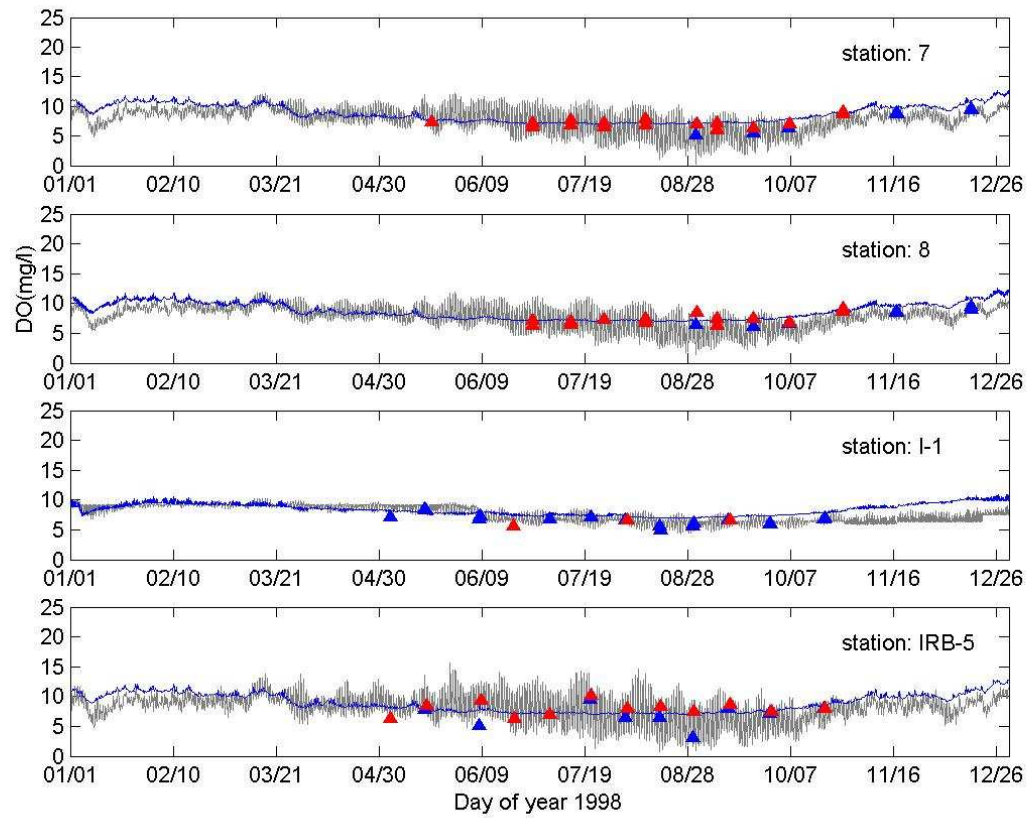


Figure 4.33: DO calibration summary 2 in the year 1998 (model results in grey lines, DO saturation in blue lines, and field data in triangles (blue: morning; red: afternoon))

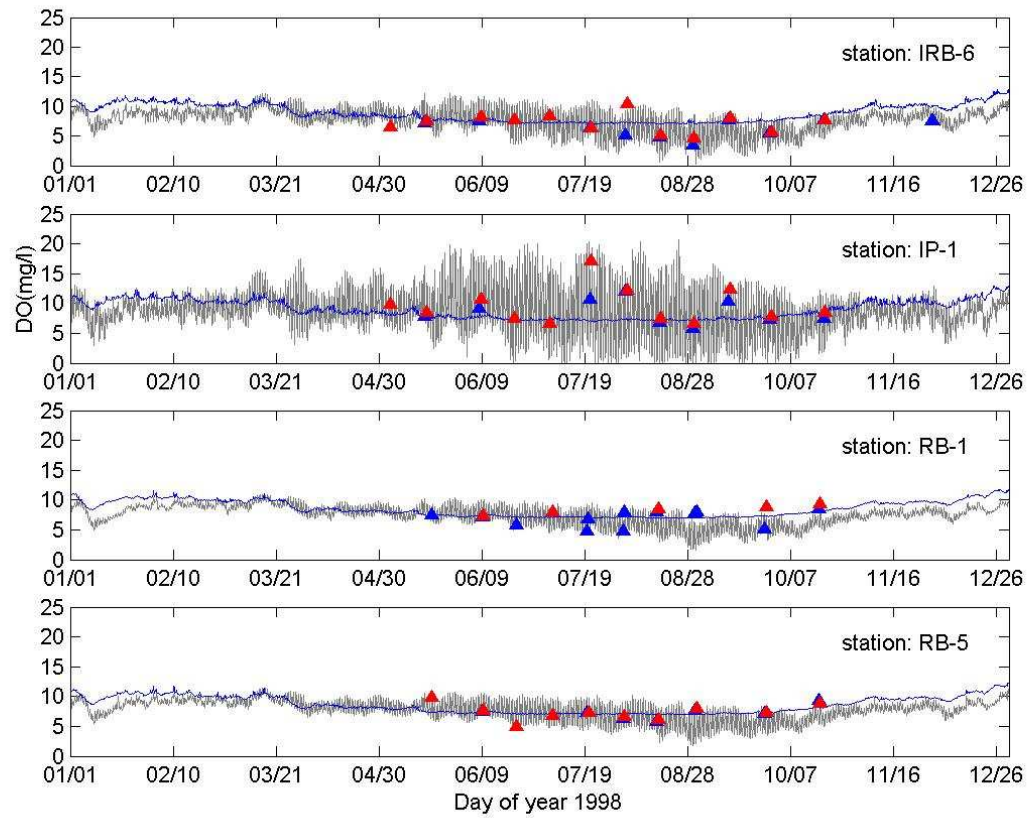


Figure 4.34: DO calibration summary 3 in the year 1998 (model results in grey lines, DO saturation in blue lines, and field data in triangles (blue: morning; red: afternoon))

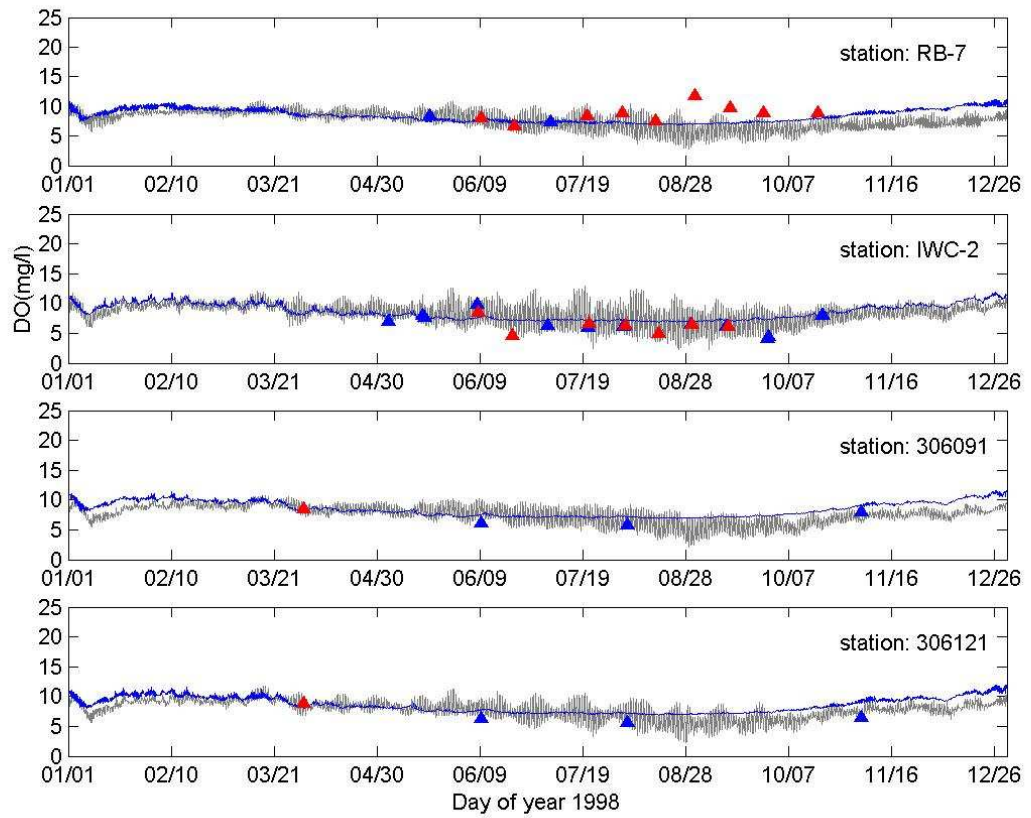


Figure 4.35: DO calibration summary 4 in the year 1998 (model results in grey lines, DO saturation in blue lines, and field data in triangles (blue: morning; red: afternoon))

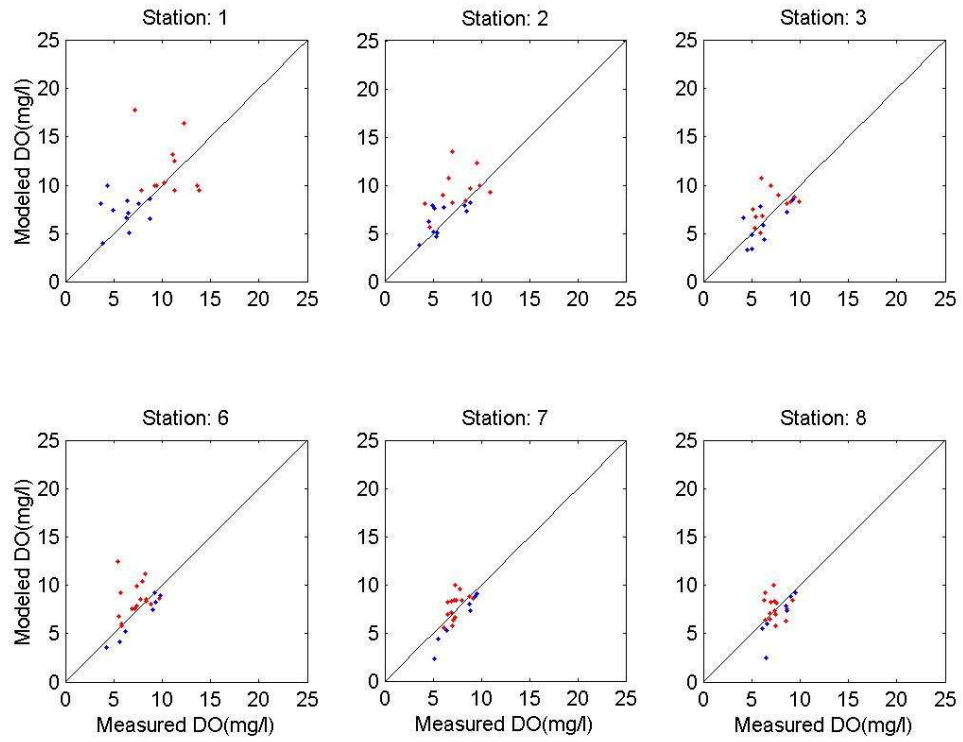


Figure 4.36: Scatterplot comparison between model and data for DO in the year 1998 (blue: morning; red: afternoon. part 1)

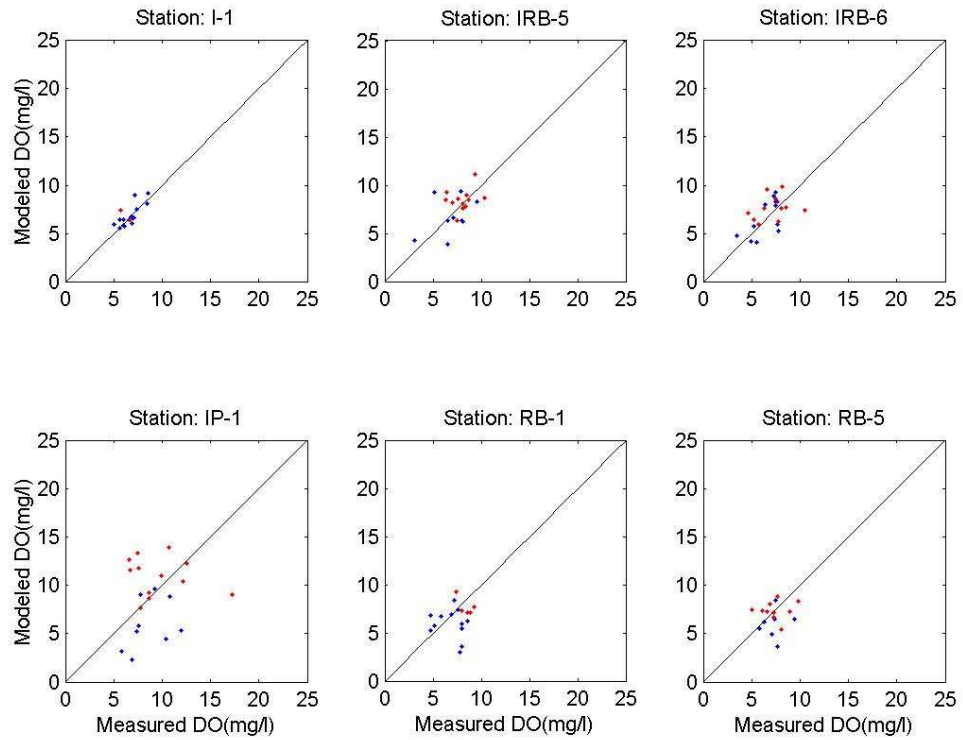


Figure 4.37: Scatterplot comparison between model and data for DO in the year 1998 (blue: morning; red: afternoon. part 2)

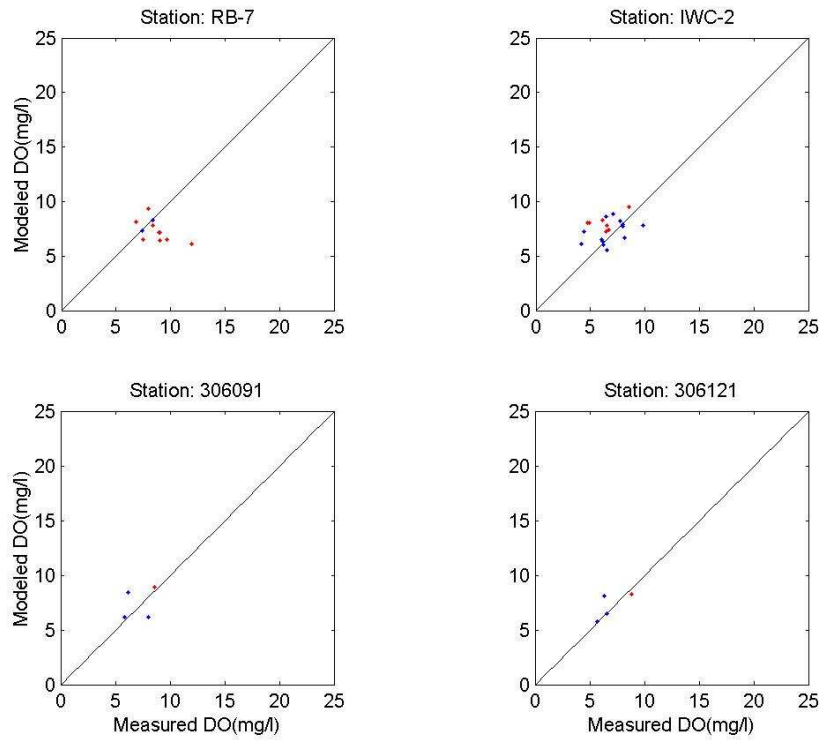


Figure 4.38: Scatterplot comparison between model and data for DO in the year 1998 (blue: morning; red: afternoon. part 3)

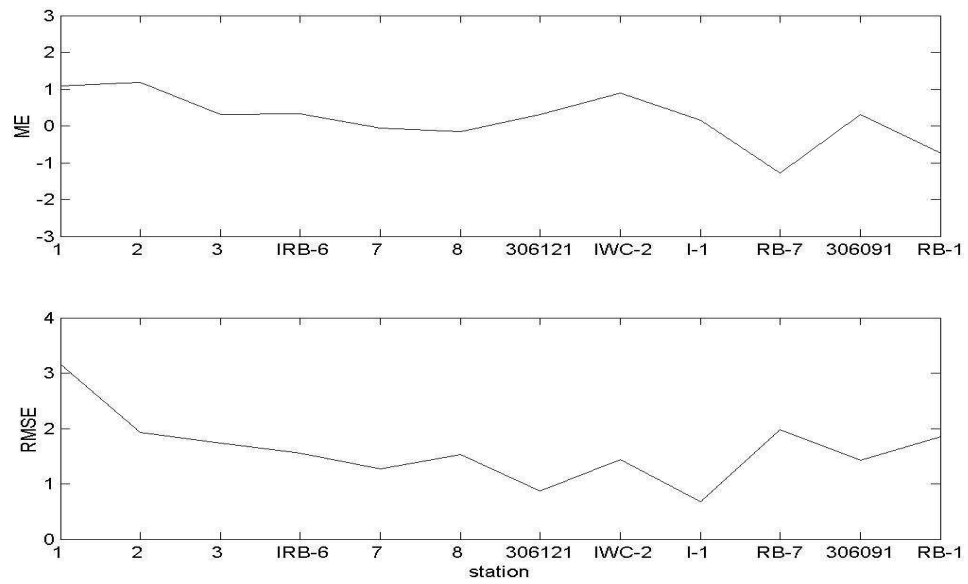


Figure 4.39: Transect plot of statistical parameters for DO in the year 1998

Chapter 5

MODEL-DATA COMPARISON AND MODEL VALIDATION

In this chapter, the calibrated model systems are applied to the calendar year 1999 for validation. The two years, 1998 and 1999, provide different freshwater inflows, tidal boundary conditions, DO loadings and atmospheric boundary conditions. It is, therefore, anticipated that calibrating and validating the model systems for these two years will establish the robustness of the models used in the present study. The data used here for validation are the same database as for calibration.

5.1 Hydrodynamic Model Validation

Figure 5.1 shows the time series comparison between the model prediction and the USGS gage data at Rosedale Beach in 1999. It shows that the model simulates the astronomical tide very well, generally. But during some time in the months February and March, the model underestimates the tidal elevation. This can also be seen in Table 5.1 that the mean error is negative. From the point of the view of tidal phase, the model and data are in phase for the whole year, unlike the year 1998. Therefore, the present model does not have phase problem. However, it seems that the model cannot predict the surface elevation well at some specific time based on the known information. It is possibly due to some missing data at the tidal boundary in Indian River Inlet.

In the year 1999, the stations chosen for comparison are slightly different from the year 1998 because of the availability of data. 14 stations have been selected to

compare with the model simulation for temperature and salinity (Figures 5.2 to 5.15). The figures show that the model again simulates the temperature well by successfully reproducing the seasonal variations for all the stations. The model also captures the general trend of salinity variations of the whole year. At some stations, the model even gets better simulations than the year 1998. Similar to the year 1998, both the tables and figures show that the temperature results have a better agreement than salinity (Figures 5.16 to 5.21, Tables 5.2 to 5.3). Figure 5.22 shows that the model overestimates the temperature slightly in most regions of the Bays except the upper portion of Indian River. The RMSE is almost uniform all over the Bays this year, which is the same as the year 1998. The results also indicate that the salinity simulations have a little better agreement this year, though the model underpredicts the results at some stations in Indian River Bay (Figure 5.23). There is a spatial trend along the Bays that the RMSE of the salinity decreases from the upper portion of Indian River to Indian River Inlet. In this year, there still exist some data points which are far from the model results. This seems inevitable based on the known conditions, but the model still successfully predicts the variations of both temperature and salinity within the whole year. The statistical analysis also indicates the good agreement with the measured data.

5.2 Water Quality Model Validation

In the year 1999, the chlorophyll concentrations are higher than the year 1998 all over the Bays. Based on the calibrated linear relation between P_{av}/R and Chlorophyll in Chapter 4, the average daily photosynthesis rate and respiration rate are calculated for those regions (Table 5.4, Figure 5.24). The water quality model results have been compared with the time series data station by station in the year 1999 (Figures 5.25 to 5.28). The figures show that the model captures the trend of DO yearly variations well generally. Almost all the measured data are within the range of model simulations at all stations. The model also successfully simulates the

diurnal DO swings at all stations during the year, with the minimum value at sunrise and maximum value at sunset. Figures 5.29 to 5.31 show clearly the performance of the model simulation. Again, the results at most of the stations are predicted well, but stations 1 and IR-2, which are far from the lines. Station 2 seems to get better simulations than the calibration results. These simulation results repeat the performance of the year 1998, and probably the problems are caused by same reasons. Some other stations have the errors between model and data, too, but they are smaller as shown in the Table 5.5. Figure 5.32 also shows the RMSE in the upper portion of Indian River is larger than the other regions, while the ME is small all over the Bays, except that station IWC-2 overestimates the DO. In this year, the model still predicts the large diurnal DO swings in the summer and fall, and the minimum values of DO concentration still exist in the end of summer for all the stations. This should be a common feature in the Delaware Inland Bays as described in Chapter 1.

5.3 Summary

From the time series comparison and scatterplot comparison, plus the error analysis of all the stations, both the hydrodynamic model and water quality model are capable of reproducing the yearly variation trends. Although input conditions are very limited, especially for the DO simulation, the coupled models still achieve good agreement with field data. For the water quality model, the simulation results are not as good as the hydrodynamic model, because water quality model is based on the performance of hydrodynamic model. The errors of hydrodynamic model have been brought to the water quality model. Although the errors are not big, they affect the performance of the DO simulation and increase the errors.

In the year 1999, the seasonal variation of water temperature in the Bays is prominent, too. In summer, mean water temperature in the Bays is $26.7^{\circ}C$ and standard deviation is $2.2^{\circ}C$; in winter, mean water temperature is $7.5^{\circ}C$ with a

standard deviation of $2.7^{\circ}C$; while mean water temperatures in spring and fall are in between, which are $14.5^{\circ}C$ and $16.9^{\circ}C$ respectively, and the standard deviations are $5.2^{\circ}C$ and $5.0^{\circ}C$ respectively. The water temperature is a little different from the year 1998.

The salinity in the Bays this year has the same features as the year 1998. The salinity is not uniform all over the Bays. The water in the upper and middle portions of the Indian River Bays is fresher than the water near the inlet. There is a significant longitudinal salinity gradient in the Indian River Bay. The salinity in the Indian River Bay has a wide range of diurnal variations than in Rehoboth Bay because of the sharp mixing between the sea water and fresh water. But the yearly variations of the salinity are different from the year 1998. So, the hydrodynamic properties between these two years are different, while the model can still capture the characteristics successfully.

In the year 1999, the DO variation has the similar characteristics as in 1998. There are large diurnal DO swings in summer and fall, while at other times, the diurnal DO range is small and very close to the saturation level. During the summer and fall, there exists many times when the DO concentration is below 4 mg/l , as well as some time up to 20 mg/l , especially in the upper portion of Indian River Bay.

In this chapter, the models have been verified using different time series data. Through the comparison with data, it demonstrates that the models are capable of capturing the general trends of the whole simulation time very well.

Table 5.1: Statistical parameters for tide (m) validation (year 1999)

	Rosedale
ME	-0.083
MAE	0.125
RE	0.165
RMSE	0.188

Table 5.2: Statistical summary for temperature ($^{\circ}C$) validation (year 1999)

	1	2	3	6	7	8	IR-2
N	29	31	30	30	30	30	15
ME	-1.149	-0.676	-0.321	0.168	0.432	0.810	-1.089
MAE	1.100	0.819	0.860	0.987	0.998	1.121	0.830
RE	0.046	0.035	0.037	0.043	0.045	0.052	0.031
RMSE	1.362	1.018	1.043	1.148	1.169	1.290	1.121
	IRB-2	IRB-4	RB-1	IWC-2	306091	306121	306321
N	15	17	13	15	4	4	4
ME	1.634	0.990	0.637	1.390	1.623	1.821	1.266
MAE	0.814	0.935	0.671	0.627	1.026	1.537	1.631
RE	0.037	0.039	0.026	0.027	0.055	0.084	0.092
RMSE	0.955	1.121	0.903	0.776	1.108	1.567	1.996

Table 5.3: Statistical summary for salinity (ppt) validation (year 1999)

	1	2	3	6	7	8	IR-2
N	29	31	30	30	30	30	15
ME	1.003	-0.145	-1.828	-1.690	-2.526	-2.429	-2.760
MAE	2.297	2.100	1.467	1.199	1.228	1.345	2.185
RE	0.186	0.123	0.066	0.051	0.047	0.049	0.099
RMSE	2.820	2.612	1.878	1.551	1.725	1.932	2.614
	IRB-2	IRB-4	RB-1	IWC-2	306091	306121	306321
N	15	17	13	15	4	4	4
ME	-2.004	-3.118	-0.429	-1.413	-0.875	-1.369	0.150
MAE	0.536	0.979	0.913	0.722	0.632	1.319	0.875
RE	0.017	0.035	0.033	0.023	0.021	0.044	0.028
RMSE	0.705	1.208	1.132	0.868	0.742	1.449	1.070

Table 5.4: Calibration parameters for RCA model in the year 1999 (Unit of chlorophyll is $\mu g/l$; units of both photosynthesis rate and respiration rate are $gC/m^2 - day$)

	IRI	RB	WC	IRB	RAC
Chlorophyll	10.30	17.20	23.60	33.50	60.00
Pav	0.31	0.55	0.59	0.94	1.56
R	0.30	0.54	0.62	0.90	1.50

Table 5.5: Statistical summary for DO (mg/l) validation (year 1999)

	1	2	3	6	7	8	IR-2
N	29	31	30	30	30	30	15
ME	0.287	0.228	0.049	-0.280	0.070	-0.081	-0.636
MAE	3.006	1.816	1.614	1.705	1.302	1.297	3.188
RE	0.279	0.205	0.202	0.189	0.161	0.162	0.326
RMSE	3.859	2.458	2.054	2.066	1.756	1.687	3.873
	IRB-2	IRB-4	RB-1	IWC-2	306091	306121	306321
N	15	17	13	15	4	4	4
ME	0.042	-0.513	0.003	1.281	-0.576	-0.579	-0.809
MAE	0.667	1.734	1.541	0.831	1.198	0.425	0.721
RE	0.106	0.230	0.220	0.134	0.166	0.058	0.094
RMSE	0.854	2.160	1.821	0.958	1.255	0.427	0.835

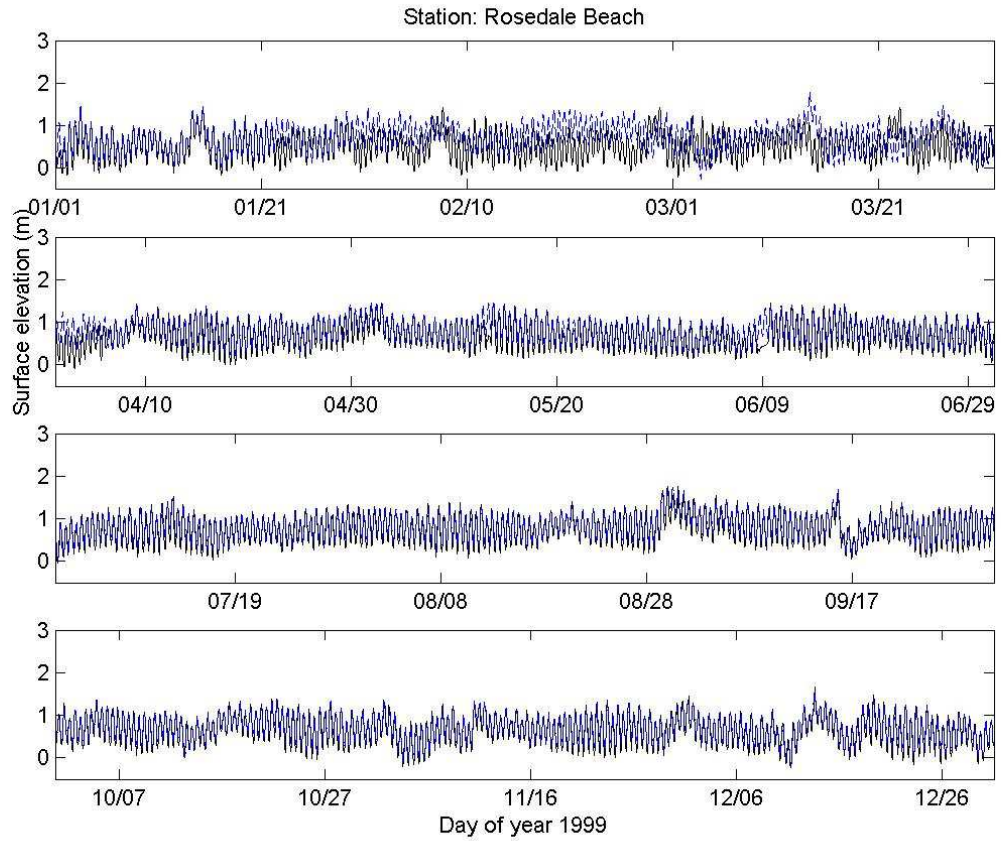


Figure 5.1: Tide validation result at Rosedale Beach in Indian River Bay in the year 1999 (model results in black solid lines, and field data in blue dash lines)

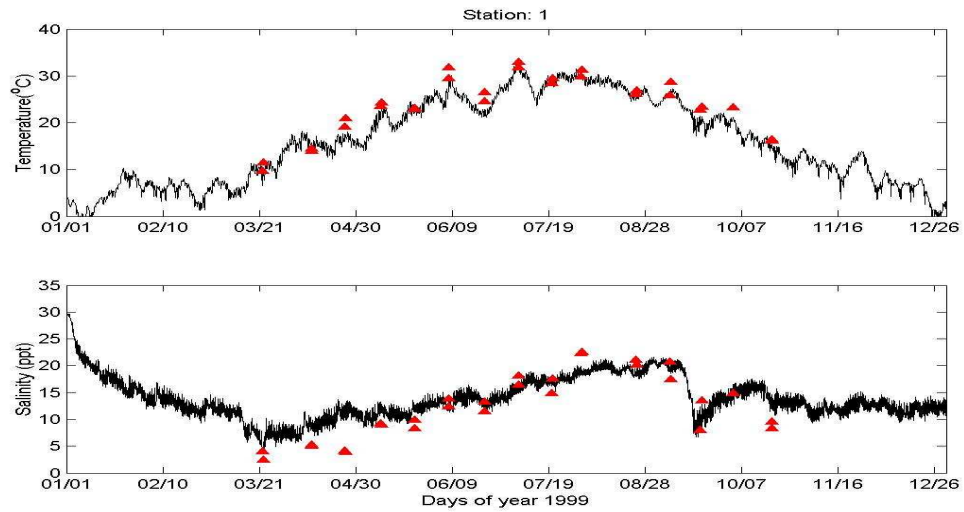


Figure 5.2: Temperature and salinity validation result at Conectiv's station 1 in the year 1999 (model results in black solid lines, and field data in red triangles)

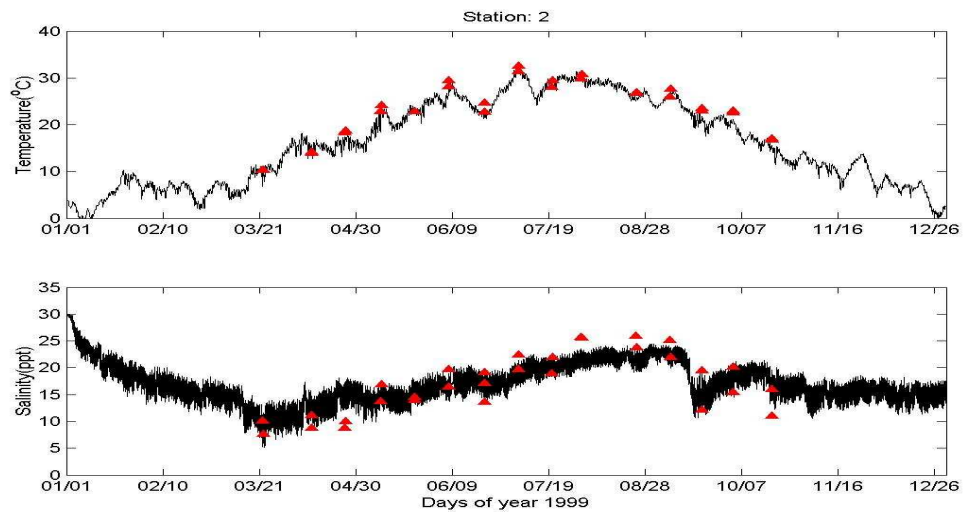


Figure 5.3: Temperature and salinity validation result at Conectiv's station 2 in the year 1999 (model results in black solid lines, and field data in red triangles)

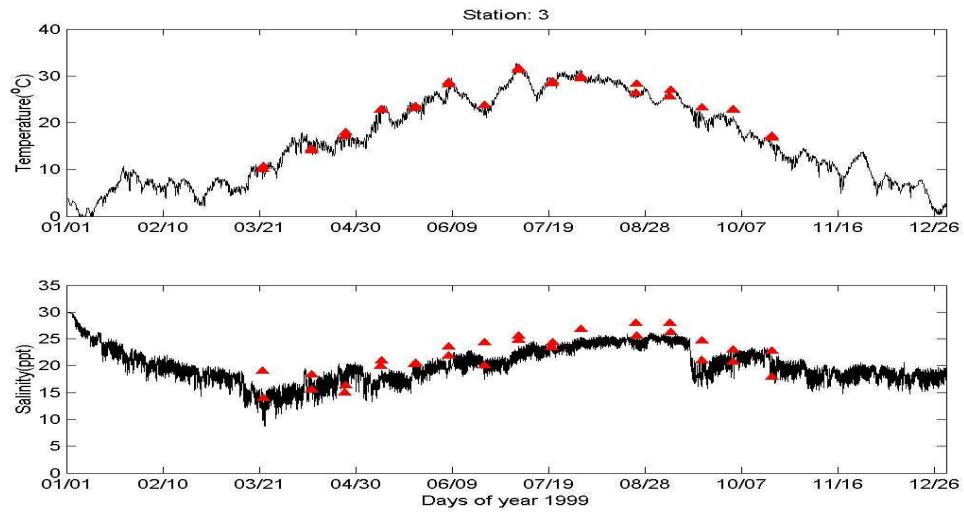


Figure 5.4: Temperature and salinity validation result at Conectiv's station 3 in the year 1999 (model results in black solid lines, and field data in red triangles)

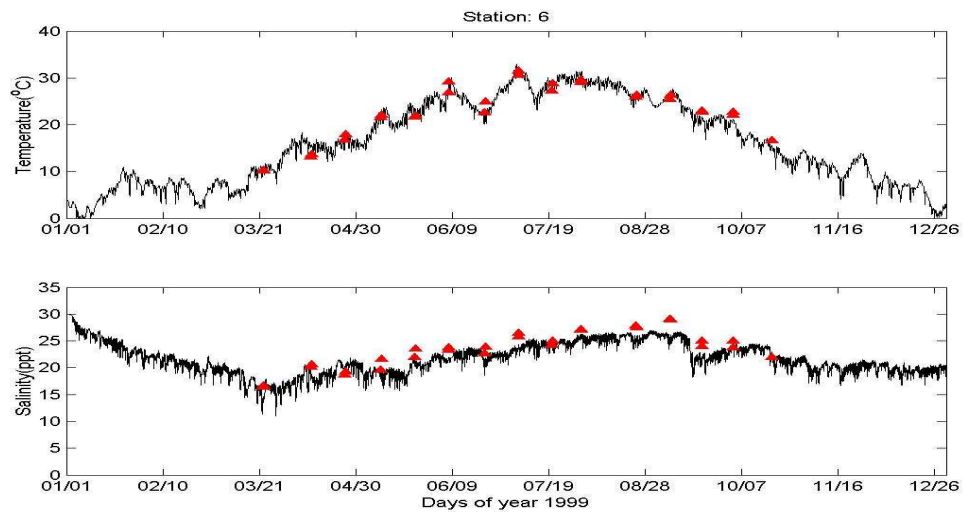


Figure 5.5: Temperature and salinity validation result at Conectiv's station 6 in the year 1999 (model results in black solid lines, and field data in red triangles)

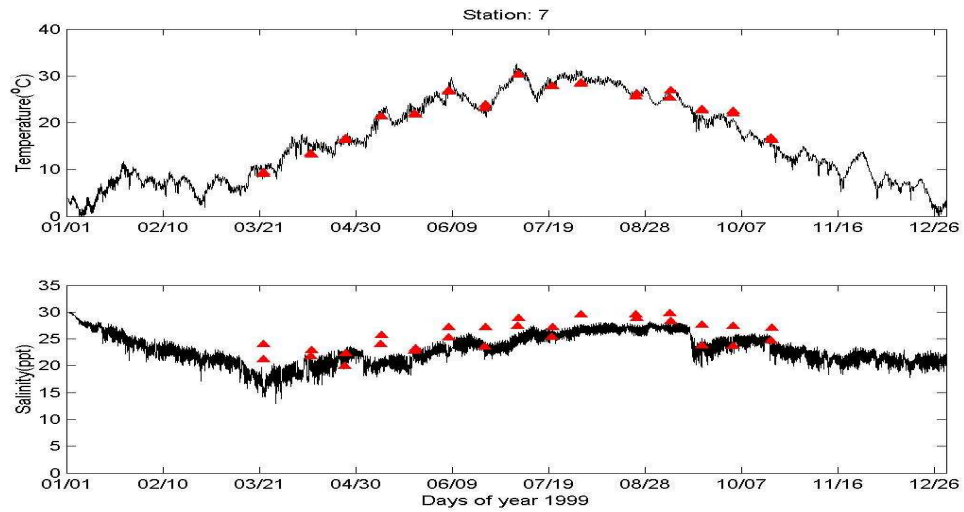


Figure 5.6: Temperature and salinity validation result at Conectiv’s station 7 in the year 1999 (model results in black solid lines, and field data in red triangles)

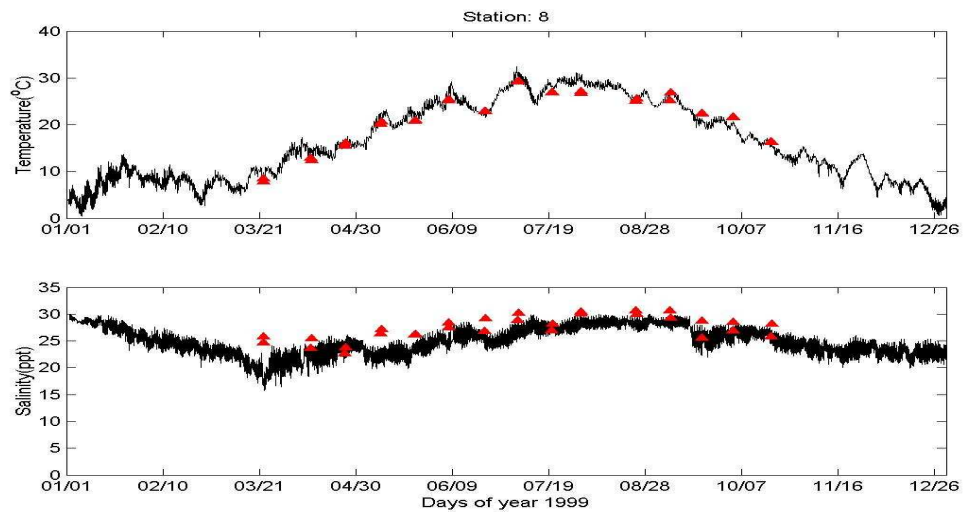


Figure 5.7: Temperature and salinity validation result at Conectiv’s station 8 in the year 1999 (model results in black solid lines, and field data in red triangles)

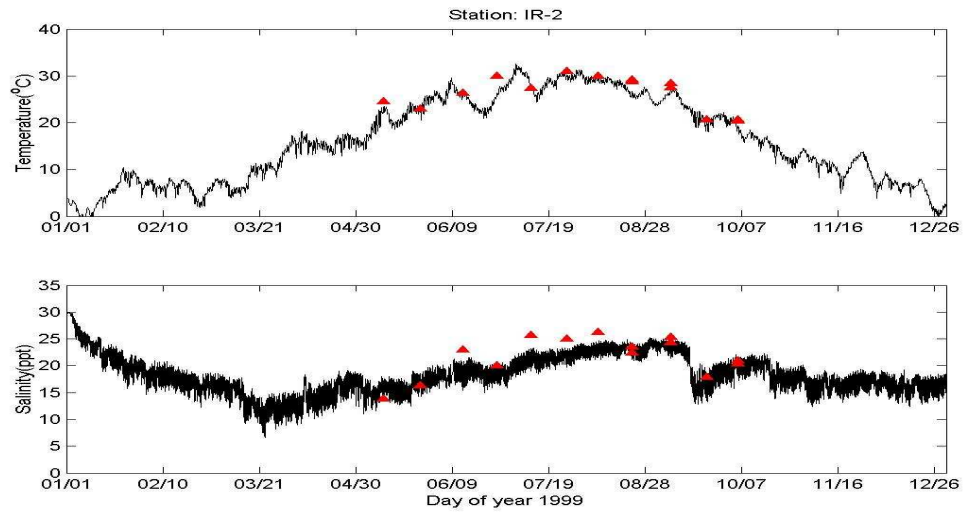


Figure 5.8: Temperature and salinity validation result at State’s Pfisteria station IR-2 in the year 1999 (model results in black solid lines, and field data in red triangles)

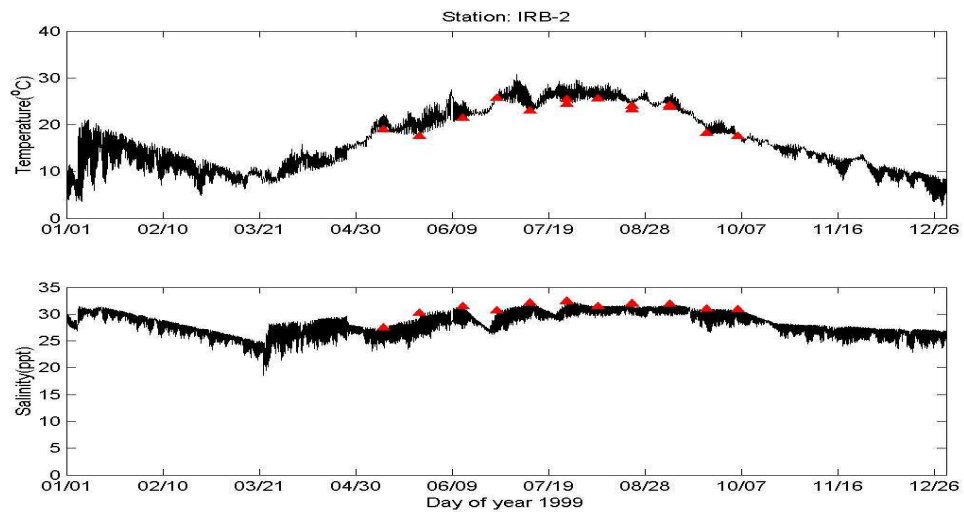


Figure 5.9: Temperature and salinity validation result at State’s Pfisteria station IRB-2 in the year 1999 (model results in black solid lines, and field data in red triangles)

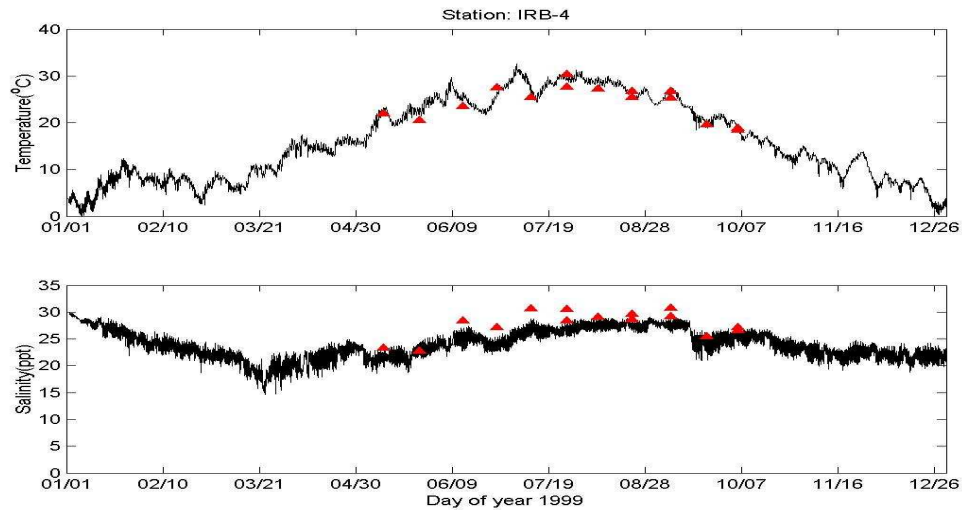


Figure 5.10: Temperature and salinity validation result at State’s Pfiesteria station IRB-4 in the year 1999 (model results in black solid lines, and field data in red triangles)

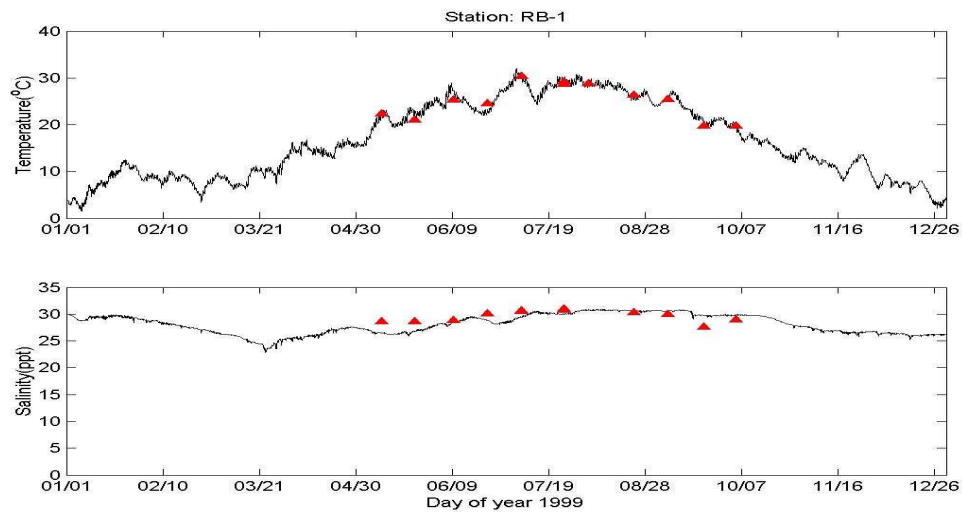


Figure 5.11: Temperature and salinity validation result at State’s Pfiesteria station RB-1 in the year 1999 (model results in black solid lines, and field data in red triangles)

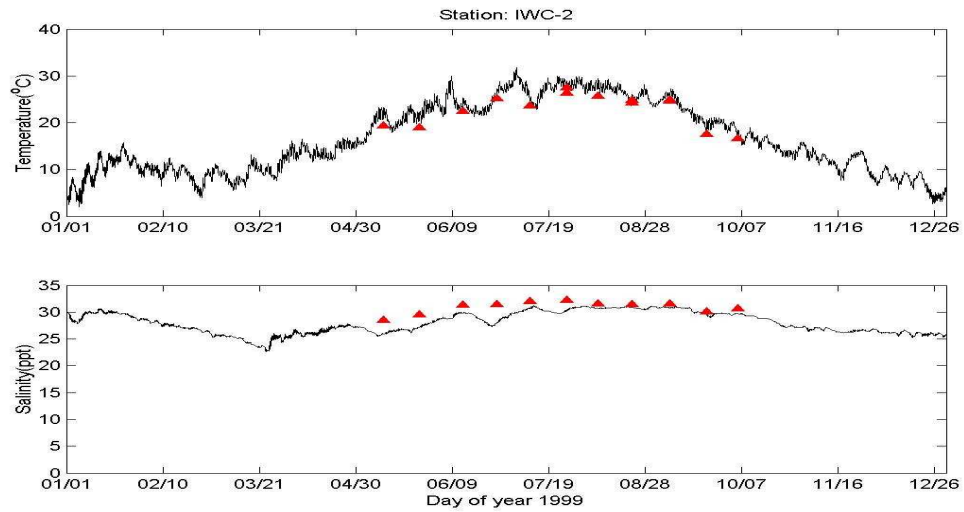


Figure 5.12: Temperature and salinity validation result at State's Pfiesteria station IWC-2 in the year 1999 (model results in black solid lines, and field data in red triangles)

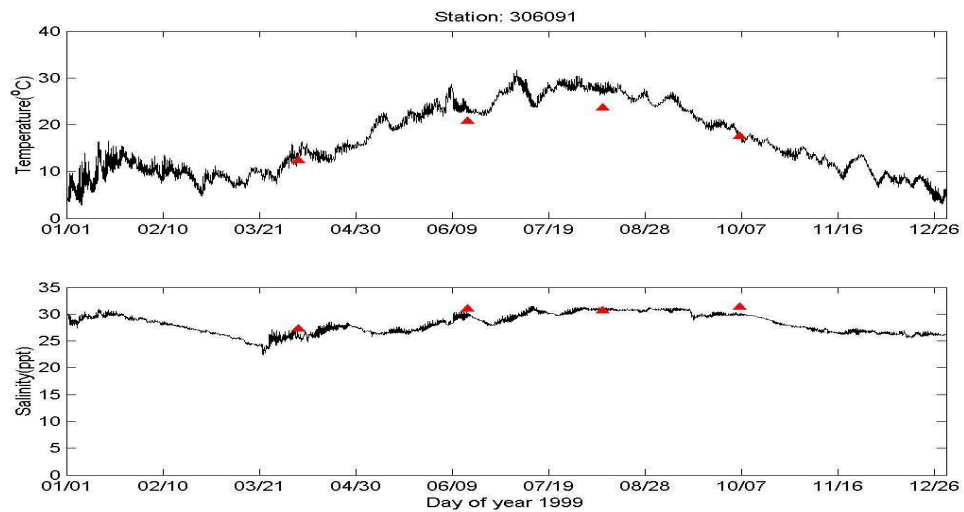


Figure 5.13: Temperature and salinity validation result at STORET station 306091 in the year 1999 (model results in black solid lines, and field data in red triangles)

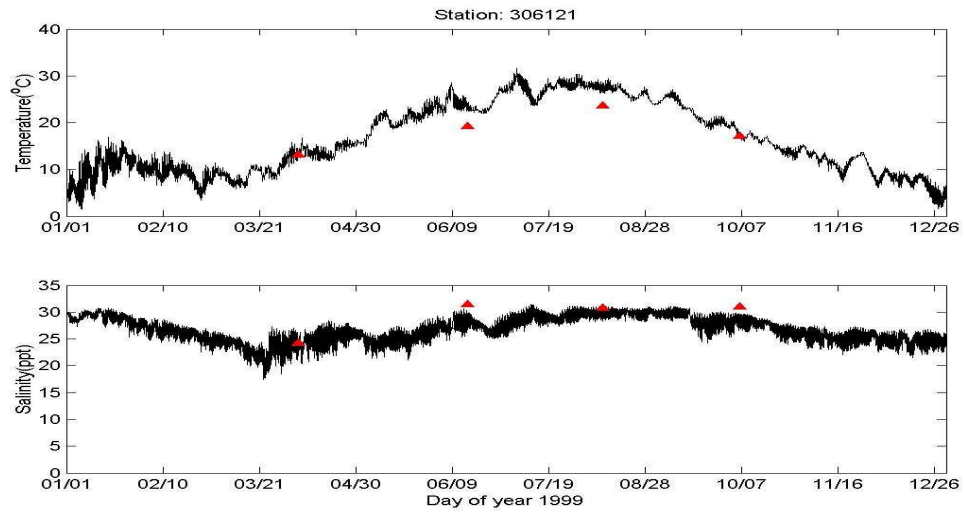


Figure 5.14: Temperature and salinity validation result at STORET station 306121 in the year 1999 (model results in black solid lines, and field data in red triangles)

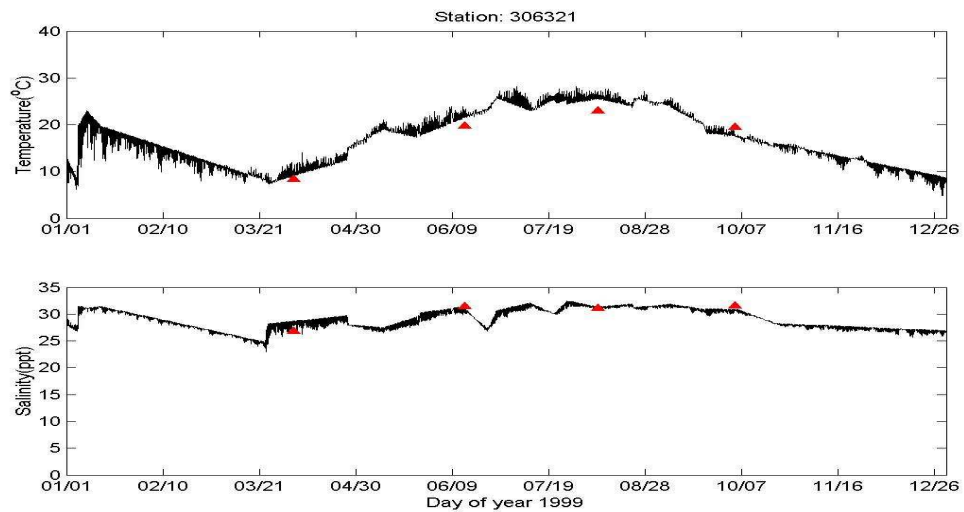


Figure 5.15: Temperature and salinity validation result at STORET station 306321 in the year 1999 (model results in black solid lines, and field data in red triangles)

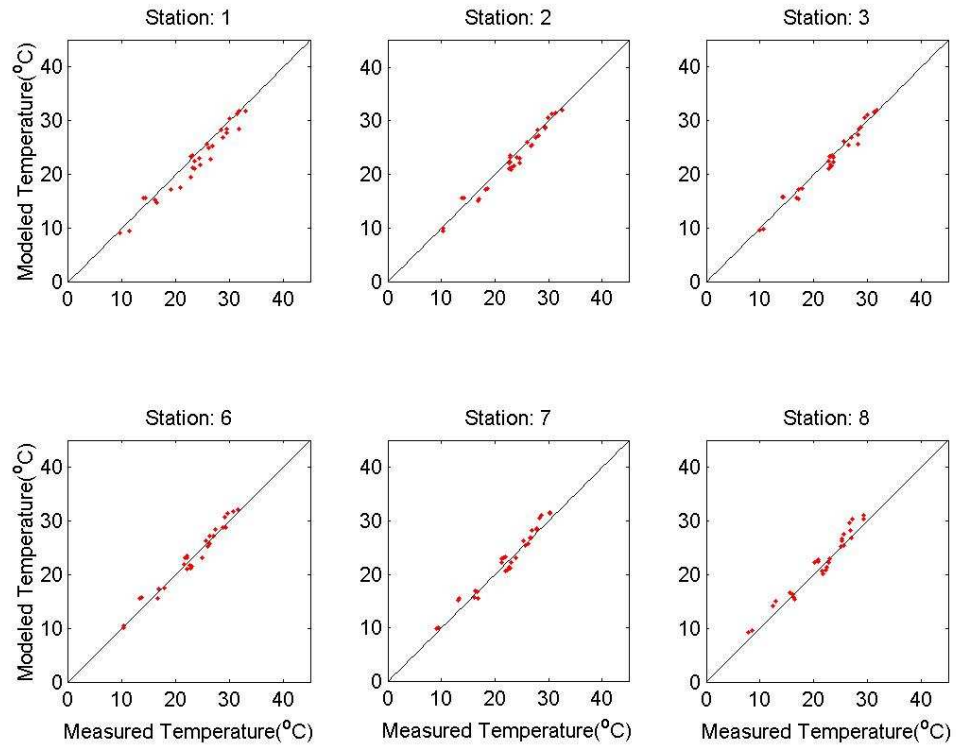


Figure 5.16: Scatterplot comparison between model and data for temperature in the year 1999 (part 1)

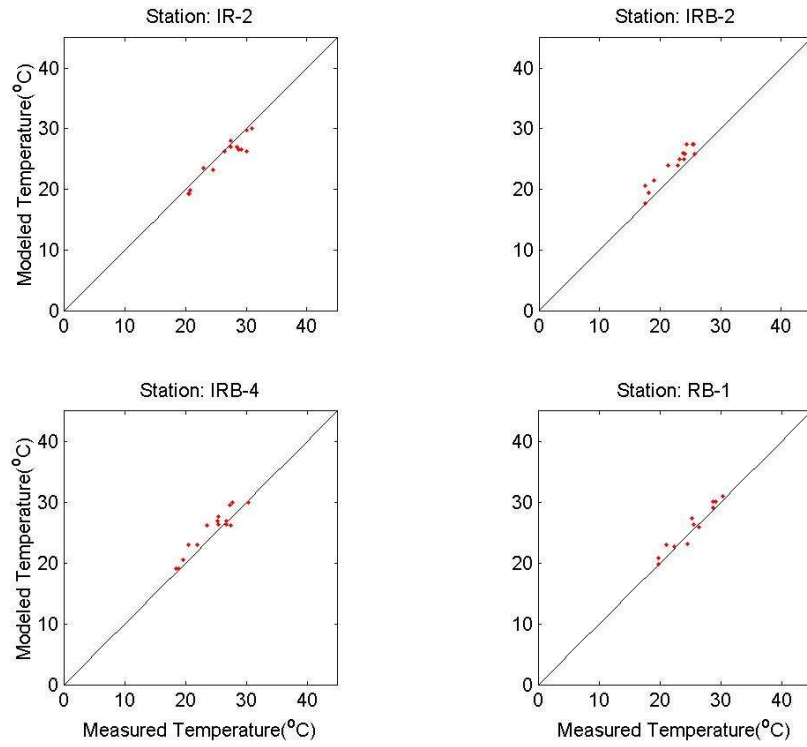


Figure 5.17: Scatterplot comparison between model and data for temperature in the year 1999 (part 2)

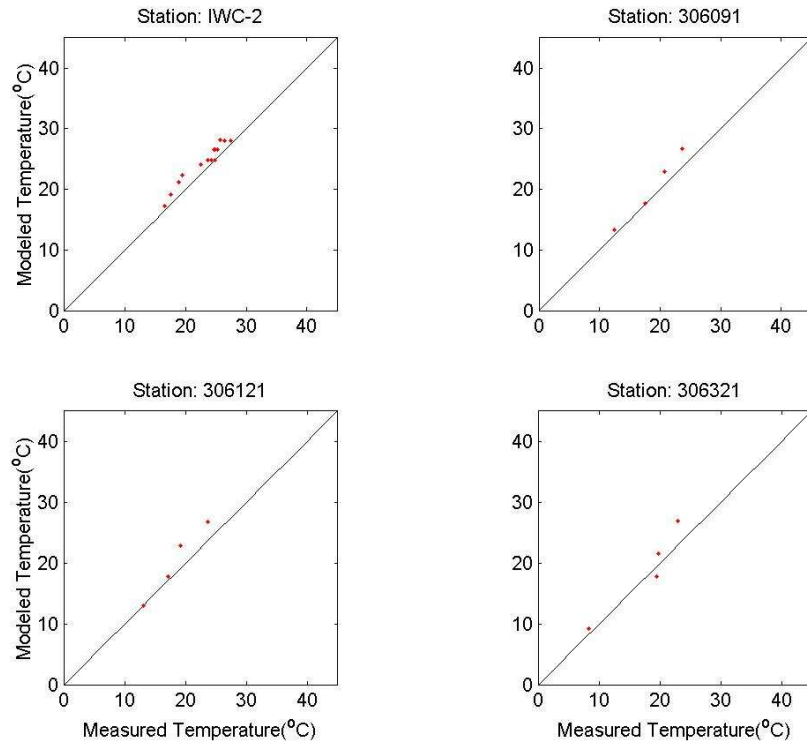


Figure 5.18: Scatterplot comparison between model and data for temperature in the year 1999 (part 3)

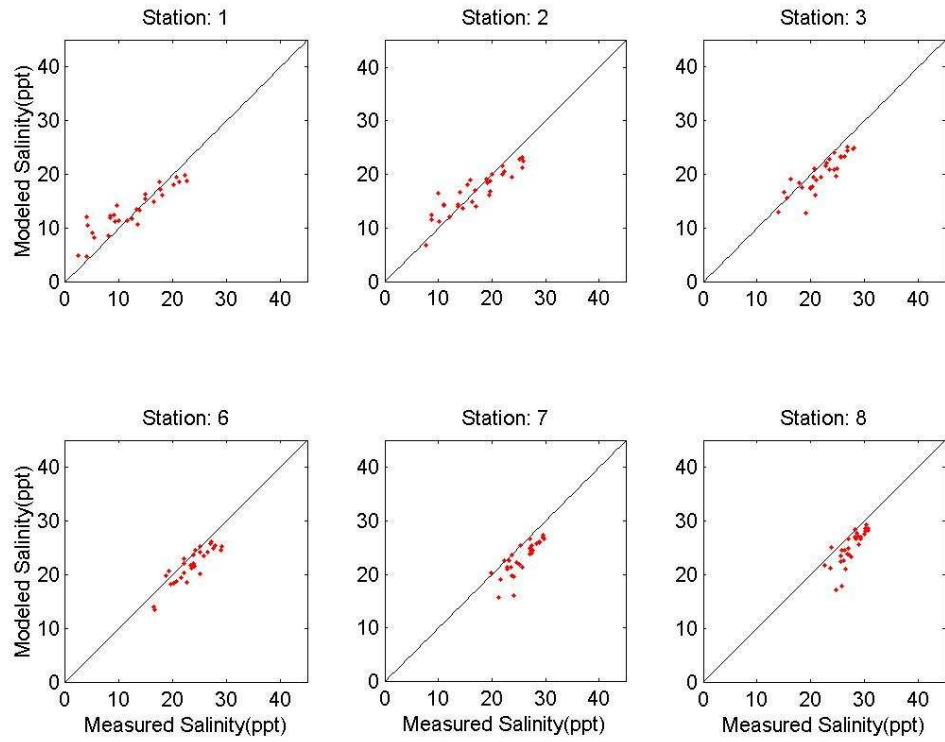


Figure 5.19: Scatterplot comparison between model and data for salinity in the year 1999 (part 1)

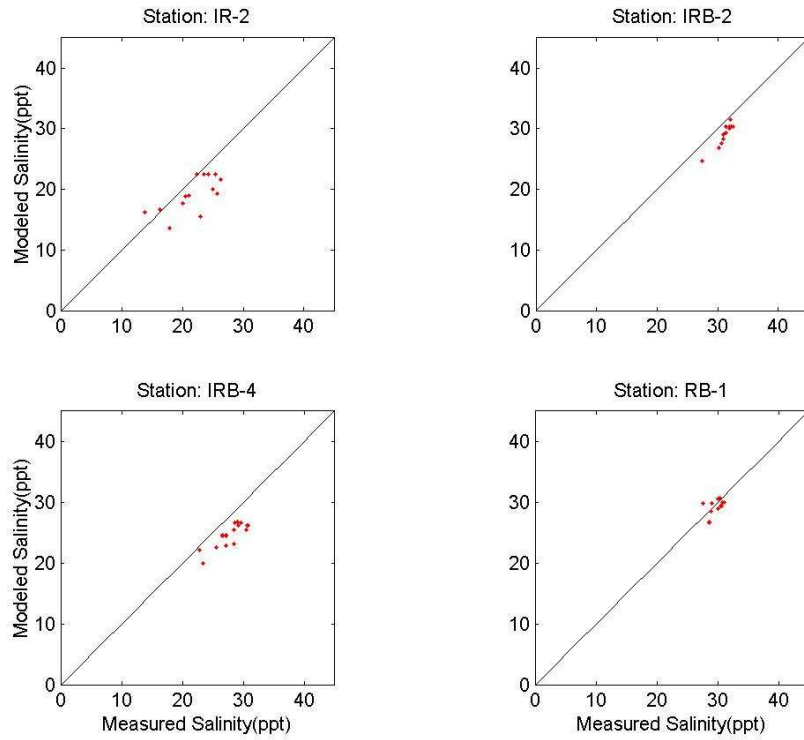


Figure 5.20: Scatterplot comparison between model and data for salinity in the year 1999 (part 2)

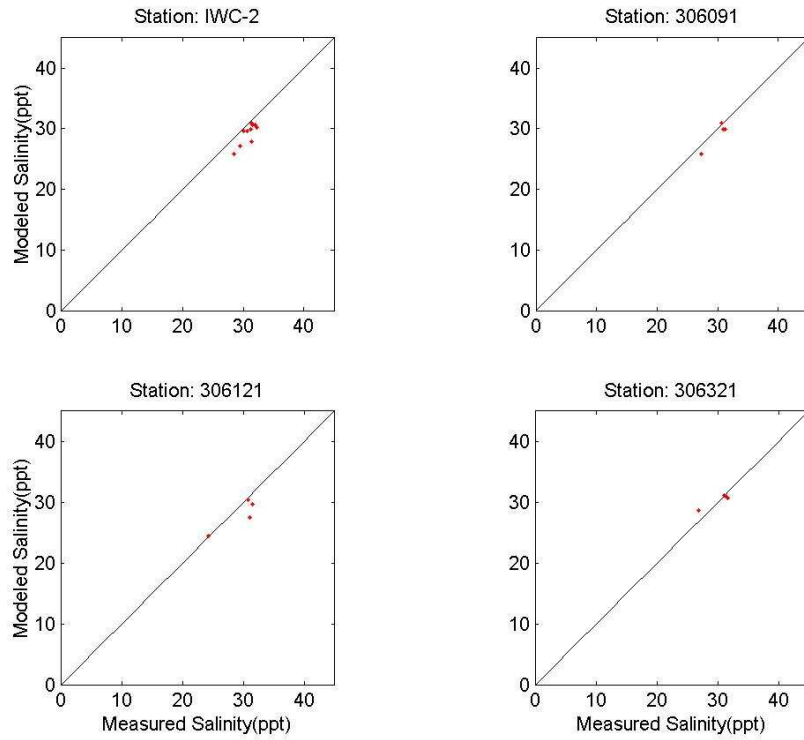


Figure 5.21: Scatterplot comparison between model and data for salinity in the year 1999 (part 3)

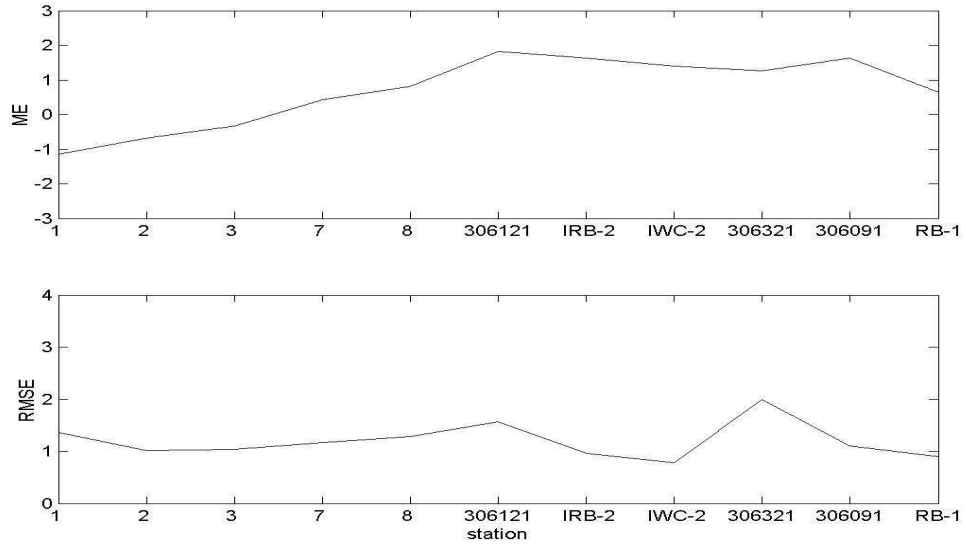


Figure 5.22: Transect plot of statistical parameters for temperature in the year 1999

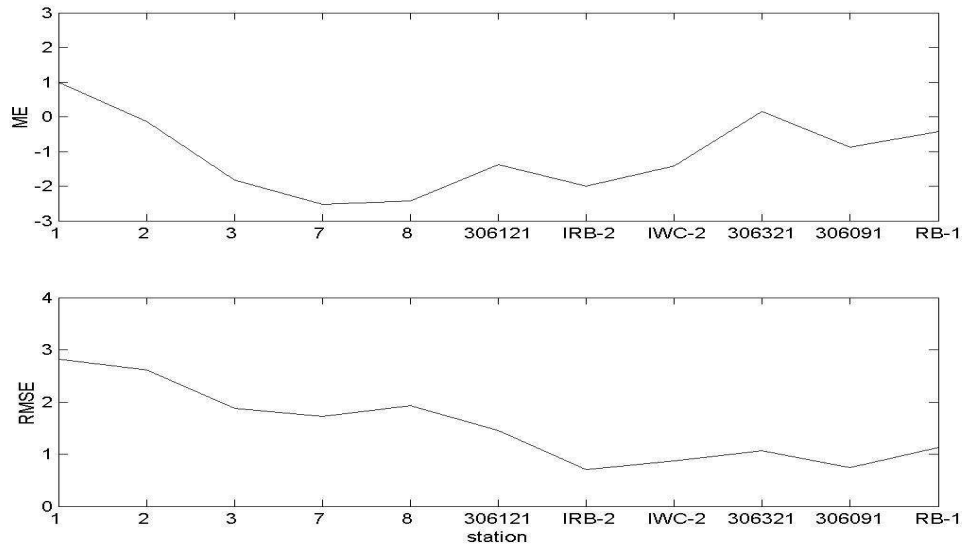


Figure 5.23: Transect plot of statistical parameters for salinity in the year 1999

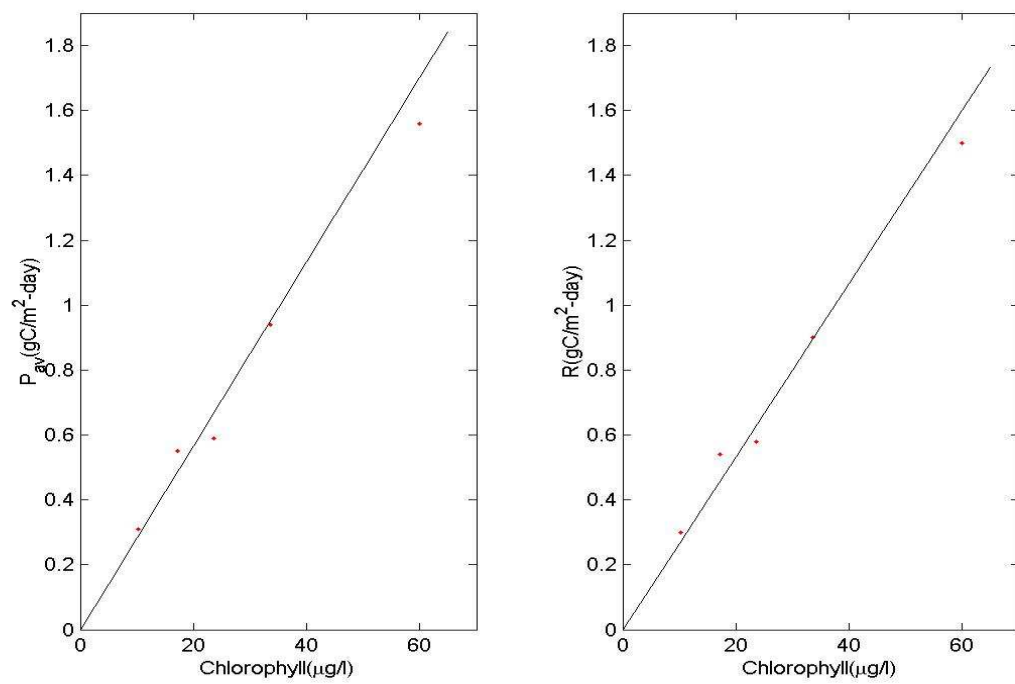


Figure 5.24: Linear relation between P_{av} and Chlorophyll (left panel), and R and Chlorophyll (right panel) in the year 1999

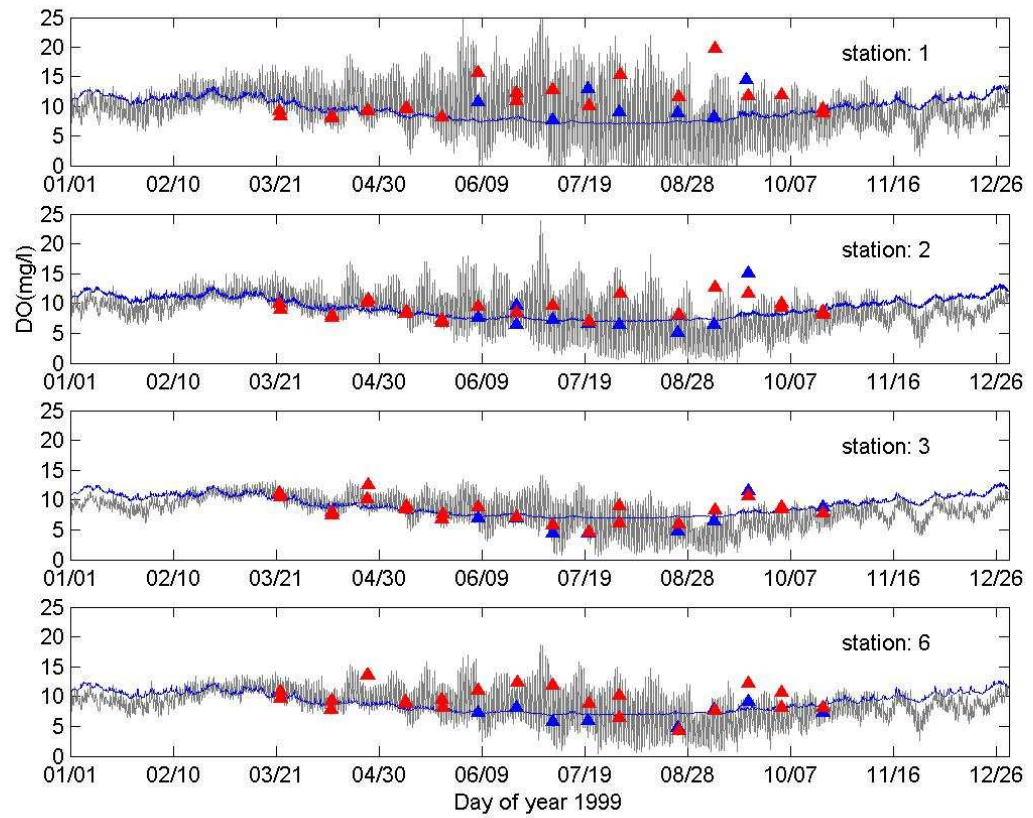


Figure 5.25: DO calibration summary 1 in the year 1999 (model results in grey lines, DO saturation in blue lines, and field data in triangles (blue: morning; red: afternoon))

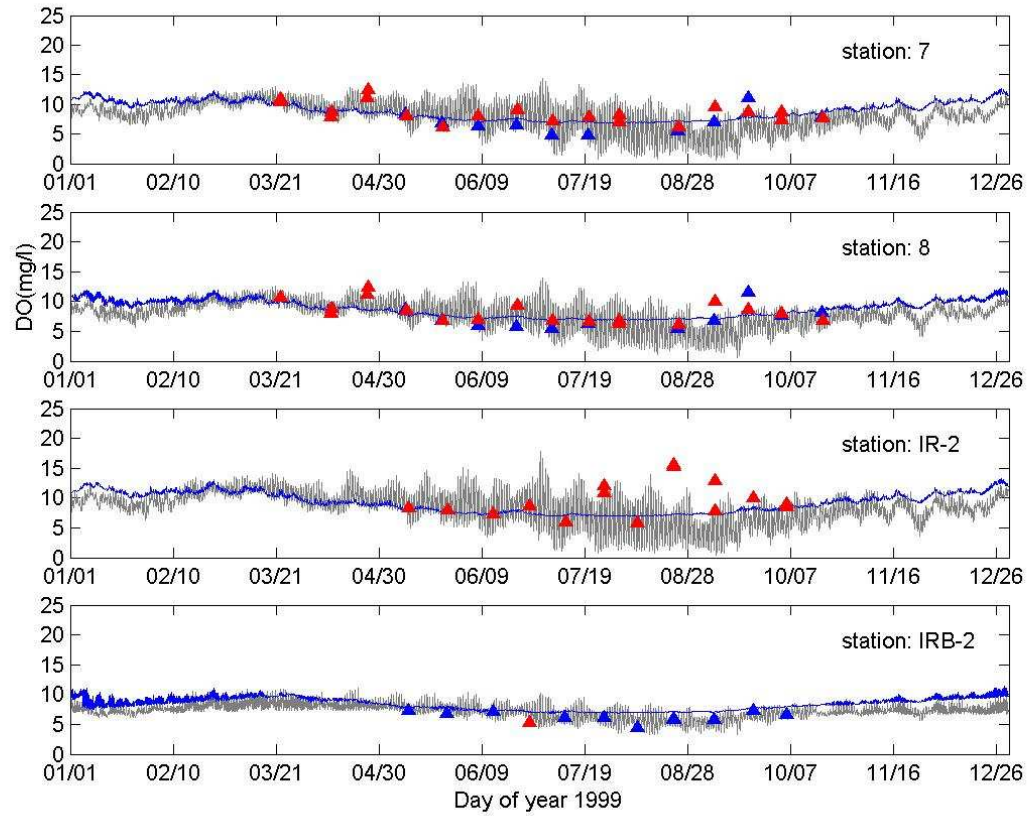


Figure 5.26: DO calibration summary 2 in the year 1999 (model results in grey lines, DO saturation in blue lines, and field data in triangles (blue: morning; red: afternoon))

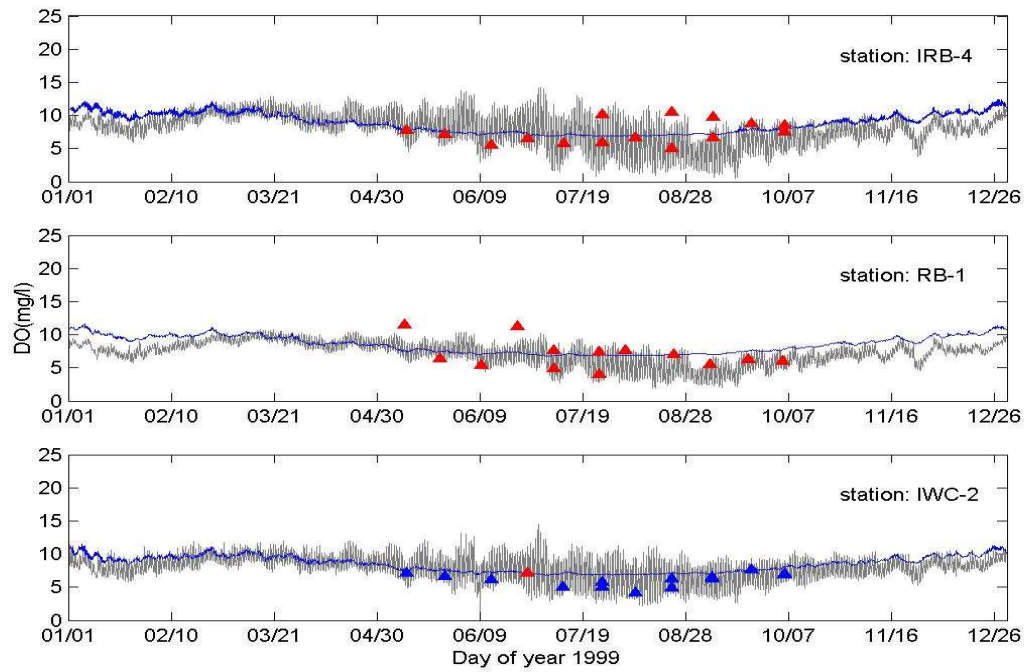


Figure 5.27: DO calibration summary 3 in the year 1999 (model results in grey lines, DO saturation in blue lines, and field data in triangles (blue: morning; red: afternoon))

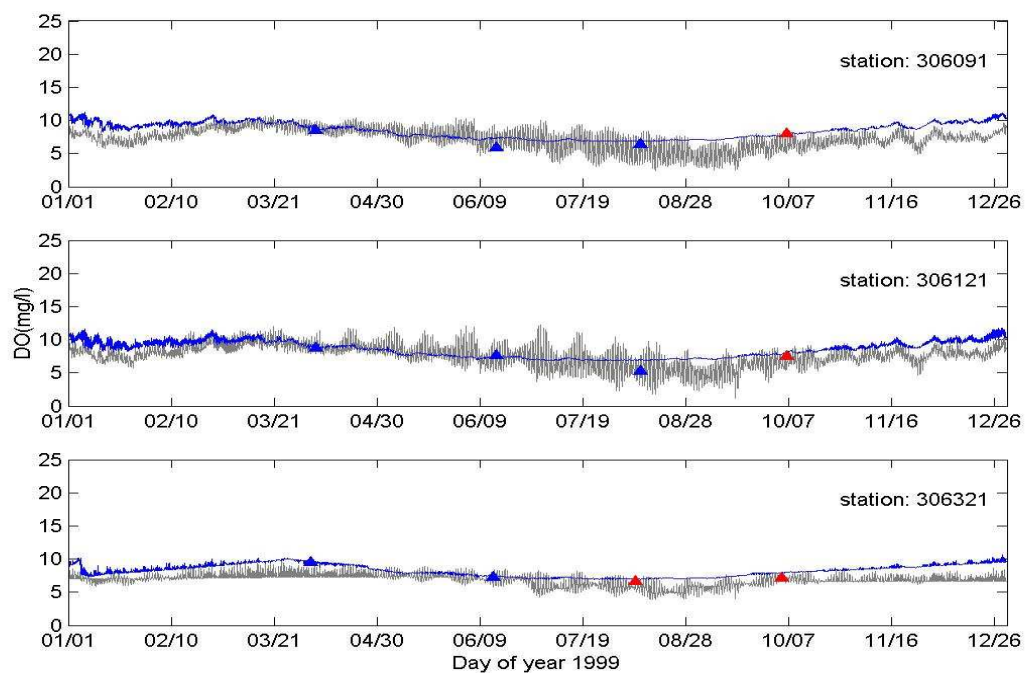


Figure 5.28: DO calibration summary 4 in the year 1999 (model results in grey lines, DO saturation in blue lines, and field data in triangles (blue: morning; red: afternoon))

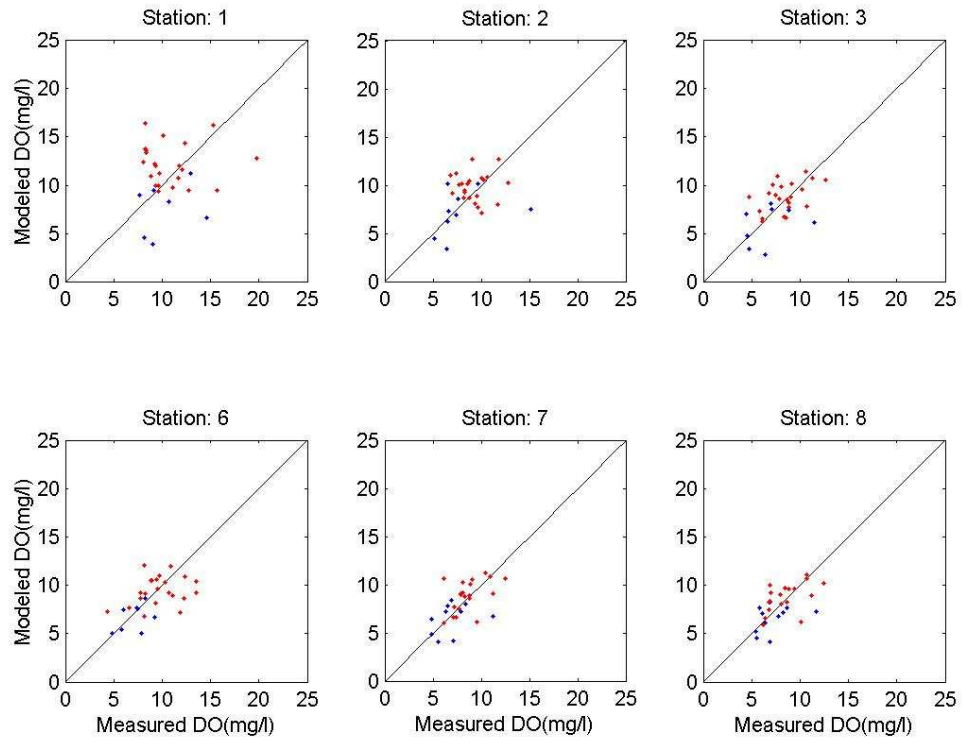


Figure 5.29: Scatterplot comparison between model and data for DO in the year 1999 (blue: morning; red: afternoon. part 1)

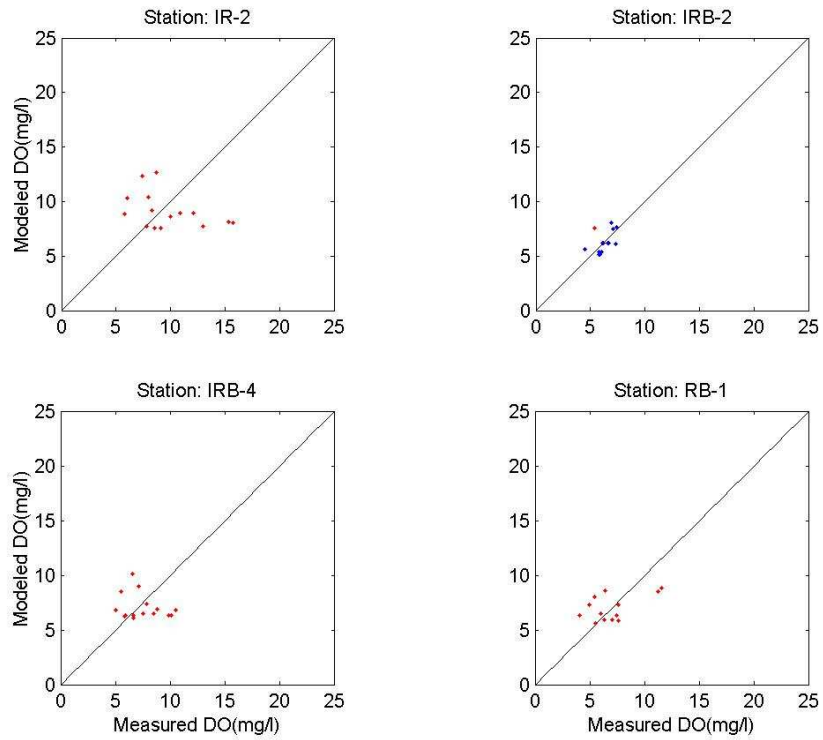


Figure 5.30: Scatterplot comparison between model and data for DO in the year 1999 (blue: morning; red: afternoon. part 2)

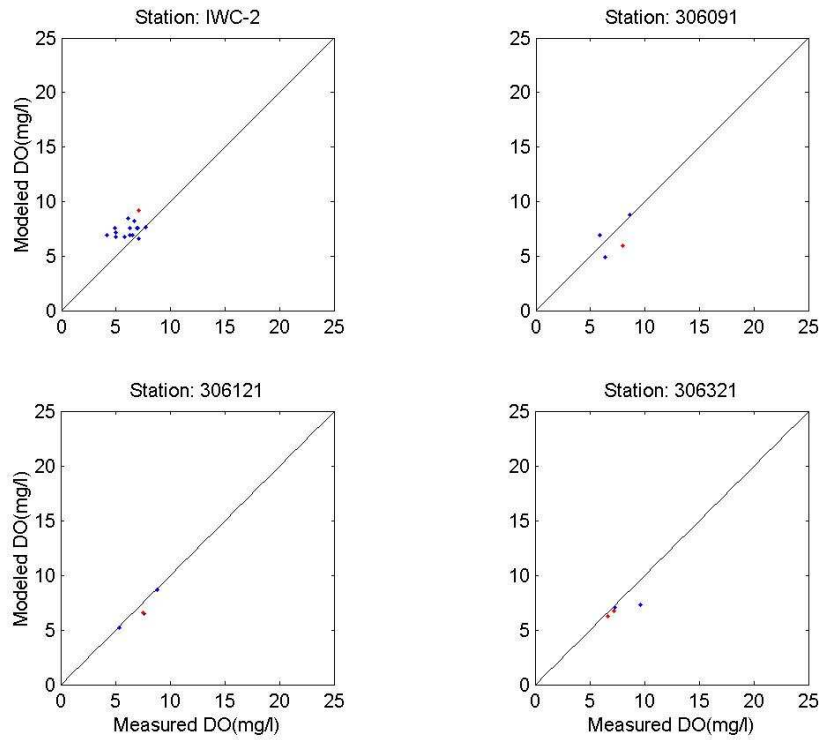


Figure 5.31: Scatterplot comparison between model and data for DO in the year 1999 (blue: morning; red: afternoon. part 3)

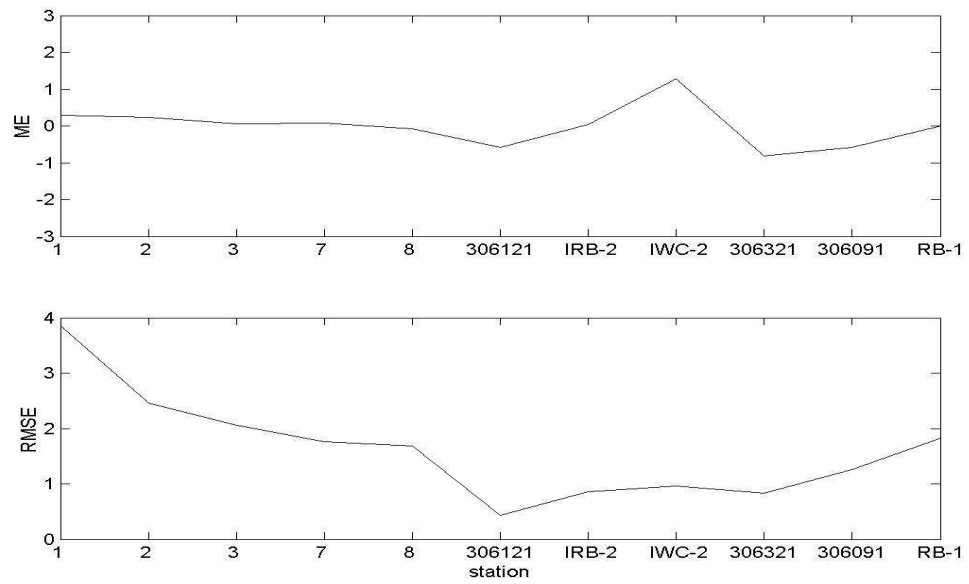


Figure 5.32: Transect plot of statistical parameters for DO in the year 1999

Chapter 6

CONCLUSION AND DISCUSSION

6.1 Conclusion

The purpose of this study is to calibrate the hydrodynamic model and water quality model in Delaware Inland Bays. First, brief descriptions of ECOMSED and RCA are presented. Then these two models are set up for Delaware Inland Bays. Physical processes include tidal current, freshwater discharges and air-sea interaction for the ECOMSED model, and biological processes include plants photosynthesis, respiration and reaeration for the RCA model. The hydrodynamic model provides dynamic transport to drive the water quality model. In order to couple these two models, ECOMSED is run first, then the bathymetry and grid information is stored in one file, and the physical transport calculated by ECOMSED is stored in another file for the desired periods. These two files are used as input files for RCA.

The coupled model systems are calibrated and verified with the field data. The data are provided by Division of Water Resource, DNREC. The database contains several data sources and provides the time series data station by station. Based on these data, the models have been implemented for two different years, one for calibration, and the other for verification. The models' simulations during these two periods are compared with the field data for surface elevation, water temperature, salinity, and DO. The simulated results show that the models are able to capture the yearly variation trends successfully. The error analysis also shows the models have good agreements with the field data.

The tidal surface elevation results show that the Inland Bays are dominated by the semi-diurnal tide, M_2 . The water temperature shows seasonal variations in the Bays for these two years. In summer, mean water temperature in the Bays is above $26^\circ C$; in winter, mean water temperature is around $8^\circ C$; while in spring and fall, mean water temperature are about $15^\circ C$ and $17^\circ C$, respectively. The salinity is not uniform all over the Bays. The water in the upper and middle portions of the Indian River Bays is fresher than the water near the inlet. There is a significant longitudinal salinity gradient in the Indian River Bay. The salinity in the Indian River Bay has a wide range of diurnal variations than in Rehoboth Bay.

The DO shows large diurnal swings in summer and fall. In the upper portion of Indian River Bay, the simulations reveal a series of large diurnal oscillations between super-saturation and near-anoxic conditions in these two seasons. In the winter, the diurnal oscillations still exist, but the minimum DO concentrations are mostly above 4 mg/l .

The success of this study indicates that numerical models are effective tools for diagnosing water quality problems in shallow waters.

6.2 Limitations and Proposed Future Work

In this study, a comprehensive numerical modeling approach is used to study the water quality problem in Delaware Inland Bays. Although the models can simulate the long-time variations well generally, the model-data comparisons indicate the model results are still not ideal. As shown in the last two chapters, at some stations, a few data points are far from the prediction. This situation often happens in the shallow waters near the freshwater discharge sites. It is mentioned that the models are not sensitive enough to predict the peak points in the field measurements. Numerical models are simplified representations of the natural world, and the results that they generate are only as good as their inputs. In this study, the available input data are not detailed enough during the simulation time. For example, the

DO loadings from rivers have very few time series data, sometimes even one data or no data in a month. These boundary conditions lead to some incorrect predictions for the DO results. It should predict more accurately if we could input the boundary conditions more frequently.

For the DO simulation in this study, the water quality model is not as complicated as the eutrophication model. DO is the only state variable calculated here, and other nutrients are not considered. Therefore, the influences of these nutrients to DO are neglected in this model. Actually, this water quality model is the beginning for the DO calculation. The eutrophication model will be considered to simulate all the water quality variables if all the required data are available for the calculation.

In this study, the simulated results are only compared with long time series data station by station, but the number of the data at these stations is limited. If we could obtain the field data at some of these stations at a higher frequency for a short time period, for example, several measurements per day for continuous 10 days or more, the models would be calibrated much better hopefully.

BIBLIOGRAPHY

- Ahsan, Q., and A. F. Blumberg, 1999. "Three-dimensional hydrothermal model of Onondaga Lake, New York", *J. Hydr. Engrg.*, 125, 912–923.
- Andres, A. S., K. S. Savidge, J. R. Scudlark, and W. J. Ullman, 2002. "Delaware Inland Bays Water Quality Database", Delaware Geological Survey Digital Product 02- 02, version 7.02.
- Arakawa, A., and V. R. Lamb, 1977. "Computational design of the basic dynamical process of the UCLA General Circulation Model", *Methods in Computational Physics*, 17, Academic Press, 173–265.
- Baden, S. P., L.-O. Loo, L. Pihl, and R. Rosenberg, 1990. "Effects of eutrophication on the benthic communities including fish: Swedish west coast. *Ambio*, 19, 113–122.
- Blumberg, A. F., and G. L. Mellor, 1980. "A coastal ocean numerical model", In: *Mathematical Modelling of Estuarine Physics, Proceedings of an International Symposium, Hamburg, August 24–26, 1978. J. Sundermann and K.P. Holz, Eds.*, Springer-Verlag, Berlin.
- Blumberg, A. F., and G. L. Mellor, 1987. "A description of a three-dimensional coastal ocean circulation model", In: *Three-Dimensional Coastal Ocean Models*, N. Heaps, Ed., 1–16, *American Geophys. Union*.
- Blumberg, A. F., and H. J. Herring, 1987. "Circulation modeling using orthogonal curvilinear coordinates", In: *Three-Dimensional Models of Marine and Estuarine Dynamics*, J. C. J. Nihoul, and B. M. Jamart, Eds., Elsevier Pub. Company, 55–88.
- Blumberg, A. F., and J. J. Fitzpatrick, 1999. "Strategy for coupling hydrodynamic and water quality models for addressing long time scale environmental impacts", *Proc., 2nd Int. Symp. on Envir. Hydraulics*, Environmental Hydraulics, Rotterdam, The Netherlands.

- Brackbill J. U., and J. S. Saltzman, 1982. "Adaptive zoning for singular problems in two dimensions", *Journal of Computational Physics*, 46, 342–368.
- Caffrey, J. M., 2003. "Production, respiration and net ecosystem metabolism in U.S. estuaries", *Environmental Monitoring and Assessment*, 81, 207–219.
- Center for the Inland Bays, 1995. "A comprehensive conservation and management plan for Delaware's Inland Bays", 173pp., retrieved from <http://www.inlandbays.org/pdfs/ccmpmain.pdf> on April 27, 2006.
- Chapra, S. C., 1997. "Surface water-quality modeling", WCB/McGraw-Hill, 844pp.
- Connolly, J. P., A. F. Blumberg, and J. D. Quadrini, 1999. "Modeling fate of pathogenic organisms in coastal waters of Oahu, Hawaii", *J. Envir. Engrg.*, 125, 398–406.
- Cox, B. A., 2003. "A review of dissolved oxygen modeling techniques for lowland rivers", *The Science of the Total Environment*, 314–316, 303–334.
- D'Avanzo, C., and J. N. Kremer, 1994. "Diel oxygen dynamics and anoxic events in an eutrophic estuary of Waquoit Bay, massachusetts", *Estraries*, 17, 131–139.
- DiToro, D. M., D. J. O'Connor, and R. V. Thomann, 1970. "A dynamic model of the phytoplankton population in the Sacramento-San Joaquin Delta", In: Nonequilibrium system in natural water chemistry, symposium of the American Chemical Society, Division of Water, Air, and Waste Chemistry, Houston, Texas, 131–180.
- Domenici, P., J. F. Steffensen, and R. S. Batty, 2000. "The effect of progressive hypoxia on swimming activity and schooling in Atlantic herring", *J. of Fish Biology*, 57, 1526–1538.
- Edinger, J. E., D. K. Brady, and J. C. Greyer, 1974. "Heat exchange and transport in the environment", *Rep. No. 14, Cooling Water Res. Project (RP-14)*, Electric Power Research Institute, Palo Alto, Calif.
- Entrix, Inc., 2001. "DRAFT ecological risk-based 316(a) demonstration for the Indian River Power Plant", New Castle, DE.

- Gutiérrez-Magness, A. L., and J. P. Raffensperger, 2003. "Development, calibration, and analysis of a hydrologic and water-quality model of the Delaware Inland Bays watershed", Water-Resources Investigations Report 03-4124, 42pp.
- Hagy, J. D., W. R. Boynton, C. W. Keefe, and K. V. Wood, 2004. "Hypoxia in Chesapeake Bay, 1950-2001: long-term change in relation to nutrient loading and river flow", *Estuaries*, 27, 634-658.
- HydroQual, Inc., 2002. "A Primer for ECOMSED, Version 1.3, Users Manual", March.
- HydroQual, Inc., 2004. "User's Guide for RCA, Release 3.0", June.
- Janzen, C. D., and K.-C. Wong, 1998. "On the low-frequency transport processes in a shallow coastal lagoon", *Estuaries*, 21, 754-766.
- J. E. Edinger Associates, Inc., 2004. "Enhancement and expansion of hydrodynamic and water quality modeling system for the Delaware Inland Bays for TMDL analysis", Delaware Department of Natural Resources and Environmental Control.
- Karim, M. R., M. Sekine, and M. Ukita, 2002. "Simulation of eutrophication and associated occurrence of hypoxic and anoxic condition in a coastal bay in Japan", *Marine Pollution Bulletin*, 45, 280-285.
- Karpas, R. M., 1978. "The hydrography of Indian River and Rehoboth-Delaware's small bays", Master Thesis, University of Delaware, 179pp.
- Karpas, R. M., and P. Jensen, 1977. "Hydrodynamics of coastal Sussex County estuaries, Report on task 2331 for the coastal Sussex County water quality analysis", Del. Sea Grant Coll. Program, University of Delaware.
- Keulegan, G. H., 1967. "Tidal flow in estuaries, water-level fluctuations of basins in communication with seas", *Tech. Bull. 4.*, Comm. on Tidal Hydraul., Army Corps of Eng., Vicksburg, Miss, 89pp.
- Lanan, G. A., and R. A. Dalrymple, 1977. "A coastal engineering analysis of Indian River Inlet, Delaware", *Ocean Eng. Tech. Rep. 14*, Del. Sea Grant Coll. Program, University of Delaware, 227pp.

- Large, W. G., and S. Pond, 1982. "Sensible and latent heat flux measurements over the ocean", *J. Phys. Oceanogr.*, 12, 464–482.
- Lu, X., and K.-C. Wong, 1994. "The subtidal Lagrangian current in Delaware's inland bays under low wind conditions", *Estuarine, Coastal and Shelf Science*, 39, 353–365.
- Mellor, G. L., and T. Yamada, 1982. "Development of a turbulence closure model for geophysical fluid problems," *Rev. Geophys. Space Phys.*, 20, 851–875.
- Orel, G., E. Vio, D. Del Piero, and F. Aleffi, 1986. "Episodes of oxygen deficiency of the sea floor, benthic populations and fisheries", *Nova-Thalassia*, 8, 267–280.
- Price, K. S., 1998. "A framework for a Delaware Inland Bays environmental classification", *Environmental Monitoring and Assessment*, 51, 285–298.
- Qin, W., 2005. "Application of the spectral wave model SWAN in Delaware Bay", Master Thesis, University of Delaware, 113pp.
- Rajar, R., and M. Cetina, 1997. "Hydrodynamic and water quality modeling: An experience. *Ecological Modeling*, 101,195–207.
- Rosati, A., and K. Miyakoda, 1998. "A general circulation model for upper ocean circulation", *J. Phys. Oceanogr.*,18, 1601–1626.
- Shi, F., 2006. "CoastGrid, a software for curvilinear grid generation", CACR Report, Center for Applied Coastal Research", University of Delaware, Newark, Delaware.
- Steele, J. H., 1962. "Environmental control of photosynthesis in the sea", *Limnol. Oceanogr.*, 7, 137–150.
- Wang, D.-P., 1979a. "Subtidal sea level variations in Chesapeake Bay and relations to atmospheric forcing", *J. Phys. Oceanogr.*, 9, 413–421.
- Wang, D.-P., 1979b. "Wind driven circulation in the Chesapeake Bay, winter 1975", *J. Phys. Oceanogr.*, 9, 564–572.
- Wang, L. T., 2005. "Locating ground water discharge areas in Rehoboth and Indian River Bays, Delaware using Landsat 7 imagery", Master Thesis, University of Delaware, 128pp.

- Wang, T., 2005. "Hypoxia in shallow coastal waters: a case study in Onancock Creek, Virginia", Master Thesis, College of William and Mary, 129pp.
- Weston, R. F., Inc., 1993. "Report to the Delaware Inland Bays National Estuary Program", Technical Report prepared for the Delaware Department of Natural Resources and Environmental Control.
- Wong, K.-C., 1991. "The effect of coastal sea level forcing on Indian River Bay and Rehoboth Bay, Delaware", *Estuarine, Coastal and Shelf Science*, 32, 213–229.
- Wong, K.-C., 2002. "On the wind-induced exchange between Indian River Bay, Delaware and the adjacent continental shelf", *Continental Shelf Research*, 22, 1651–1668.
- Wong, K.-C., and J. DiLorenzo, 1988. "The response of Delaware's inland bays to ocean forcing", *J. Geophys. Res.*, 99, 14209–14222.
- Wong, K.-C., and X. Lu, 1994. "Low frequency variability in Delaware's inland bays", *J. Geophys. Res.*, 99, 12683–12695.